NTNU

Norwegian University of
Science and Technology

Updated Norwegian In Situ Rock Stress Database

Aurora Louise Lucia Simonsen

Geotechnology
Submission date: June 2018
Supervisor: Charlie Chunlin Li, IGP

Norwegian University of Science and Technology
Department of Geoscience and Petroleum

NTNU
Norges teknisk-naturvitenskapelige universitet

Fakultet for ingeniørvitenskap

Institutt for geovitenskap og petroleum

Masteroppgave - oppgavetekst

Studentens navn: Aurora Louise Lucia Simonsen

Studieretning: Ingeniør – og miljøgeologi/ Ingeniørgeologi og bergmekanikk

Tittel: Updated Norwegian In Situ Rock Stress Database

Veileder: Professor Charlie Chunlin Li

Utfyllende tekst for oppgaven:

The purpose of this thesis is to develop an updated Norwegian in situ rock stress database comprised of stress data from 1990 until present time. The database will contain stress data obtained with different measurement and estimation methods, from both onshore and offshore Norway, as well as Svalbard. Parameters in the database will include stress orientations, stress magnitudes, description of location with focus on overburden and topography and geological information about the site. The data collected will be presented graphically and analysed with focus on the database parameters.

The work that is to be done for this thesis can be summarised by three main objectives:

- Develop an updated Norwegian in situ rock stress database
- Collect as much in situ rock stress data from the last 28 years as possible
- Present the data collected graphically and analyse the data with focus on the database parameters

06.06.2018

Faglærer

Preface

This master thesis is written at The Department of Geoscience and Petroleum at the Norwegian University of Science and Technology (NTNU) as a part of the study program Geotechnology. The associated work has been carried out during the spring semester of 2018, and is a continuation of the project report with the same title from the autumn semester of 2017.

I would like to thank my supervisor Professor Charlie C. Li at NTNU for his guidance, for the information he has provided for me on the topics discussed in this project and for getting me in touch with relevant people in the industry. Furthermore, I would like to thank Conrad Lindholm at NORSAR for inviting me to their office to learn about the focal mechanism method when I was working on the project report. I am very grateful for the focal mechanism data he sent me which makes up about half of data in the database.

I want to express my thanks to everyone who helped me collecting data. I would especially like to thank Johannes Hope at Statkraft, Gunnar Birgisson at Sweco, Roger Olsson at NGI and Freyr Palsson at Norconsult. They were a great help by informing me of relevant projects and getting me in thouch with right people on the projects. They also confirmed that the work I was doing was relevant for the industry which kept me motivated during the semester.

Finally, I would like to express my gratitude to the companies that have allowed me to use their data:

- Bane NOR SF
- Eidsiva Vannkraft AS
- NGI
- Norconsult AS
- NORSAR
- Skanska Norge AS
- Statens vegvesen Region vest
- Statens vegvesen Vegdirektoratet
- Statkraft AS
- Statoil ASA
- Store Norske Spitsbergen Kullkompani AS
- Sweco Norge AS

Trondheim, 07.06.2018

Aurora L. L. Simonsen

Summary

This thesis presents an updated Norwegian in situ rock stress database and collected in situ rock stress data. In situ rock stresses are the stresses that are present in the ground before any disturbance. Knowledge of in situ stresses is of importance for the safety and stability of man-made structures in rock masses, and they also play a fundamental role in the development of geological structures. The database created for this thesis consists of four tables where one serves as the main table. The main table contains information about the in situ stress field, about bedrock and description of location. The other tables contain test data from rock stress measurements and data uncertainty.

Throughout the work of this thesis there have been collected 115 data records that were obtained with different measurement (overcoring and hydraulic fracturing) and estimation (borehole breakouts, drilling-induced-fractures and focal mechanism) methods. Measurement data makes up 36 % of the database and the data has overburdens from 11–1300 m. Estimation data makes up 64 % of the data and the data covers a depth range from about 1000 m–50 km.

A N–S and a WNW–ESE major horizontal stress orientation dominate the estimation data from offshore Norway and western, mid and eastern Norway. This is consistent with the ridge push effect from the mid-Atlantic ridge. The measurement data from onshore Norway had scattered orientations that could be caused by local effects. The major horizontal stress generally exceeded the vertical stress in the Norwegian region with an average ratio of 1.2. Calculations indicated that the sedimentary rocks had more stress anisotropy than igneous and metamorphic rocks, and that the Precambrian rocks had higher stress magnitudes than Cambrian-Silurian rocks. It also seemed that the stress gradients decreased with increasing overburden. However, the calculations are based on small data sets which reduces the reliability of the results. To improve the reliability of the results and get more information about stress orientations, more in situ rock stress data should be collected, especially from onshore Norway.

The effect of topography on the in situ stress field was evaluated by studying four data points located in mountain sides. The effect of topography on the principal stress orientations seemed to decrease inwards in the rock mass. There were also indications of horizontal stress concentration beneath the valleys.

Sammendrag

Denne avhandlingen presenterer en oppdatert norsk in situ bergspenningsdatabase og samlet in situ bergspenningsdata. In situ bergspenninger er spenninger som er til stede i grunnen før eventuelle forstyrrelser. Kunnskap om in situ bergspenninger er viktig for sikkerheten og stabiliteten av menneskeskapte strukturer i bergmasser, de spiller også en fundamental rolle i utviklingen av geologiske strukturer. Databasen som har blitt laget består av fire tabeller hvor en av dem fungerer som hovedtabell. Hovedtabellen inneholder informasjon om in situ spenningstilstand, om berggrunn og beskrivelse av lokalitet. De andre tabellene inneholder testdata fra bergspenningsmålinger og datausikkerhet.

Gjennom arbeidet med denne avhandlingen har det blitt samlet 115 datapunkter som er funnet med ulike måle- (overboring og hydraulisk frakturering) og estimeringsmetoder (borehullsbreakouts, boreindusterte sprekker og fokalmekanisme). Måledata utgjør 36 % av databasen og dataene har overdekning fra 27–1300 m. Estimeringsdata utgjør 64 % av dataen og dekker et dybdeintervall fra ca. 1000 m–50 km.

En N–S og en WNW–ESE-retning på største horisontalspenning dominerte estimeringsdataene fra kontinentalsokkelen og Vest-, Midt- og Øst-Norge. Dette stemmer med retningen på trykkeffekten fra den midtatlantiske rygg. Måledataene fra fastlands-Norge hadde spredte retninger som kan være forårsaket av lokale effekter. Den største horisontalspenningen var generelt høyere enn vertikalspenningen med et gjennomsnittsforhold på 1.2. Beregninger indikerte at sedimentære bergarter hadde høyere bergspenningsanisotropi enn magmatiske og metamorfe bergarter, og at prekambriske bergarter hadde høyere spenningsstørrelser enn bergarter fra Kambro-Silur. Det var antydning til at størrelsen på spenningsgradientene avtok med økende overdekning. Beregningene er basert på små datasett, noe som reduserer påliteligheten av resultatene. For å øke påliteligheten av resultatene og for å få mer informasjon om spenningsstørrelser, burde mer in situ bergspenningsdata bli samlet, spesielt fra fastlands-Norge.

Effekten av topografi på in situ spenningsfeltet ble evaluert ved å studere fire datapunkter lokalisert i fjellsider. Det virket som effekten av topografi på hovedspenningsretningene ble redusert innover i bergmassen. Det var også indikasjoner på horisontale spenningskonsentrasjoner under dalene.

Contents

List of Figures

List of Tables

Chapter 1

Introduction

This chapter serves as an introduction to the thesis and covers background for the project, objectives, related work and a structure of the thesis. The work presented in this thesis is a continuation of the project report with the same title. The project report was written during the autumn of 2017 as a part of the course TGB4500 Engineering Geology and Rock Mechanics Specialisation project at the Norwegian University of Science and Technology (NTNU). The main purpose of the project report was to provide the theoretical basis for this thesis. Therefore, most of Chapter 2 (theory Chapter) and Section 3.2.1, 3.3 and 3.4 (in method Chapter) are similar to contents of the project report.

1.1 Background

There are many different aspects when dealing with rocks where knowledge about in situ rock stresses is important. Knowledge about in situ stresses can be used when evaluating seismic risks, to understand dynamic processes in relation to plate tectonics and in earthquake predictions (Stephansson et al., 1986). For geologists and geophysicists, knowledge of in situ stresses is of importance because they play a fundamental role in the development of geological structures (Amadei and Stephansson, 1997).

For engineering purposes, knowledge of the in situ rock stresses is important for safe construction and operation of man-made structures in rock (Hanssen, 1997). The rock mass is

pre-stressed and these stresses will control the stress development after excavation (Li, 2015). Thus, the stability of underground and surface excavations in rock can be improved if the in situ stress stat is known. Knowledge about in situ rock stresses is also helpful at the designing stage of underground openings. At the designing stage, knowledge of stresses can be used in numerical modelling to optimise geometry, dimensions and orientation of the opening relative to the in situ stress state. If this is done successfully, possible stress-related problems like rock failure and development of fractures can be reduced or eliminated (Amadei and Stephansson, 1997).

There has already been collected in situ rock stress data in different databases, with the largest being the global World Stress Map (WSM) database (World Stress Map, 2017). Rock stress data from Norway has been collected in a regional stress database called the Fennoscandian Rock Stress Database (FRSDB), which was later incorporated in the WSM database (Stephansson et al., 1991). The FRSDB database is not continuously updated (Fejerskov, 1996) and, apart from five data records added in 2016, there has not been added Norwegian stress data to the WSM for about 25 years. Consequently, Norway is today one of the areas with the lowest density of data records in the WSM database (Carafa and Barba, 2013).

The combination of the importance of knowledge of in situ rock stresses and the low number of Norwegian in situ stress rock data collected in databases, makes it clear that there is need for an updated Norwegian in situ rock stress database.

1.2 Objectives

The purpose of this thesis is to develop an updated Norwegian in situ rock stress database comprised of stress data from 1990 until present time. The database will contain stress data obtained with different measurement and estimation methods, from both onshore and offshore Norway, as well as Svalbard. Parameters in the database will include stress orientations, stress magnitudes, description of location with focus on overburden and topography and geological information about the site. The data collected will be presented graphically and analysed with focus on the database parameters.

The work that is to be done for this thesis can be summarised by three main objectives:

1. Develop an updated Norwegian in situ rock stress database
2. Collect as much in situ rock stress data from the last 28 years as possible
3. Present the data collected graphically and analyse the data with focus on the database parameters

1.3 Related Work

This section will introduce in situ rock stress databases that contain Norwegian rock stress data. This involves the global WSM project, the regional FRSDB and two Norwegian doctoral theses. In addition to the WSM database, there exists another global in situ rock stress database called the Quantitative World Stress Map. Its focus is on rock-type specific in situ stress magnitudes versus depth, but no data from Norway has been included so far and it will therefore not be presented (Zang et al., 2012).

1.3.1 World Stress Map Project

The World Stress Map (WSM) project was initiated as a global cooperative project in 1986 with the purpose to collect and interpret in situ tectonic stress data. The first version of the WSM database was released in 1989 and composed of 3574 data records (Zang et al., 2012). Since, the collection of data has expanded and the newest version from 2016 contained 42 870 data records (World Stress Map, 2017). The map based on the data from WSM 2016 is presented in Figure 1.1. The Figure shows orientation of the major horizontal in situ stress in the Earth's crust, where the colours of the bars represent tectonic stress regime in that area, categorised after Figure 1.2.

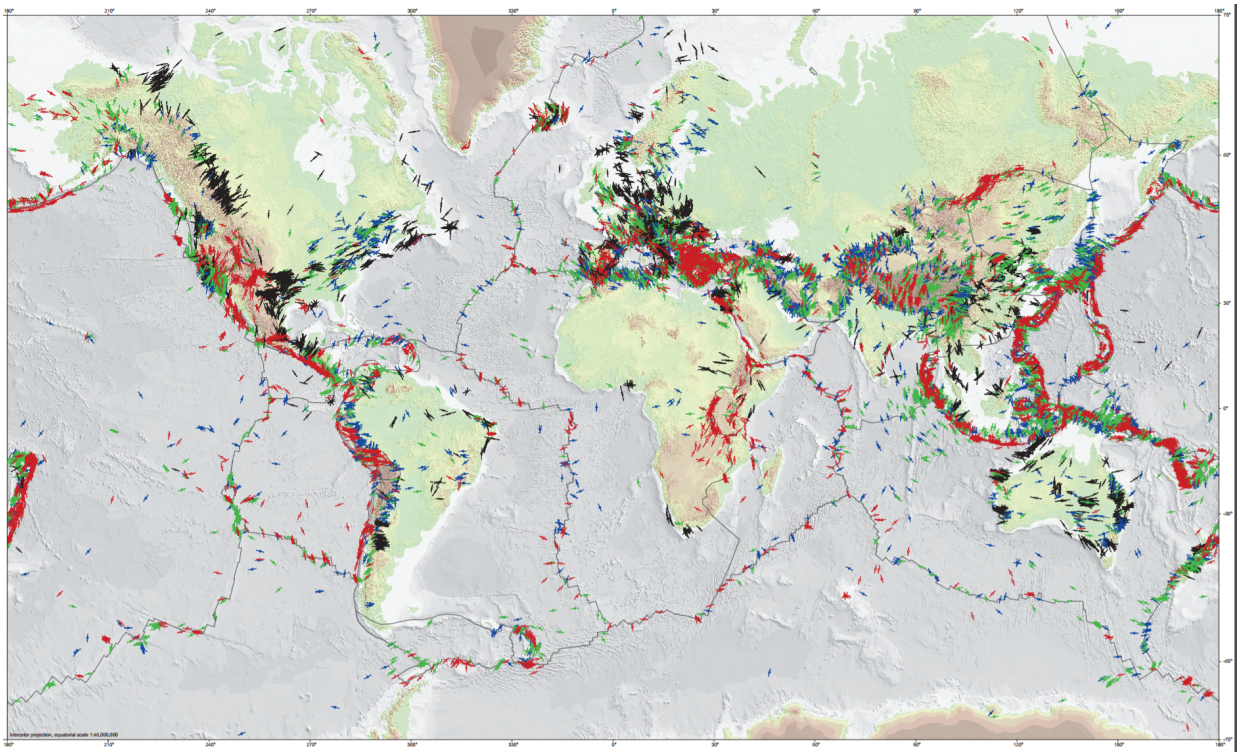

Figure 1.1: Word Stress Map released in 2016. The bars show σ_H orientation and the colours show tectonic stress regimes. Accessed from World Stress Map (n.d.) 20.01.2018.

The tectonic stress regimes express different faulting styles that are determined by relative stress magnitude of the horizontal stresses with respect to the vertical stress. The main faulting styles used in the WSM is normal faulting, strike-slip faulting and reverse faulting. Extension of tectonic plates gives normal faulting, compression of plates gives reverse faulting and sideways movement of plates gives strike-slip faulting (Zoback and Zoback, 2002). Normal faulting is marked by red in Figure 1.1 and 1.2, strike-slip faulting by green and reverse faulting by blue. In situ stresses, principal stresses and horizontal/vertical stresses will be discussed in Section 2.1.1.

The stresses in the Earth's crust can also be categorised based on their lateral extent as either continental, regional or local stresses (Zoback, 1992). According to Zoback and Zoback (2002), the WSM project mainly focuses on regional tectonic stress patterns. However, recently more data not likely to be representative for long intraplate stress patterns has been added to the WSM database (Heidbach et al., 2010).

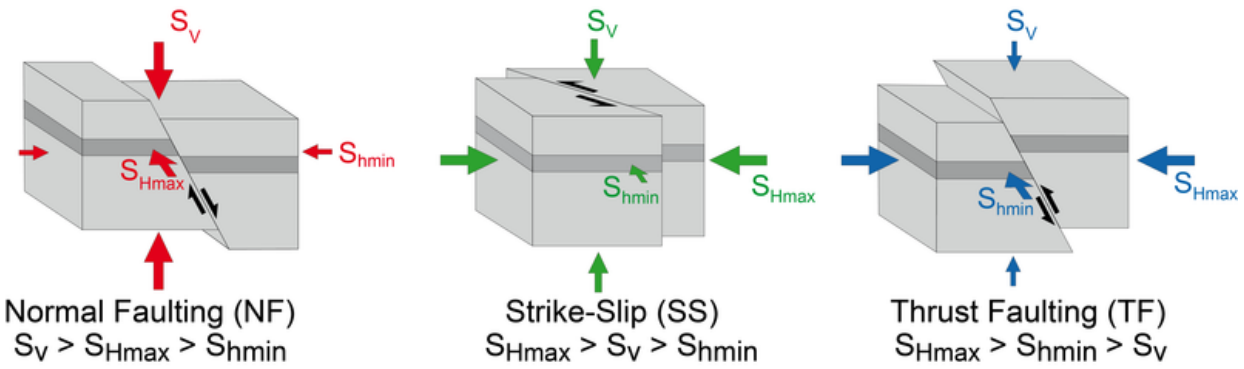

Figure 1.2: Tectonic regimes in the WSM project. For normal faulting (left), $\sigma_V = \sigma_1$ and $\sigma_h = \sigma_3$. Strike-slip faulting (middle) gives $\sigma_H = \sigma_1$ and $\sigma_h = \sigma_3$. For reverse faulting (right), $\sigma_H = \sigma_1$ and $\sigma_V = \sigma_3$. Accessed from World Stress Map (n.d.) 23.01.2018.

Quality Ranking Scheme

An internationally accepted quality ranking scheme is used to standardise the data in the WSM database. That it is internationally accepted guarantees global comparability of stress data (Zang et al., 2012). The main goal with this scheme is to assess how reliable each data point represents the stress field (Zoback and Zoback, 2002).

The quality scheme is composed of letters from A to E that represents the quality of the data. A–C quality are considered reliable for the use in analysing stress patterns in the WSM (Zang et al., 2012). For A quality data, the orientation of the major horizontal in situ stress shall be accurate within ±15°, while for B ±20° and for C ±25°. In addition to orientation accuracy, there are other requirements that are considered when assigning data quality. These requirements include among others number of measurements, standard deviation and distance to from free surface. Table A.1 and A.2 in Appendix A.4 show parts of the quality ranking scheme that are relevant for the stress determination methods presented in Chapter 3.

1.3.2 Fennoscandian Rock Stress Database

The Fennoscandian Rock Stress Database (FRSDB) was initiated in 1986 as a joint project in Norway, Sweden and Finland. The main purpose of the FRSDB was to determine whether there existed any regional stress trends or systematic stress variations related to rock properties or to geological structure. Another purpose with the database, was to use it as a base for

further research in Norway, Sweden and Finland (Stephansson et al., 1986). The first version of the FRSDB contained 487 entries that had been collected separately in the respective countries (Stephansson et al., 1991). One of the in situ rock stress maps based on the records is presented in Figure A.1 in Appendix A.1.

Stephansson et al. (1991) presented the major results from the FRSDB that showed very large scatter in stress directions and magnitudes. The data collected was mainly from shallow depths, no data was retrieved from intermediat depths in the Earth's crust (Stephansson et al., 1986). Therefore, Stephansson et al. (1991) concluded that the scatter in the FRSDB was likely produced by heterogeneities in the uppermost part of the Earth's crust. How heterogeneities affect the in situ stress state will be discussed in Section 2.3.2.

1.3.3 Norwegian in situ stress databases

During the 1990s at NTNU, Fejerskov (1996) and Hanssen (1997) created two in situ rock stress databases as part of their doctoral work. Fejerskov (1996) established an in situ rock stress database for offshore Norway that was a part of the Regional Stress Field topic within the EU research project Integrated Basin Studies. The purpose with the Regional Stress Field was to increase the number of stress data points on the Norwegian continental shelf, as well as to increase the understanding of the stress field offshore Norway. Through the work of Fejerskov (1996), 538 data points from oil companies and research institutes were collected. The paper published by Fejerskov et al. (2000) presented a new stress map from the Norwegian region by compiling data from the WSM, the FRSDB and newer borehole breakout and focal mechanism data.

In his doctoral work, Hanssen (1997) collected existing stress measurement data from 150 onshore sites in Norway, Sweden and Finland. This data was used to evaluate the stress state in western Fennoscandia (Hanssen, 1997).

1.3.4 Relation to the thesis

The WSM database is not in direct conflict with the present thesis because it has low density of stress data from Norway and a high amount of data without stress magnitudes (Carafa and Barba, 2013; Fejerskov, 1996). The FRSDB will not be in conflict either since it has not been updated after 1989. Fejerskov (1996)'s database main focus is on offshore data, while Hanssen (1997)'s database mainly focuses on onshore data from Fennoscandia. These databases have not been updated since the 1990s. These databases will therefore not be in direct conflict with the present thesis, which focuses on newer data and data from both onshore Norway, offshore Norway and Svalbard. The paper published by Fejerskov et al. (2000) will neither be in conflict because its focus is only on stress orientations and Svalbard is not included.

1.4 Structure of the Thesis

The thesis is structured as follows:

- **Chapter 1** Introduction chapter. Background for project, objectives, related work and structure of the thesis are presented.
- **Chapter 2** In Situ Rock Stresses, theory chapter. This chapter introduces in situ rock stresses by describing how in situ stresses are generated and factors that can affect in situ stresses. The in situ stress state in Norway is also presented in this chapter.
- **Chapter 3** Stress Determination Methods, method chapter. This chapter presents different measurement and estimation methods for determination of in situ rock stresses. At the end of this chapter there is a comparison of the methods.
- **Chapter 4** Updated Norwegian In Situ Rock Stress Database, result chapter. This chapter presents the database and the data collected. Presentation of the database includes a description of the software used, the database structure and of the parameters in the database. The data collected is presented graphically by graphs and maps.
- **Chapter 5** Discussion. The data presented in Chapter 4 is discussed. Focus is on stress orientation, stress magnitudes, bedrock and topography.

- **Chapter 6** Conclusion
- **Chapter 7** Further work
- **Chapter 8** References
- **Bibliography**
- **Acronyms**
- **Appendices** Fennoscandian Rock Stress Database (FRSDB) map, equations, GSA geological timescale, World Stress Map (WSM) quality ranking scheme, figures referred to in discussion and presentation of the data collected in the database created.

Chapter 2

In Situ Rock Stresses

Stresses in rock masses can be divided into two main types: in situ rock stress and induced rock stress. In situ rock stresses are the stresses that are present in the ground before any disturbance and are also known as virgin, primitive or natural stresses. Induced rock stresses, also called secondary stresses, are stresses that originate from man-made activities such as mining and tunnel excavation (Amadei and Stephansson, 1997). This thesis will only focus on in situ rock stresses and induced stresses will therefore not be mentioned. This chapter describes what generates in situ rock stresses and factors that can affect them. The in situ stress state in Norway will also be presented. First, there will be an introduction to the subject of stress.

2.1 Stress

2.1.1 Stresses

Stress is defined as a force acting on a unit area (Zoback and Zoback, 2002, 144). For a given point in the rock mass, stress is be given by following equation:

$$\sigma = \lim_{A \to 0} \frac{\Delta F}{\Delta A} \quad [\frac{N}{m^2}] \tag{2.1}$$

Where ΔF is the force working on the area ΔA in a plane (Li, 2015).

Force is a vector, which is a quantity with magnitude and direction, but stress at a point is a tensor. A tensor exists in three-dimensional (3D) space and is a quantity with magnitude, direction and a plane under consideration. A stress tensor consists of nine separate stress components. Three of these are normal stress components and six are shear stress components. Normal stress acts perpendicular to the plane under consideration and is represented by σ_n in Figure 2.1. Shear stress acts along that plane and is represented by τ in Figure 2.1 (Harrison and Hudson, 2001). Out of the six shear stress components, only three of them are unique. Consequently, only three normal stress components and three shear stress components are required to completely specify the stress state at a point (Amadei and Stephansson, 1997).

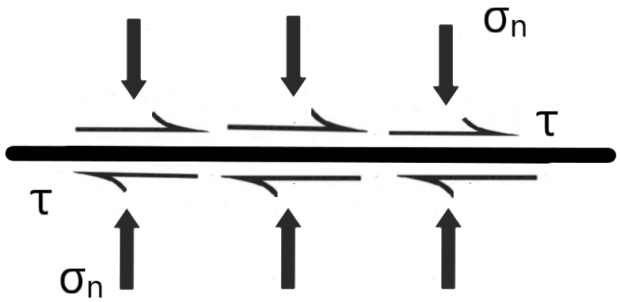

Figure 2.1: Normal and shear stresses acting on a surface.

2.1.2 Principal stresses

The 3D stress state can also be expressed by three principal stresses and their orientations. The principal stresses are normal components of the stress tensor that act on planes where the shear stress is zero (Amadei and Stephansson, 1997). This is illustrated in Figure 2.2 where σ_1 represents the major principal stress, σ_2 the medium and σ_3 is the minor principal stress. In this stress plane, the three principal stresses fully describe the stress field since there is no shear stress (Zoback and Zoback, 2002).

The Earth's surface is in contact with fluid, water or air, which cannot support shear traction. Thus, no shear force is acting on the the Earth's surface and it is therefore a principal stress plane. One of the principal stresses will be located approximately normal to the Earth's surface

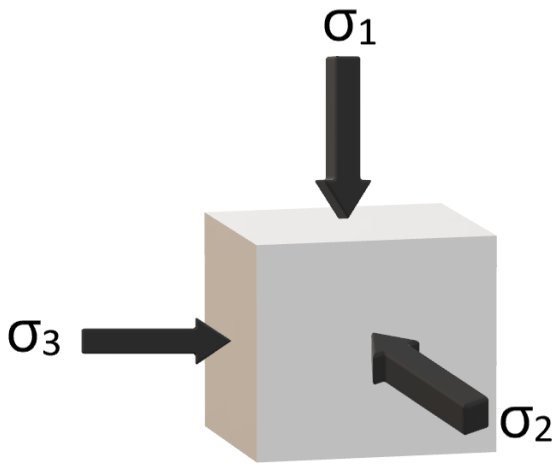

Figure 2.2: The three principal stresses acting on principal planes.

and is detonated σ_v since it is oriented vertically (σ_1 in Figure 2.2). The other two principal stresses will act approximately in the horizontal plane perpendicular to each other (σ_2 and σ_3 in Figure 2.2). One will be the major horizontal stress σ_H and the other the minor horizontal stress σ_h, in some cases $\sigma_H = \sigma_h$. It is common to assume that the principal stresses have these orientations down to several km because data has shown that this in general is true (Zoback and Zoback, 2002). The stress state can then be fully described by the orientation of σ_H or σ_h and the three magnitudes (in Figure 1.1, σ_H is used).

2.2 Components of In Situ Stress

The present in situ rock stress state in the ground is often composed of three types of in situ stress. Theses types are gravitational stress, tectonic stress and residual stress (Harrison and Hudson, 2001). This section will present these in situ rock stress types.

2.2.1 Gravitational stresses

Gravitational stresses are stresses caused by the weight of the overlying material and are also known as overburden stresses (Harrison and Hudson, 2000). If ρ is the average density of the overlying rock, the vertical gravitational stress is given by following Equation:

$$\sigma_v = \rho \cdot g \cdot z \quad [MPa] \tag{2.2}$$

Where g is the gravitational acceleration and z is the depth in meters down to the stress field.

Since the unit weight of rocks generally varies between 0.025 and 0.033 MN/m^3, the vertical gravitational stress should increase literary with depth with a stress gradient in this interval (Amadei and Stephansson, 1997, 27). In Figure 2.3, measured global vertical stresses are plotted against depth. From the Figure it can be seen that the stress gradient of 0.027 MPa/m is a good fit to the data. This indicates that the magnitude of the vertical in situ stress is primarily a result of gravitational stress only (Li, 2015). However, the data show some scatter. Factors likely to create the scatter include geological heterogeneities, tectonic forces or local topography (Jaeger et al., 2007). These factors will be discussed later in this chapter.

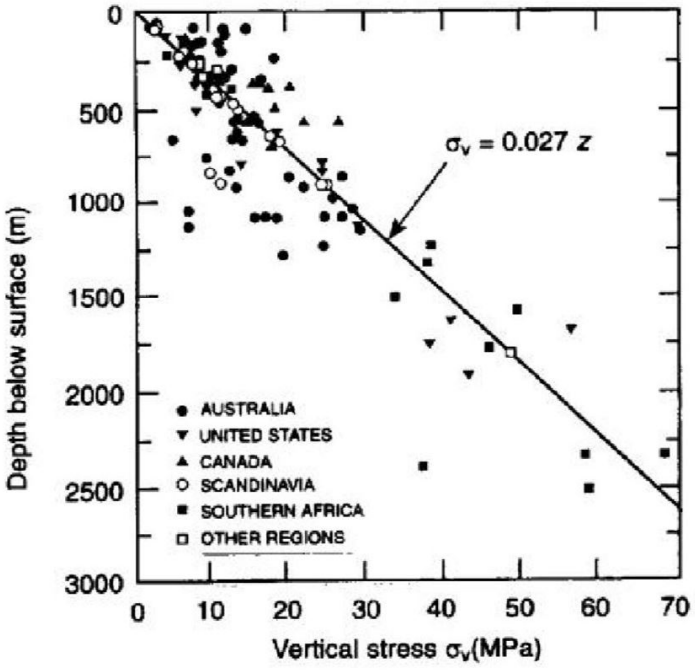

Figure 2.3: Worldwide collection of in situ stress data (Brown and Hoek, 1978).

The most used relationship between horizontal and vertical gravitational stress is derived from Hooke's law (Harrison and Hudson, 2000). Hooke's law states that there is a linear relationship between strain ϵ and stress σ in elastic material (see Appendix A.2.1). In rock mechanics, rock is usually considered as an elastic material (Myrvang, 1996). When the expression for horizon-

tal gravitational stress was derived, it was assumed that the rock could not expand freely in the horizontal direction because it was restrained by adjacent elements. The horizontal strain was therefore zero. It was also assumed that $\sigma_H = \sigma_h$ (Harrison and Hudson, 2000). Solving Hooke's Equations for three dimensions (Equation A.9 in Appendix A.2.1) with those assumptions gave:

$$\sigma_h = \frac{\nu}{1-\nu} \cdot \sigma_v \tag{2.3}$$

ν is an elastic rock parameter called Poisson's ratio and is defined as the negative ratio of lateral to axial strain in a material subjected to uniaxial stress. ν is usually positive because compression is considered positive in rock mechanics (Jaeger et al., 2007).

For horizontal stress, the deviation between theoretical gravitational and measured stress has shown to be even greater than for vertical stress. Theoretical predictions of horizontal stress assume independence of depth when no lateral strain is permitted. Measurements have however shown that the deviation is biggest at shallow depths (Amadei and Stephansson, 1997). According to Harrison and Hudson (2000), this deviation is mainly caused by tectonic, stress residual stress, anisotropy and discontinuity (will be discussed later in this chapter).

2.2.2 Tectonic stresses

Tectonic stresses are stresses caused by relative displacement of the tectonic plates. The displacement of the tectonic plates subjects the Earth's crust to tectonic forces, and these forces induce stresses. If the stresses are high enough, fractures, joints and faults can develop in the rock mass (Harrison and Hudson, 2001). Tectonic stresses can be categorised as either active or remnant. Active tectonic stresses are stresses caused by current straining of the Earth's crust, while remnant tectonic stresses are caused by past tectonic events that have only been partially relieved (Amadei and Stephansson, 1997).

Collection of data has shown that there are two main groups of active tectonic forces: broad-scale tectonic forces and local tectonic stresses. Broad-scale tectonic forces are plate-boundary forces that drive or resist plate motion and are indicated by point 1, 2, 3 and 4 in Figure 2.4.

Point 1 illustrates shear traction that happens at the base of the lithosphere. Point 2 illustrates slap pull, slap pull represents a balance between the forces on the subducted lithosphere. Point 3 illustrates ridge push from mid-oceanic ridges, which is caused by the ridge elevation. Whereas point 4 illustrates trench suction at subduction zones, which is caused by extension of the plate to fill the gap (Zoback et al., 1989).

Local tectonic stresses consist of point 5, 6 and 7 in Figure 2.4 and are caused by bending stresses, isostatic compensation and downbending of the oceanic lithosphere. Bending stresses can be generated by sediment loading, deglaciation and mountains (Zoback et al., 1989). For sediment loading to create bending stresses, the sedimentation rate must be high. These stresses will decrease with increasing time after sedimentation (Fejerskov and Lindholm, 2000). The isostatic compensation is an adjustment of the lithosphere density relative to the overlying load (Zoback et al., 1989).

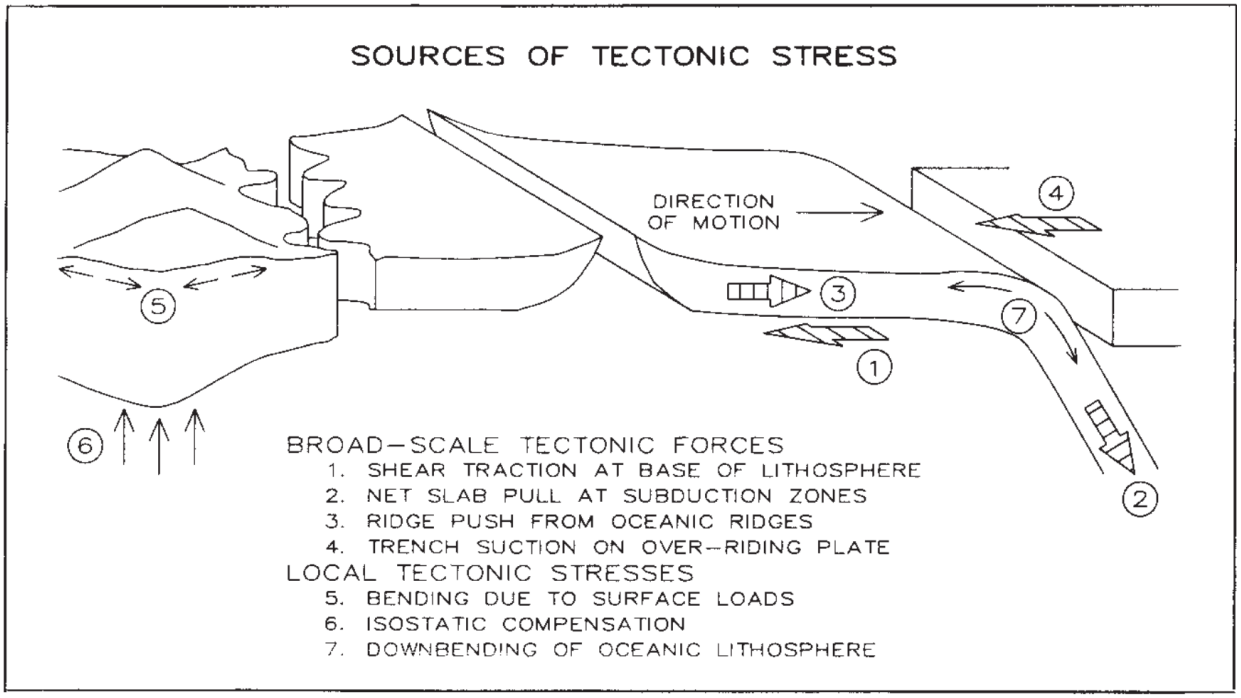

Figure 2.4: The tectonic forces that are responsible for the tectonic stresses (Zoback et al., 1989).

2.2.3 Residual stresses

Residual stresses are stresses that remain in the rock mass when the external forces are removed. These stresses are also known as internal or locked-in stresses. Residual stresses are generated when a load over the rock mass is reduced or removed, or by change in conditions. Load reduction can be caused by erosion, weathering, deglaciation or land uplift. Change in condition involves temperature changes such as magma cooling (Amadei and Stephansson, 1997, 65). Remnant tectonic stresses are actually residual stresses, but are categorised as tectonic since they are a result of tectonic activity like faulting, folding and jointing (Amadei and Stephansson, 1997).

Residual stresses are self-equilibrating, which means that they are related to a system of balanced compressive and tensile forces. Load reduction or temperature change will make the rock mass relax, and the interlocking fabric of the rock will create restraints. This will generate an equilibrium with balanced forces. From Equation 2.2, it is evident that reduction in vertical gravitational stress due to reduction in load will be larger than the horizontal gravitational stress reduction. This is partly the reason why the horizontal in situ stress is bigger than the vertical in some areas (Li, 2015).

2.3 Factors Affecting the In Situ Stress Field

When analysing the in situ stress field in the ground, it is common to assume that the rock mass is isotropic, continuous and homogeneous. However, any rock mass is to a degree anisotropic, heterogeneous and/or discontinuous. This makes it almost impossible to predict the in situ stress field exact (Amadei and Stephansson, 1997, 24). This section will look closer at how anisotropy, heterogeneity, discontinuity, geological structures and topography affect the in situ stress field.

2.3.1 Anisotropy

A rock is anisotropic if the properties of the rock vary with direction (Harrison and Hudson, 2001, 160). Anisotropy of a rock mass is caused by either the mineral composition, the jointing pattern or by geological structures in the rock mass such as foliation or stratification (Li, 2015). According to Amadei et al. (1987), most rock masses close to the Earth's surface have properties that change with direction and are therefore anisotropic. Layered sedimentary rocks and foliated metamorphic rocks, like slate and schist, show distinct anisotropy and one (or more) direction(s) of symmetry (Amadei et al., 1987). Whereas none-foilated metamorphic rocks like gneiss show less anisotropy (Myrvang, 2001). With increasing depth, the Earth's crust becomes more isotropic (Stephansson et al., 1991).

Models proposed by Amadei et al. (1987) showed that the gravitational stress field was related anisotropy caused by the rock mass structures. However, it was mainly the magnitude and orientation of the two horizontal stresses that were dependent on anisotropy of the rock mass. The models showed that the vertical stress was unaffected and therefore independent on anisotropy. Amadei and Stephansson (1997) concluded that when no lateral strain was permitted, the in situ stress state would depend on the orientation of the symmetry planes such as layers and foliations.

2.3.2 Heterogeneity

A rock mass is heterogeneous if its properties varies from point to point, which is normally the case for rock masses in the upper part of the Earth's crust. Common heterogeneities are dikes, layers of sedimentary rocks (strata) and ore bodies (Harrison and Hudson, 2000). A heterogeneous rock mass can affect both the magnitude and orientation of the in situ rock stresses, and produce scattered field measurements (Amadei and Stephansson, 1997). According to Li (2015), there have been observed stress jumps and varying stress fields close to heterogeneities.

If the rock stiffness (commonly expressed by E-modulus) varies in adjacent rock layers, or with dikes/ore bodies and the surrounding rock mass, this will cause variations in the stress field

(Amadei and Stephansson, 1997). The stress will be higher in the rock with the highest stiffness because stress is dependent on stiffness: $\sigma = E \cdot \epsilon$ (Hooke's law). This also applies for weakness zones. If a weakness zone is surrounded by a more competent rock, there will be stress concentration in the competent rock close to the weaker rock mass (Li, 2015). This is illustrated in Figure 2.5 where the weakness zone causes stress concentration in the surrounding, more competent rock.

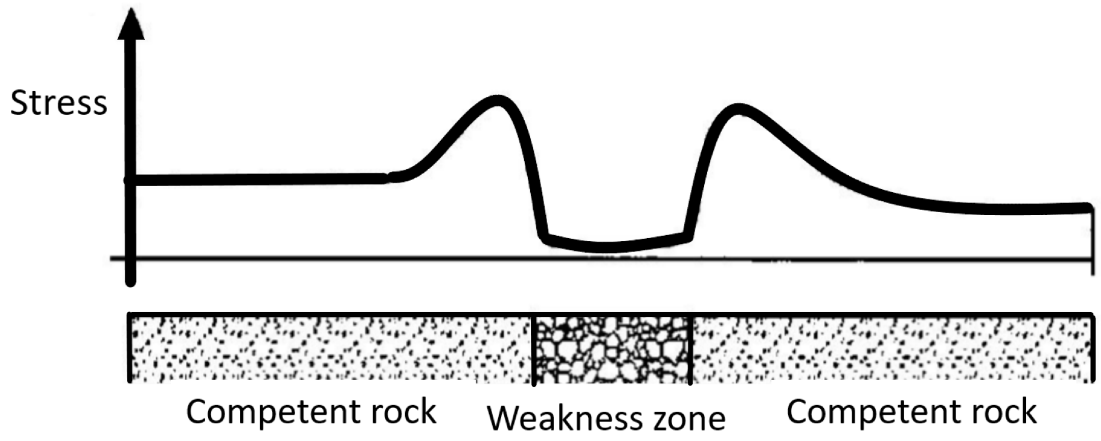

Figure 2.5: Stress distribution around a weakness zone. Modified after Myrvang (1996).

2.3.3 Discontinuity

A discontinuity is defined as a separation of the rock continuum with zero tensile strength. Discontinuities change the stress field around it because the stress field will reflect the geometry of the discontinuity. The impact zone will be dependent on the size of the discontinuity (Harrison and Hudson, 2001).

Fracture is a common discontinuity because all rock masses have fractures of some scale. Figure 2.6 shows how a fracture can affect the stress field around it. The principal stresses, indicated by the crosses, have a change in magnitude and direction close to the fracture. If stress measurements are carried out in this area, this might cause spread in the data results (Harrison and Hudson, 2000). According to Amadei and Stephansson (1997, 45), there are three main types of stress changes expected around discontinuities. The three types are dependent on the relative stiffness of the material in the discontinuity compare with the surrounding rock:

1. Open discontinuity: the discontinuity has zero strength and will be a principal stress

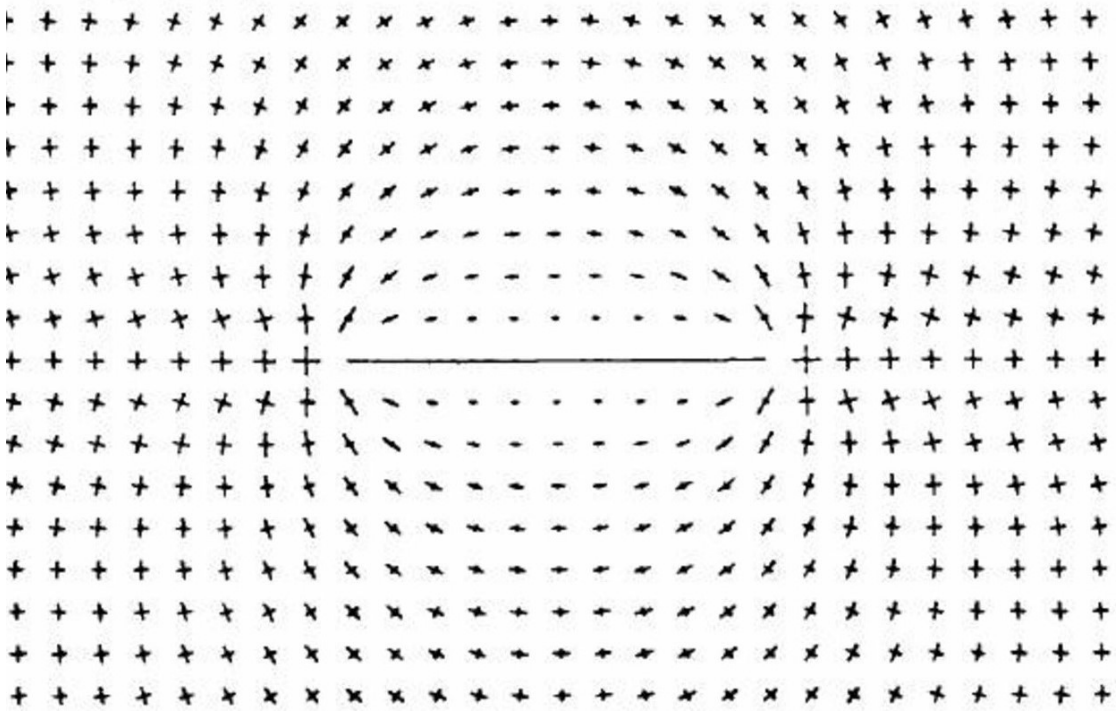

Figure 2.6: The effect a fracture can have on a two-dimensional hydrostatic stress ($\sigma_1 = \sigma_2$) field. The crosses represent magnitude and direction of the principal stresses (Hyett, 1990).

plane. The major principal stress will be parallel with the discontinuity and the minor principal stress will be perpendicular to it with a value of zero.

2. Discontinuity with same material as surrounding rock: principal stresses will be unaffected.

3. Discontinuity with rigid material: the discontinuity is a principal stress plane. The major principal stress will be redirected perpendicular to discontinuity and the minor principal stress will be parallel with it.

2.3.4 Geological structures

Geological structures are structures like faults, folds, joints and dikes (Li, 2015, 4-14). Just as for heterogeneities and discontinuities, geological structures may disturb the in situ stress field by rotating the stresses. In situ stress determinations have shown that geological structures in the size range from microscale to major thrust faults can disrupt the in situ rock stresses (Amadei and Stephansson, 1997).

Faults will generate stress concentration at the contact point between the blocks in the fault, with stress refraction developing adjacent to the fault (Stephansson et al., 1991). The principal stresses will, like for discontinuities, be located perpendicular to and parallel with the fault plane (Myrvang, 2001). Whereas folds create stresses with compressive and tensile stresses in beddings (Li, 2015). An illustration of this can be seen in Figure 2.7.

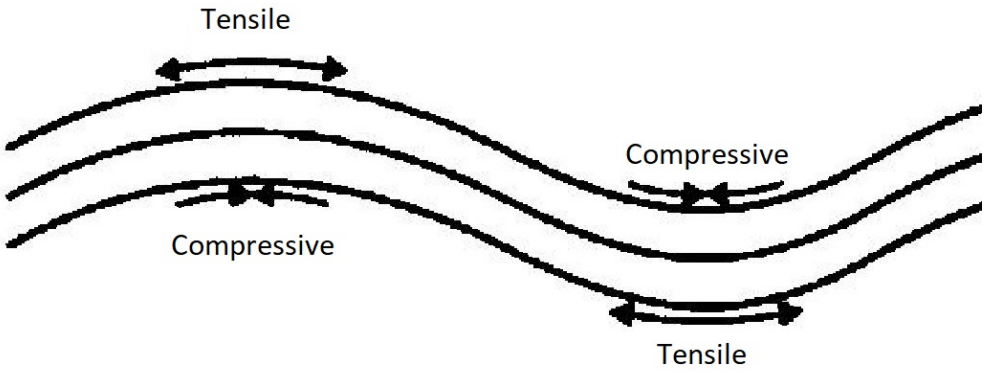

Figure 2.7: Compressive and tensile stresses in folds. Modified after Myrvang (1996).

2.3.5 Topography

When the ground surface is not horizontal, but composed of valleys and mountains as in Figure 2.8, the mountain sides will create an unbalanced stress distribution. The principal stresses will not be entirely vertical and horizontal, but two of the principal stresses will be parallel to the slope surface and the third will be perpendicular to the slope surface. Out of the two slope-parallel principal stresses, one is usually inclined and oriented downhill, while the other is more horizontal (Li, 2015).

If the stress field is purely gravitational, σ_1 will be oriented downhill. Since the principal stress perpendicular to the slope surface will be σ_3, σ_2 will be in the slope-parallel stress in the horizontal direction. If there is horizontal tectonic loading in addition to gravitational stress, the horizontal and slope-parallel stress will increase and can become σ_1. In mountainous areas, there will also be stress concentration and increased horizontal stresses at valley bottoms (point 1 in Figure 2.8). While at mountain tops (point 2 in Figure 2.8) the horizontal stress may be low due to lack of surrounding rock mass (Amadei and Stephansson, 1997). According to

Myrvang (2001), the magnitude of σ_3 will increase inwards in the rock mass, while σ_1 and σ_2 will remain constant.

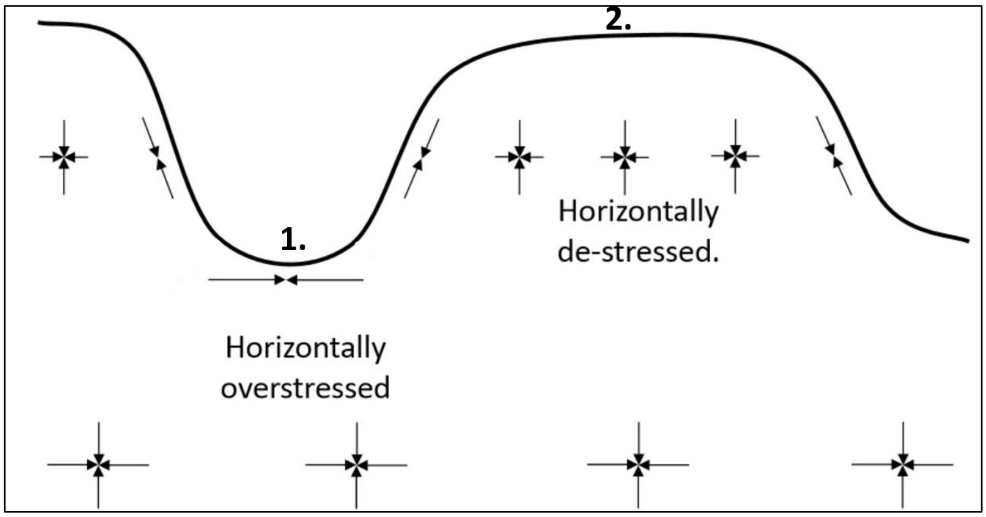

Figure 2.8: Principal stress orientations indicated by crosses in an area with mountains and valleys. Modified after (Li, 2015).

The effect topography has on the in situ stress field will be dependent on the size of the valleys and mountains. Broad structures will affect the stress field to a greater depth than narrow structures. In addition, rock masses with vertical planes of aniostropy will be more affected than isotropic masses or masses with horizontal planes of anisotropy (Amadei and Stephansson, 1997). However, with increasing depth the principal stresses will approach vertical and horizontal orientations as shown in Figure 2.8 (Li, 2015).

2.4 In Situ Stresses in Norway

It is common to express the relationship between the horizontal and vertical stress by a factor K (Myrvang, 2002):

$$\sigma_H = K \cdot \sigma_v \tag{2.4}$$

Collection of in situ stress data has shown that in most parts of Norway, the major horizontal stress is greater than the vertical stress. K is therefore often > 1 and lager than what Equation 2.3 in Section 2.2.1 indicates (Myrvang, 2002). According to Fejerskov (1996) and Myrvang

(2002), ridge push from the mid-Atlantic plate spreading is the primary source for tectonic stress in Norway. It is also likely the main reason for the high horizontal stresses in Norway (Fejerskov, 1996). See Section 2.2.2 and Figure 2.4 for explanation of the ridge push effect.

In reference to σ_H orientations, some trends have been identified in the Norwegian region. Data from northern Norway and the Barents Sea mainly have a N–S orientation. In mid-Norway and the Norwegian Sea, σ_H is more rotated toward WNW–ESE direction. The dominating trend in western Norway and northern North Sea is WNW–ESE with a secondary trend of NNE–SSW orientation. The rotation from N–S to WNW–ESE orientation is could be caused by the ridge push from the mid-Atlantic plate spreading, but other factors may contribute (Fejerskov et al., 2000). Figure 2.9 shows the direction of σ_H in Norway. σ_H stress trends will be discussed in more detail in Section 5.2.

On regional scale, research has shown that the stresses to some degree are affected by the unloading due to deglaciation, and by the post-glacial uplift of the land (Bungum et al., 2010). The σ_H orientation along the coastal areas in mid and western Norway coincide with deglaciation models. In these ares the stresses act perpendicular to the coast (can be seen in Fejerskov and Lindholm (2000) stress map in Figure A.4) (Fejerskov and Lindholm, 2000). However, according to Fejerskov and Lindholm (2000) the effect of deglaciation is small compared to other mechanisms. Sediment loading is expected to affect the stresses on the continental shelf, but the effect has been difficult to determine since it acts in the same direction as the ridge effect (Fejerskov, 1996). Whereas topography has been found to affect the stress fields on local scale in areas with mountains and fjords or valleys (Myrvang, 2001). The stresses will be reoriented to align with the fjords or valleys (Fejerskov et al., 2000). In Figure 2.9 it can be seen that direction of σ_H is parallel with the Caledonian mountain range.

Lithology has also shown to affect the in situ stress field in Norway. There have been measured exceptionally high horizontal stresses in Precambrian rocks, and in igneous Permian rocks (Myrvang, 1996). About 50 % of mainland Norway is composed of rocks of Precambrian age (older than 540 Million years (MA)), mainly gneiss and granite. Around 2 % is of Permian age (around 250 MA old) located around Oslo. The Permian rocks mainly originate from rift development and are therefore mainly igneous (Nilsen and Broch, 2012). See Appendix A.3 for geological timescale.

Caledonian rocks of Cambrian-Silurian age (540-420 MA) generally show lower stresses than average (Myrvang, 2001). According to Myrvang (2001), the higher degree of jointing of the Caledonian rocks compared with the Precambrian rocks is most likely the reason for this. The Caledonian mountain range was formed when two tectonic plates collided in the Cambrian-Silurian period. Around 30 % of the bedrock is of Cambrian-Silurian age. The areas of Cambrian-Silurian rocks mainly consist of metamorphic rocks that are a part of the Caledonian mountain range, but there also exist some sedimentary rocks around Oslo (Nilsen and Broch, 2012). However, that rocks of Cambrian-Silurian age show lower stresses is not always the case as there have been recorded high stresses in Caledonian rocks (Myrvang, 2001). Areas composed of Precambrian, Permian and Cambrium-Silurian rocks are indicated in Figure 2.9.

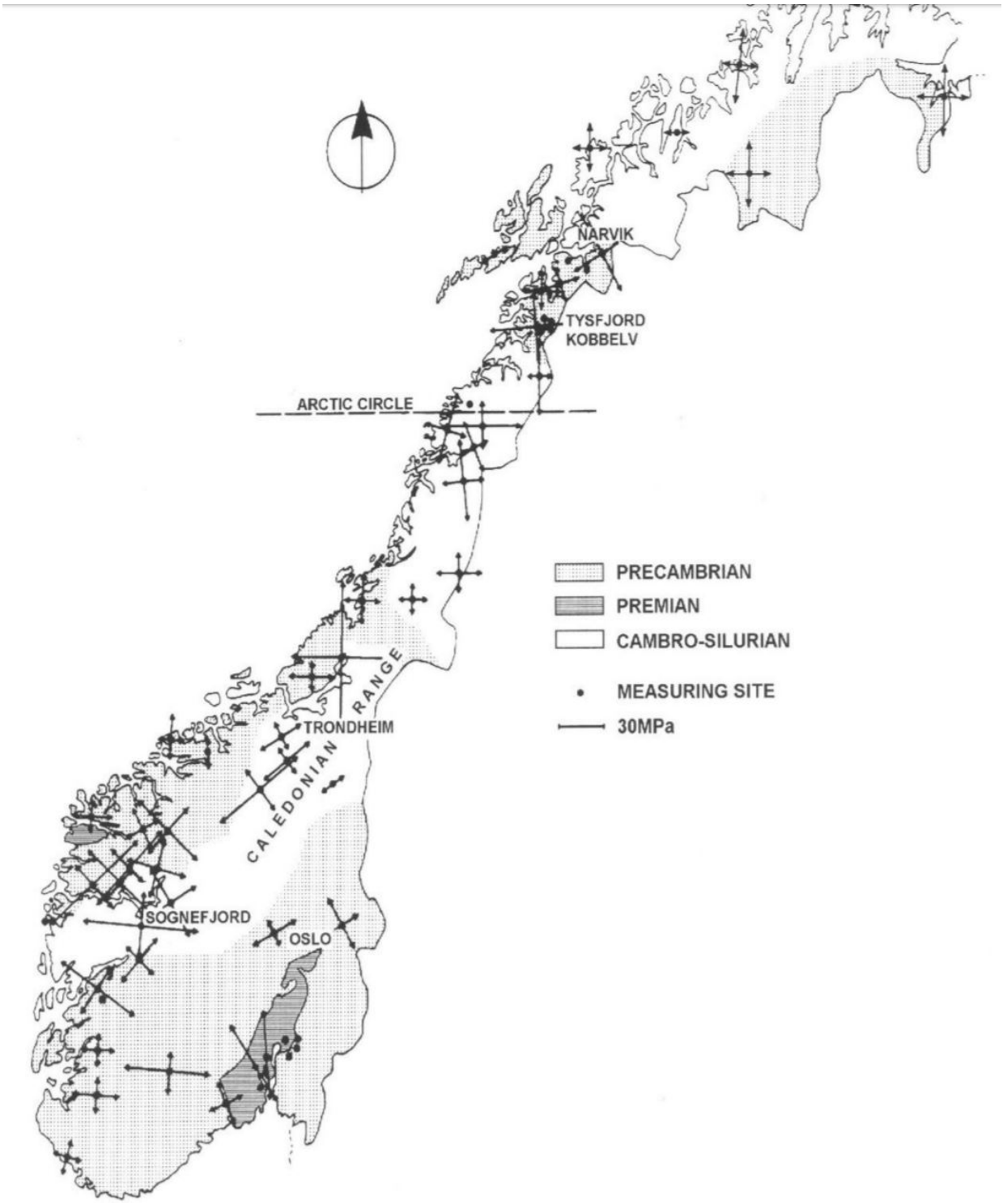

Figure 2.9: Direction of the horizontal in situ stresses in Norway (Myrvang, 1996).

Chapter 3

Stress Determination Methods

There exist a variety of different methods developed to analyse the in situ rock stresses. The stress determination methods can be divided in two main categories; measurement methods and estimation methods (Harrison and Hudson, 2000). Stress measurement methods disturb the in situ conditions by inducing strain, deformation or open fractures, whereas the estimation methods observe rock mass behaviour without disruptions (Ljunggren et al., 2003). It is difficult to determine in situ stresses exactly due to uncertainly related to rock mass parameters, and it is therefore common to present in situ stress data with a range or a confidence interval (Amadei and Stephansson, 1997).

Based on data from the FRSDB, the WSM and the work of Fejerskov (1996) and Hanssen (1997), it is likely that the data collected will be obtained with either overcoring methods, hydraulic methods, estimation methods in boreholes or the focal mechanism method. This chapter will therefore present these methods. Theory, test procedure and strengths/weaknesses for each method will be discussed. At the end of the chapter there is a comparison of the methods presented.

3.1 Overcoring Methods

Overcoring methods are measurement methods that isolate rock cores from the rock mass to destress the cores and monitor the responses. To obtain accurate results from overcoring, it

is important conduct measurements outside the influence zone of the underground opening. This is usually at a distance at least 1.5 times the diameter of the opening (Myrvang, 1996). The most used overcoring methods are the Doorstopper method, overcoring with the US Bureau of Mines (USBM) gauge, overcoring with the Council for Scientific and Industrial Research (CSIR) triaxial strain cell and overcoring with the Commonwealth Scientific and Industrial Research Organization (CSIRO) Hollow Inclusion (HI) cell (Amadei and Stephansson, 1997). These methods will be presented in this section.

Common for each of these methods, is the use of strain gauges. A strain gauge is a device with four metallic strips that are attached to a thin layer of paper or plastic (Myrvang, 2001). The metallic strips in the strain gauge are glued directly to the rock sample. When the test section is overcored, stress is relieved which causes elastic strain of the rock sample. The strips are stretched and this changes their electrical resistance. The elastic strain is linearly related to the change in electrical resistance (Li, 2015)

3.1.1 Two-dimensional overcoring

Two-dimensional (2D) overcoring methods allow determination of principal stresses in the plane perpendicular to the borehole axis, when the orientations of the principal stresses are known or can be assumed (Leeman, 1969). Knowledge of stress orientations is essential since stress along the borehole will affect measurement results. The method is therefore mainly carried out at locations where it can be assumed that the stress parallel with the borehole axis is small or zero. This usually involves vertical boreholes close to the tunnel surface or horizontal holes in vertical pillars (Ljunggren et al., 2003).

Even though 2D overcoring is developed to determine principal stresses perpendicular to the borehole, it is possible to find the complete three-dimensional stress field. This is done by carrying out measurements in three different holes at an angle from one another (Leeman, 1969; Amadei and Stephansson, 1997).

The Doorstopper method

The Doorstopper method was first described in South Africa by E. R. Leeman in 1964, and is named after the cell that is used (Amadei and Stephansson, 1997). The method utilises strain relief at the bottom of a borehole to find the in situ stress state (Leeman, 1969). The CSIR Doorstoppe cell consists of a cylindrical silicon rubber plug with a strain gauge rosette attached to the bottom of the plug (Jaeger et al., 2007). A strain gauge rosette is a multi-direction strain gauge consisting of either three or four singe strain gauges at an angle from one another (Li, 2015). The strain gauge configuration in the Doorstopper cell applied by The Foundation of Technical and Scientific Research (SINTEF) at NTNU is shown in Figure 3.1a. Figure 3.1b shows a photo of a Doorstopper cell in use by SINTEF in November 2017.

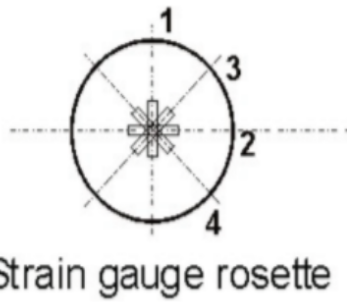

(a) Strain gauge rosette (SINTEF, 2014).

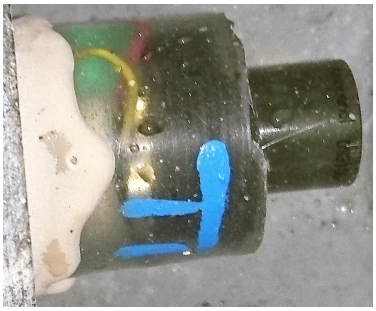

(b) Doorstopper cell in profile.

Figure 3.1: Doorstopper cell applied by SINTEF.

Figure 3.2 shows the installation and test procedure as applied by SINTEF. First a hole is drilled to a wanted depth and the bottom of the hole is flattened. The Doorstopper cell is glued to the bottom of the hole with installation tool. The first strain reading is carried out. The borehole is then overcored with a larger diameter. This relieve the stresses at the end of the borehole. The core is broken off with the Doorstopper cell still attached to the core and the second strain recording is done (SINTEF, 2014).

When the elastic properties E-modulus and ν of the rock are known, the secondary principal stresses in the borehole can be found by using Hooke's law for 2D state (Equation A.5 in Appendix A.2.1). In the calculations, it is assumed continuous, homogeneous, isotropic and linear-elastic rock behaviour (Sjöberg et al., 2003). To find the in situ stresses, the values obtained from Equation A.5 have to be adjusted with correction factors (Li, 2015).

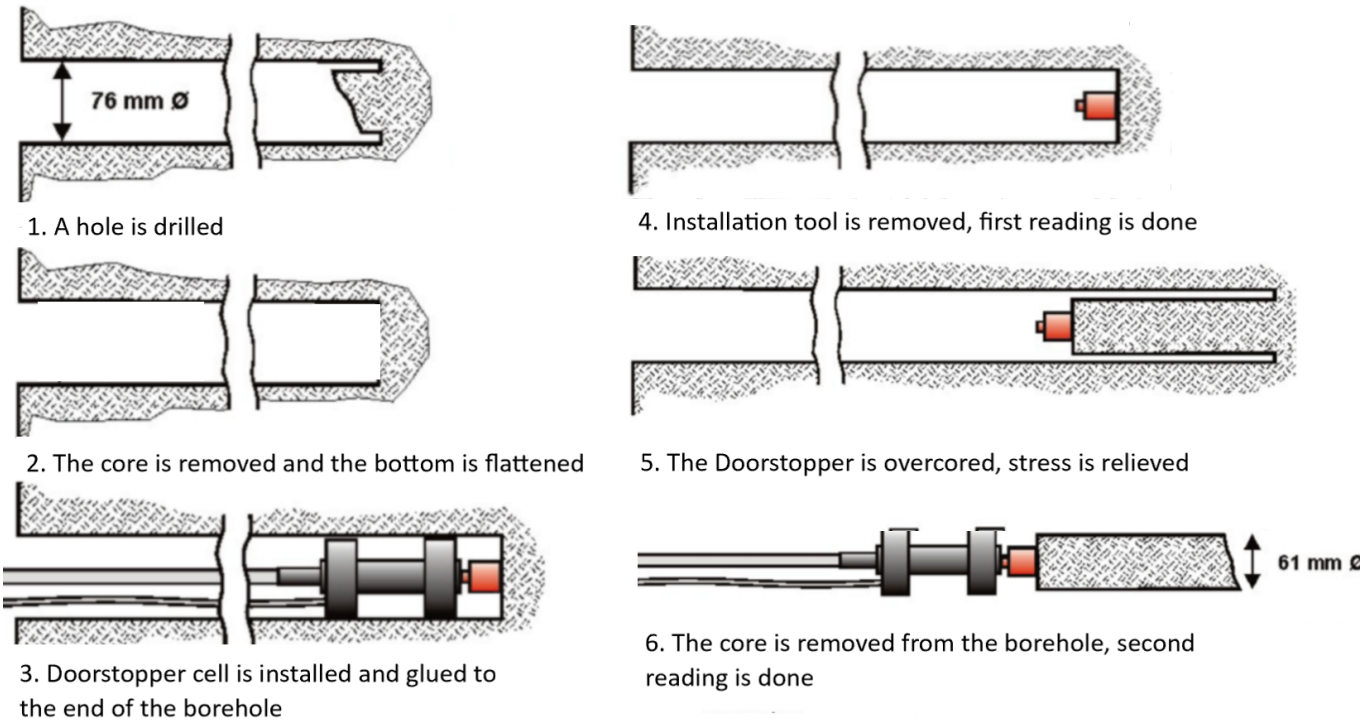

Figure 3.2: 2D Doorstopper overcoring procedure as applied by SINTEF. Modified after SINTEF (2014).

Overcoring with USBM gage

The 2D overcoring method with the US Bureau of Mines (USBM) gauge was developed at the USBM in the 1960s and is widely used, especially in The US and Canada (Myrvang, 2001; Ljunggren et al., 2003). In opposition to the Doorstopper method, this method measures change in the pilot hole diameter rather than elastic strain of the rock core (Ljunggren et al., 2003). The USBM gauge is a cylindrical deformation meter (Ljunggren et al., 2003). It is of stainless steel with three pistons equally spaced around its circumference. The pistons are connected to three cantilevers inside the gauge (Jaeger et al., 2007). There are four strain gauges glued to each cantilever, which is illustrated to the right in Figure 3.3 (Myrvang, 2001). To the left in Figure 3.3, there is an illustration of a modern version of the USBM gauge.

Figure 3.4 shows the overcoring procedure with the USBM gauge. First a hole is drilled, then a pilot hole of roughly the same diameter as the gauge is drilled further in. The gauge is inserted into the pilot hole. The pistons are tensioned to make good contact with the hole wall. The pilot hole is then overcored with a larger diameter to a depth of at least one overcore diame-

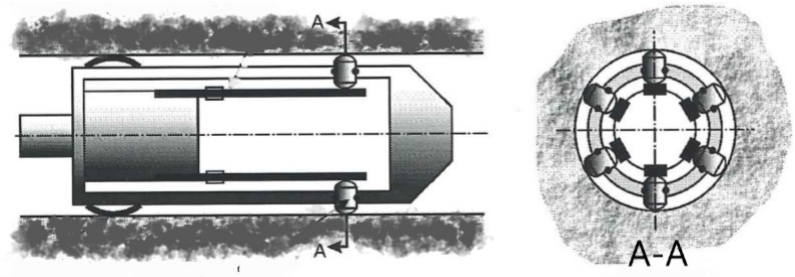

Figure 3.3: USBM cell, cross section to left and profile to right. Modified after Myrvang (2001).

ter past the gauge. This relieves an area around the gauge of stress and this creates change in the pilot hole diameter. The radial deformation of the pilot hole is measured in three directions with the strain gauges attached to the cantilevers (Jaeger et al., 2007). The diametrical change that is measured is related to the secondary principal stresses through the Equations in Appendix A.2.2.

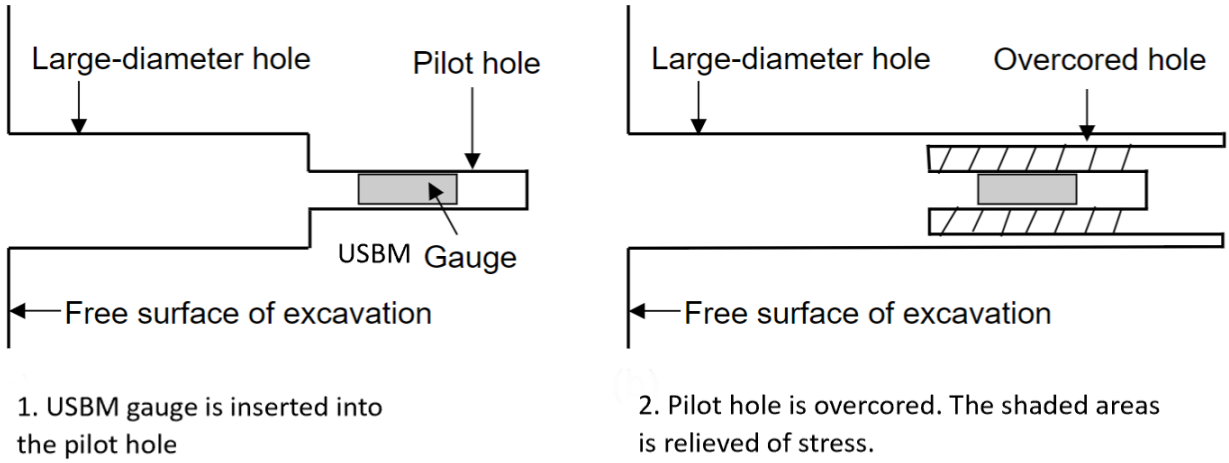

Figure 3.4: Overcoring with SBM gauge. First the gauge is insterted in the piolt hole, then the hole is overcored and the shaded area is relieved of stress. Modified after Jaeger et al. (2007).

3.1.2 Three-dimensional overcoring

Three-dimensional (3D) overcoring allows the complete 3D stress state to be determined from one borehole only (Amadei and Stephansson, 1997). As mentioned in Section 2.1.1, six independent components are required to describe a stress field in three dimensions. Consequently, at least six measurements are required to determine the stress field. To get enough measurements, three strain gauge rosettes are commonly used in 3D overcoring methods.

Three strain gauge rosettes will give a total of nine or twelve strain gauges, depending on the number of strain gauges in the rosettes. If the rock sample is anisotropic, the extra readings can be used to incorporate anisotropy in the results (Harrison and Hudson, 2000).

Stress can be calculated from strain after Hooke's law when the elastic properties (E-modulus and ν) of the rock are known (SINTEF, 2014). In the calculations, it is assumed continuous, homogeneous, isotropic and linear-elastic rock behaviour (Sjöberg et al., 2003). The hollow rock core with the measuring cell inside is broken off after overcoring. The elastic parameters of the rock can be determined from testing of this core with the measuring cell inside. This can be done by loading of the core or by biaxial testing. Attachment between the strain gauges and the rock core will then also be tested. An alternative is to test the solid rock core from the main borehole (Li, 2015). With 3D overcoring, there will occur some scatter even under seemingly ideal conditions because the measuring cells are sensitive to grain size, isotropy and homogeneity of the rock mass (Ljunggren et al., 2003; Amadei and Stephansson, 1997).

Overcoring with CSIR triaxial strain cell

Overcoring with the South African CSIR triaxial strain cell, also known as the Leeman cell, was first introduced in 1969 and was developed to determine the stress state from one borehole (Leeman, 1969). The measuring procedure with the with CSIR triaxial strain cell is similar to overcoring with the USBM gauge. The instrument is installed in a pilot hole that later is overcored (Ljunggren et al., 2003). However, like the Doorstopper method, it is elastic strain that is measured. For the standard CSIR triaxial cell, strain is measured before and after overcoring, but there are developed versions of the cell that allow continuous monitoring of the strain gauges (Amadei and Stephansson, 1997). Two modified versions of the CSIR triaxial cell will be presented in this subsection.

NTNU/SINTEF triaxial cell

The NTNU/SINTEF, formerly known as the Norwegian Institute of Technology (NTH) cell, is a modified version of the CSIR triaxial cell that is in regular use by SINTEF at NTNU. The cell is made of plastic and has three pistons with strain gauge rosettes attached. Each rosette is composed of three strain gauges (Hanssen, 1997). The strain gauge configuration and illustration

of the NTNU/SINTEF cell are shown in Figure 3.5. For this cell, measurements are commonly done down to depths of 18 m from the tunnel surface in horizontal holes (Larsen, 2017).

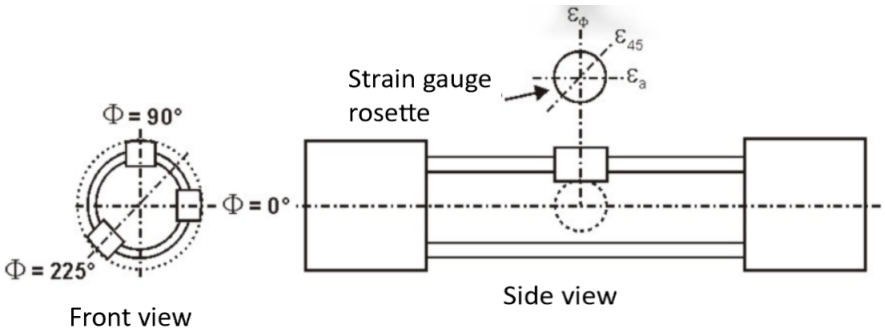

Figure 3.5: Strain gauge rosette configuration and an illustration of the NTNU/SINTEF cell. Modified after SINTEF (2014).

Figure 3.6 shows installation and the overcoring procedure for the NTNU/SINTEF cell. For this cell, strain is measured before and after overcoring like for the standard CSIR triaxial strain cell. SINTEF uses a computer program called Determination of In-Situ Stress by Overcoring (DISO) to determine the in situ stress from the measured strains. DISO provides a statistical analysis of the data and removes possible sources of error (SINTEF, 2014).

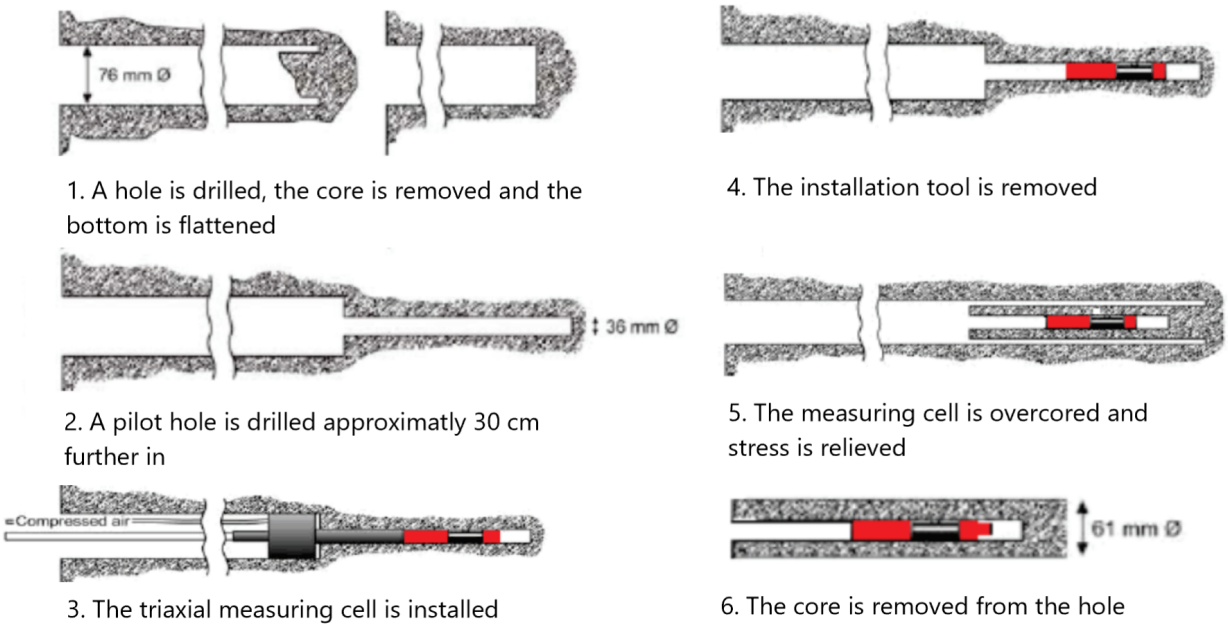

Figure 3.6: 3D overcoring as with the NTNU/SINTEF cell as applied by SINTEF. Modified after SINTEF (2014).

Borre (SSPB) probe

The Swedish State Power Board (SSPB) cell, currently known as the Borre probe, is a modified version of the CSIR triaxial cell that is suitable for deep boreholes. The probe permits measurements down to more than 500 m in water-filled boreholes. It has also been tested down to depths of 1000 m (Amadei and Stephansson, 1997). The cell is cylindrical with a length of around 55 cm. The probe has a total of nine strain gauges spread over three strain rosettes that are connected to three plastic cantilever arms. The strain gauge configuration is illustrated to the left in Figure 3.7. To the right in Figure 3.7, there is a photo of the Borre probe. The cell is recoverable, but the strain gauges are glued to the borehole wall and have to be changed for each measurement (Sjöberg and Klasson, 2003).

Figure 3.7: Strain gauge rosette configuration and a photo of the Borre probe. Modified after Sjöberg et al. (2003).

Figure 3.8 shows installation and the overcoring procedure for the Borre Probe. From the Figure it can be seen that only the outer part of the probe is inserted into the pilot hole. This is the part with the strain gauges and the plastic cantilevers. A mechanical latch is triggered by the contact with the base of the main borehole (point 4 in Figure 3.8), which pushes the protective cone further into the hole (point 5). The pressure from the nose cone presses the cantilevers and strain gauges against the borehole wall (Sjöberg and Klasson, 2003). The Borre probe includes a built-in data logger that allows continuous monitoring of the strain gauges during testing (Ljunggren et al., 2003).

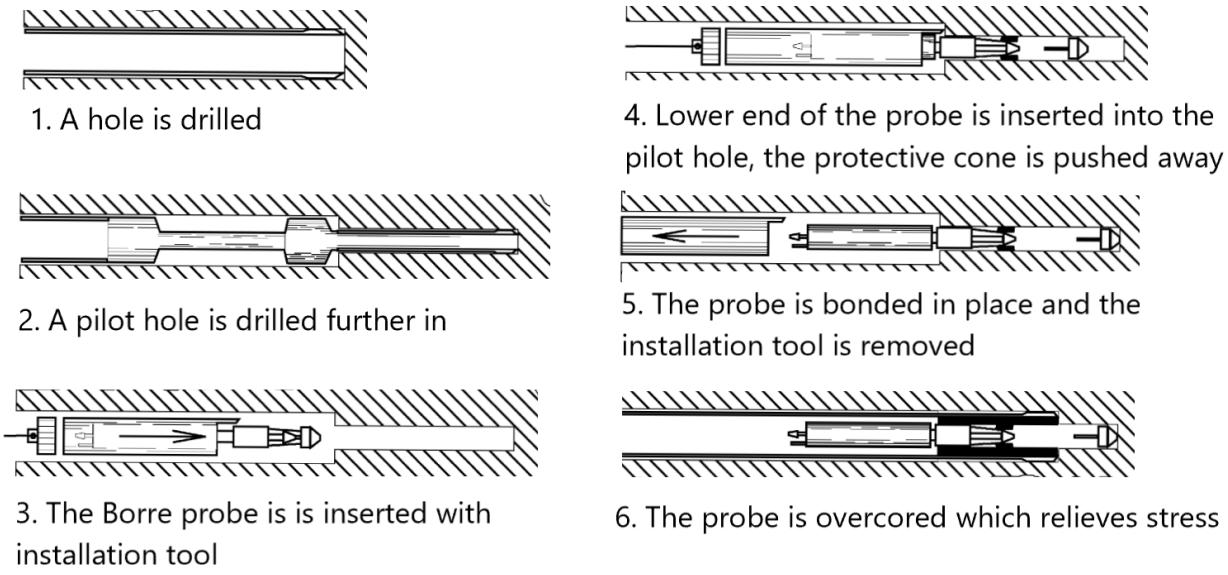

Figure 3.8: Installation and overcoring procedure for the Borre (SSPB) probe. Modified after Sjöberg et al. (2003).

Overcoring with CSIRO HI cell

Overcoring with the Commonwealth Scientific and Industrial Research Organization (CSIRO) Hollow Inclusion (HI) cell was first introduced in Australia in the early 1970s. It is therefore the newest overcoring method presented in Section 3.1, and it combines features of the USBM gauge and the CSIR triaxial cell (Worotnicki, 1993). The cell is much used around the world (Myrvang, 2001).

The CSIRO HI cell is made up of an epoxy, plastic pipe and a hollow, metallic end piece and has a total length of 9 cm. The plastic pipe consists of two layers where the outer layer is pushed away during overcoring. Strain gauge rosettes with either three or four strain gauges are used and are attached to the inner surface of the outer layer. This encapsulates the rosettes that protect them from drilling and groundwater. Configuration of the strain gauge rosette consisting of three strain gauges is illustrated to the left in Figure 3.9. To the right, there is a photo of the CSIRO HI cell. The cell has undergone modifications since its introduction, but the design has mostly remained the same (Worotnicki, 1993).

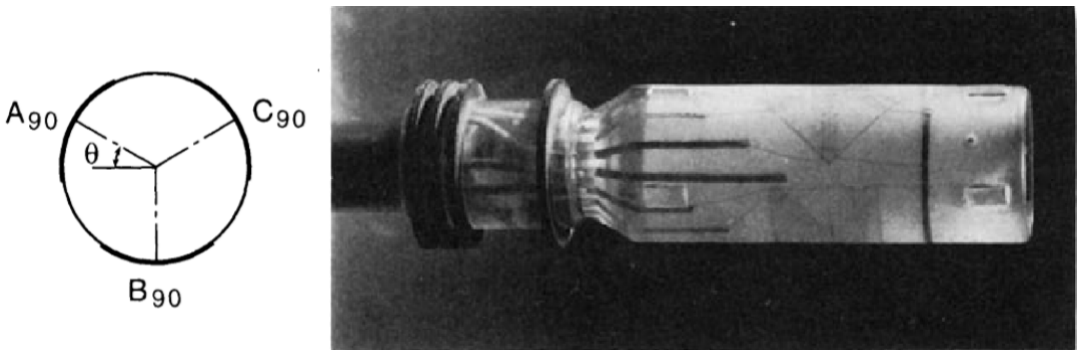

Figure 3.9: Strain gauge rosette configuration in the CSIRO HI cell and a photo the CSIRO HI cell. Modified after Hillis et al. (1999).

The test procedure is similar to overcoring with the USBM gauge and the CSIR cell, and is illustrated in Figure 3.10. When the CSIRO HI cell is installed, it is cemented with epoxy adhesive that is extruded by a piston and seals are used to confine the grout around the CSIRO HI cell. From the Figure it can be seen that the cell is permanently attached to the readout cable. This allows continuous observations of strain changes during the overcoring process (Amadei and Stephansson, 1997). The arrow shaped tool in the Figure is an orientation device (Worotnicki, 1993).

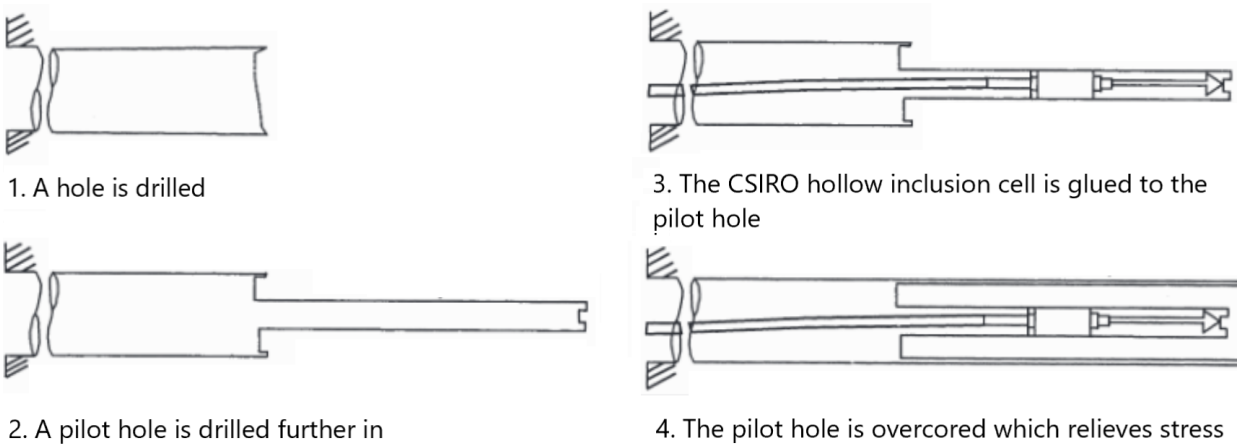

Figure 3.10: Installation and overcoring procedure for the CSIRO HI cell. Modified after Hillis et al. (1999).

3.1.3 Strengths and weaknesses

A great strength with the Doorstopper method, is that only a small piece of a intact core is required. This method is therefore suitable when it is difficult to obtain larger intact cores,

for instance in jointed rock mass or when core discing might occur. Core discing are fractures that develop perpendicular to the length axis of a rock core under high stress conditions (Ljunggren et al., 2003). The Doorstopper cell can also be used in longtime monitoring of stress changes (Li, 2015). Some advantages with the 2D USBM gauge, is that the gauge is recoverable and reusable, no cement or glue is required and it works under wet conditions. The USBM gauge can also provide continuous monitoring of strain changes (Amadei and Stephansson, 1997).

The biggest strength with the 3D overcoring methods, is that the 3D stress state can be determined from one single hole. In addition, the number of strain gauges (nine or twelve) permits least square estimate of the in situ stress field components. A strength with the CSIRO HI cell and some modified versions of the CSIR triaxial cell, is that they provide continuous monitoring during overcoring (Amadei and Stephansson, 1997).

One of the biggest weaknesses with the 2D overcoring methods is that three separate boreholes are required to determine the 3D stress field. Also, unlike the USBM gauge, the Doorstopper cell requires a flat hole bottom, glue to be installed and does not provide continuous monitoring of data (Amadei and Stephansson, 1997). A weakness with 3D overcoring is that it is more time-consuming than 2D overcoring. It takes about a day more to carry out measurements (SINTEF, 2014). In addition, for the CSIRO HI cell, the epoxy adhesive takes long time to cure and curing is difficult under wet or cool conditions (Amadei and Stephansson, 1997).

The 3D overcoring methods and 2D overcoring with the USBM gauge require rock mass with a low degree of jointing due to the overcoring lengths. These methods are therefore inapplicable under high rock stress conditions that can initiate core discing (Ljunggren et al., 2003). Another weakness with these cells, is that they often produce scattered results since they are sensitive to grain size, anisotropy and heterogeneity of the rock mass. The CSIRO HI cell is however less influenced by rock mass heterogeneity and grain size than the CSIR triaxial cells, but it is about twice as expensive (Amadei and Stephansson, 1997).

3.2 Hydraulic Methods

The concept of hydraulic stress determination methods is to induce fractures, or reopen existing fractures, in borehole walls to measure stress. These methods are therefore categorised as measurement methods (Amadei and Stephansson, 1997). Just as for overcoring, it is important conduct measurements outside the influence zone of the underground opening to obtain as accurate results as possible (a least 1.5 times the diameter of the opening) (Myrvang, 1996). According to Amadei and Stephansson (1997, 121), there are three main types of hydraulic measurement methods: hydraulic fracturing, sleeve fracturing and hydraulic testing of hydraulic testing of pre-existing fractures (HTPF). Hydraulic fracturing and HTPF will be presented in this section.

3.2.1 Hydraulic fracturing

Hydraulic fracturing is a 2D method where the stresses perpendicular to the borehole axis are considered (Ljunggren, 1990). The method was first applied in the oil industry in the 1940s to improve productivity in formations with low permeability. Hydraulic fracturing is carried out by injecting fluid into a sealed-off, fracture free section of a borehole to create fractures in the walls. These fractures are initiated when the rock mass fails in tension, which happens when the tensile stress at the borehole wall exceeds the tensile strength of the rock mass (Ljunggren et al., 2003).

The orientations of the fractures are related to the in situ stress field because the fractures will initiate at the points in the borehole that offer least resistance (Ljunggren et al., 2003). From Kirch's Equations and Figure A.2.3 (see Appendix A.2.3), it is evident that this will be in the direction parallel with the major principal stress perpendicular to the borehole axis. Kirch's Equations describe stress distribution around a circular opening in an isotropic rock mass (Li, 2015). Figure 3.11 illustrates tensile fractures developing around a borehole where the principal stresses are in the vertical and horizontal planes.

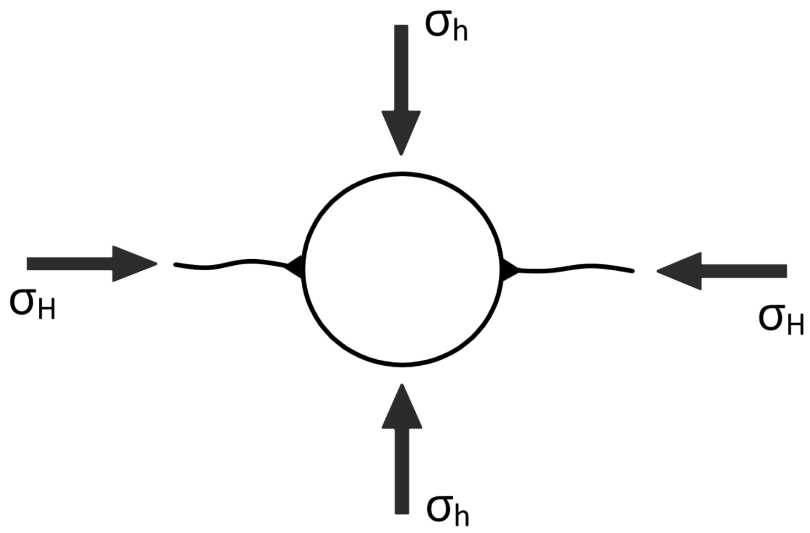

Figure 3.11: Tensile failure fractures developing around a vertical borehole with principal stresses in the vertical and horizontal planes.

Hydraulic fracturing is usually carried out with a saddle packer, a high-pressure turbine/drill pipe/hose and injection fluid. A saddle packer is an inflatable, double rubber packer system that is used to isolate the borehole test interval. It is important that the packer pressure is higher than the pressure in the test section. The high-pressure turbine, drill pipe or hose is used to convey hydraulic fluid downhole to the saddle packer. A pump system is used to inject fluid into the test section. The system is normally located at the surface, but for deep tests it can be fixed on the saddle packer (Haimson and Cornet, 2003). The hydraulic fracturing test set-up is illustrated to the left in Figure 3.12.

To inspect the borehole, an impression packer together with a magnetic compass is normally used. An impression packer is an inflatable packer with an outer layer of soft rubber. The packer creates an impression of the borehole wall when it is inflated in the test section (Haimson and Cornet, 2003). The impression test set-up is illustrated to the right in Figure 3.12. Alternatively, a borehole televiewer or a micro-scanner can be used (Ljunggren et al., 2003). To measure fluid and packer pressure, pressure transducers are used. A flowmeter is used to measure flow with time (Haimson and Cornet, 2003). There is an example of typical pressure and fracture versus time curves during testing in Figure 3.13.

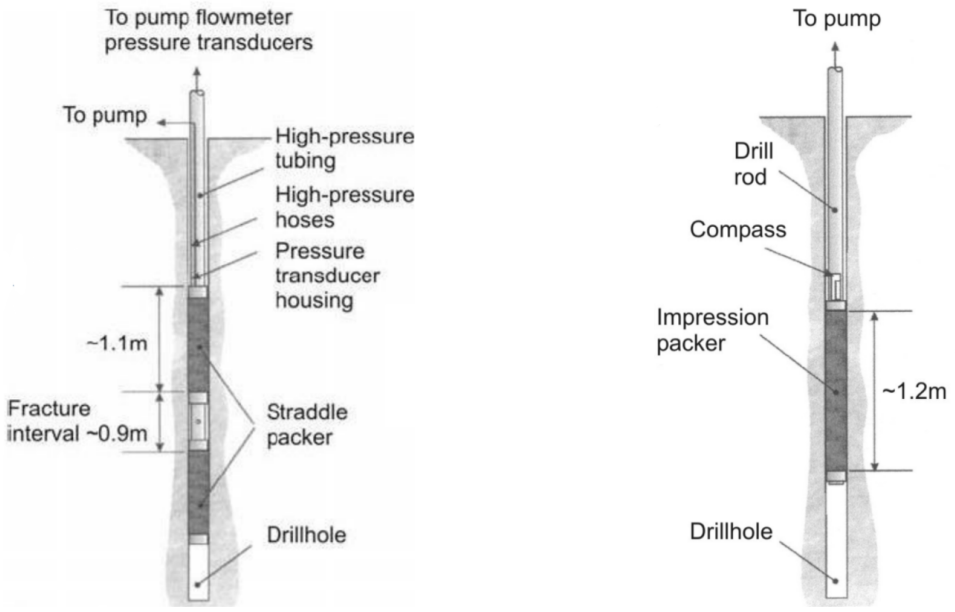

Figure 3.12: Saddle packer arrangement to the left and impression packer arrangement to the right. Modified after SINTEF (2014).

According to SINTEF (2014), hydraulic fracturing can be carried out both from the surface and from underground holes in tunnels. The orientation of the borehole should be parallel with σ_1 or σ_2, and it is important that the test section is free from fractures (Myrvang, 2002). SINTEF can perform hydraulic fracturing measurements down to a depth of 300 m in vertical holes (Larsen, 2017). The recommended test procedure is as follows (Haimson and Cornet, 2003):

1. A hole is drilled and a section of the borehole is sealed-off with a saddle packer. Hydraulic fluid, usually water, is injected into this section at a constant rate.

2. The interval pressures is increased until the rock mass fails in tension and fractures develop. The pressure level at this stage is called "the breakdown pressure"- P_b in Figure 3.13.

3. The pumping is stopped, but the test section is not vented. This causes a decrease in pressure, but the fractures will propagate further for a while.

4. At a certain pressure level, the stresses normal to the fractures plane will close the fractures. This pressure point is called the "shut-in pressure" - P_{si}, is indicated by P_s in Figure 3.13.

5. A few minutes after shut-in, normally 3–10 min, the hydraulic line is vented.

6. When the pore pressure has reached its original value (usually after a few minutes), the above pressurisation cycle should be repeated at least three times. The pressure required to reopen the fracture is measured - P_r in Figure 3.13.

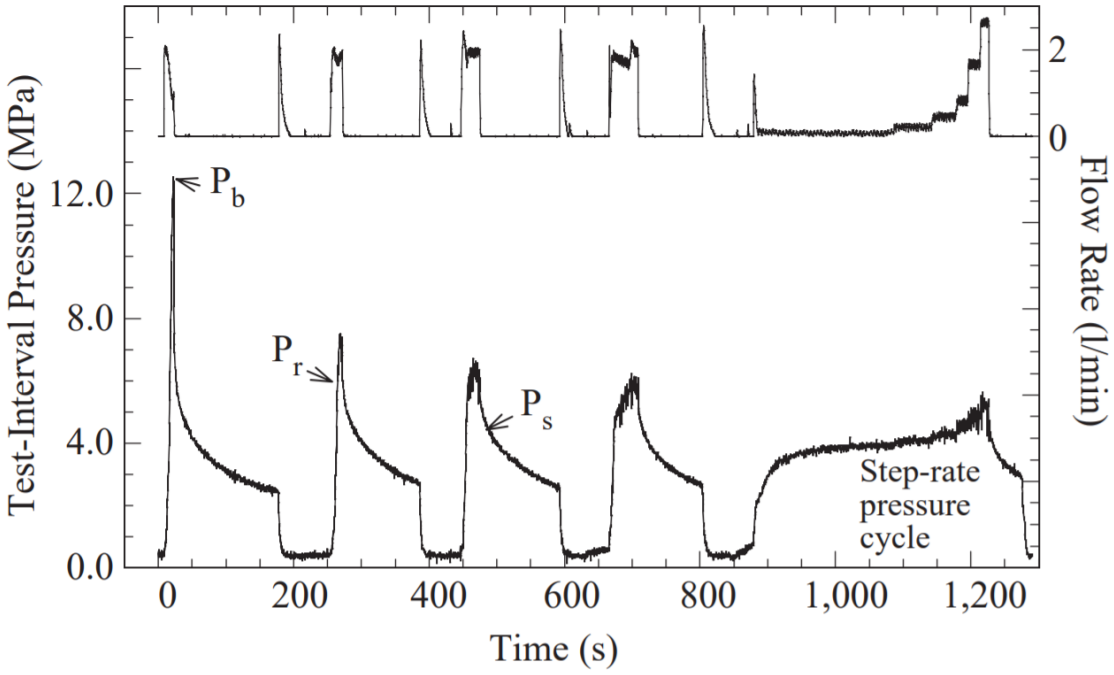

Figure 3.13: Pressure and flow rate versus time (Haimson and Cornet, 2003).

P_{si} should be measured for every cycle, and the lowest value for P_{si} will theoretically be equal to σ_3 when the borehole is located parallel with σ_1 or σ_2 (Li, 2015). In vertical boreholes where σ_V can be assumed to be σ_1 or σ_2, σ_3 will be equal to σ_h as illustrated in Figure 3.11. According to Jaeger et al. (2007), the magnitude of the major principal stress can be calculated from the following Equation:

$$\sigma_1 = \sigma_t + 3 \cdot \sigma_3 - P_b \tag{3.1}$$

Where σ_t = tensile strength of the rock, σ_3 = shut-in pressure and P_b = breakdown pressure.

The fractures have no tensile strength (Jaeger et al., 2007), so by using the reopening pressure P_r instead of P_b Equation 3.1 is reduced to:

$$\sigma_1 = 3 \cdot \sigma_3 - P_r \tag{3.2}$$

3.2.2 Hydraulic test on pre-exisiting fractures

The hydraulic testing of pre-existing fractures (HTPF) method was first introduced in 1986, and involves opening of existing fractures to measure the normal stress across them (Amadei and Stephansson, 1997). In comparison to hydraulic fracturing, HTPF is independent on borehole orientation and is 3D (Haimson and Cornet, 2003). The HTPF method involves testing on none-parallel pre-existing fractures to determine the complete stress tensor.

As mentioned in Section 2.1.1, six parameters are required to describe the 3D stress state. However, due to uncertainties related to measurements, at least eight tests should be carried out (Amadei and Stephansson, 1997). For each of these, it is important to only open one fracture and to know strike and dip angle of the fracture plane. Strike is the line of the fracture plane that represents the intersection with a horizontal plane, while dip is the angle of the fracture relative to the horizontal plane (Harrison and Hudson, 2000). These angles are found with the impression packer. The orientation should be different for each measured fracture (Haimson and Cornet, 2003).

The equipment used is the same as for the hydraulic fracturing method presented in Section 3.2.1 (Amadei and Stephansson, 1997). The test procedure is also similar to hydraulic fracturing, but the flow rate is kept lower to prevent initiation of new fractures (Haimson and Cornet, 2003). In addition, pressure is raised in a series of steps where the flow rate that maintain constant borehole pressure is measured for each step. The injection is stopped when the fracture is opened and the shut-in pressure P_{si} is recorded (Amadei and Stephansson, 1997). The procedure is repeated at least two times with step-wise pressurisation. After reaching the maximum flow rate, the pressure can also be decreased step-wise and this allows independent P_{si} determination (Haimson and Cornet, 2003). Figure 3.14 shows the the test principle for HTPF.

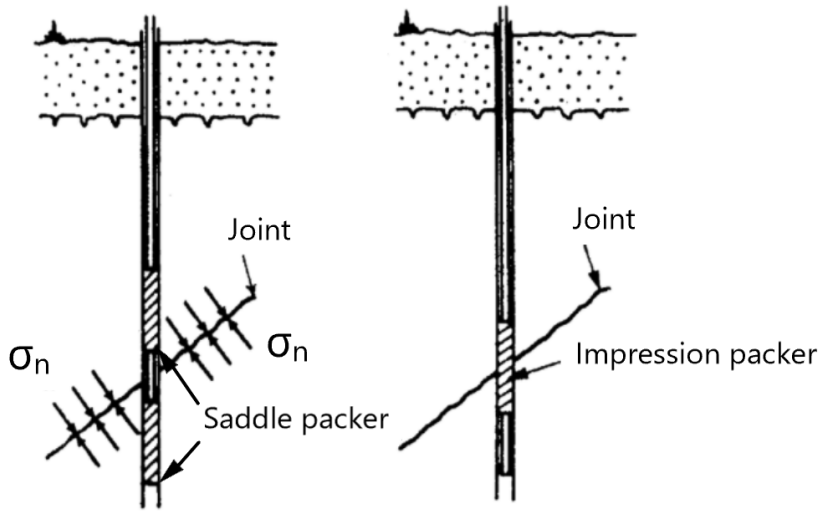

Figure 3.14: Test principle for HTPF. Modified after Ljunggren et al. (2003).

When carrying out HTPF, it is assumed that the fracture has a planar geometry and that the normal stress is uniform across the fracture's surface (Ljunggren et al., 2003). Both the breakdown P_b and the reopening P_r pressures are assumed to be measurements of the normal stress shown in Figure 3.14. The complete stress tensor is calculated from inversion of the normal stress results. When the borehole is in a principal stress direction, hydraulic fracturing and HTPF can be combined. When they are combined, only three–four tests with HTPF are required to complement the results from hydraulic fracturing (Haimson and Cornet, 2003).

3.2.3 Strengths and weaknesses

A strength with the hydraulic methods is that they, unlike the overcoring methods, measure stress directly and therefore do not require knowledge of the elastic rock properties (Jaeger et al., 2007). This eliminates possible error sources related to determination of the elastic properties, which improves their reliability. Another strength with the hydraulic methods, is that they can be done from the surface. The hydraulic methods are therefore applicable at early stages of excavation when no underground access is available (Amadei and Stephansson, 1997). An advantage with the hydraulic fracturing method is its accuracy of σ_3, which is ± 5 %. Advantages with the HTPF method include that the borehole does not need to be in a principal stress direction, that it is 3D and that it works under higher stress conditions than

hydraulic fracturing (Ljunggren et al., 2003).

A weakness with the hydraulic fracturing method, is the accuracy of the major principal stress magnitude perpendicular to the borehole axis, which is around $\pm 10 - 20$ % (Ljunggren et al., 2003). Another weakness is that the borehole has to be in a principal stress direction. If it is not, shear stress will act on the plane and P_{si} may not represent the minor principal stress (Haimson and Cornet, 2003). Hydraulic fracturing also requires rock mass of a certain quality to avoid opening existing fractures, so the borehole needs a few meters without fractures. The rock mass cannot be too fractured for HTPF either, since the method requires each measured fracture to be isolated (Amadei and Stephansson, 1997).

Other factors that affect measurement results for the hydraulic fracturing method, are geological structures and very high stresses. Geological structures may act as weakness planes and control the direction of the fractures, while very high stresses can make it difficult to fracture the rock mass. These factors will not have the same effect on the HTPF method. The HTPF method is on the other hand more time-consuming and more expensive than hydraulic fracturing (Ljunggren et al., 2003).

3.3 Estimation Methods in Boreholes

Estimation methods can be performed in existing boreholes, by analysis of rock cores related to core discing, analysis of geological structures or as focal mechanism. Core discing can only be used as an indicator for estimation and geological structures may have been formed when the in situ stress field was different than present the stress field (Ljunggren et al., 2003). This makes those methods questionable, and other estimation methods such as those preformed in boreholes and focal mechanism are usually preferred. This section will present boreholes borehole breakout analysis and drilling-induced-fractures (DIF)s, two methods that are performed in existing boreholes. Focal mechanism is presented in Section 3.4.

3.3.1 Borehole breakout analysis

Borehole breakouts are elongations of borehole cross sections that occurs under high stress concentration. When the compressive stress around a borehole is too high for the rock to sustain, spalling will occur in the borehole wall. Spalling occurs at the points of maximum compressive stress concentration, which will be at two diametrically opposed zones (Haimson and Herrick, 1986). These zones will elongate the borehole cross section and become borehole breakouts. The development of breakouts in a borehole is illustrated in Figure 3.15. Breakouts are found in almost every rock type and were first used for stress determination in 1964 (Amadei and Stephansson, 1997).

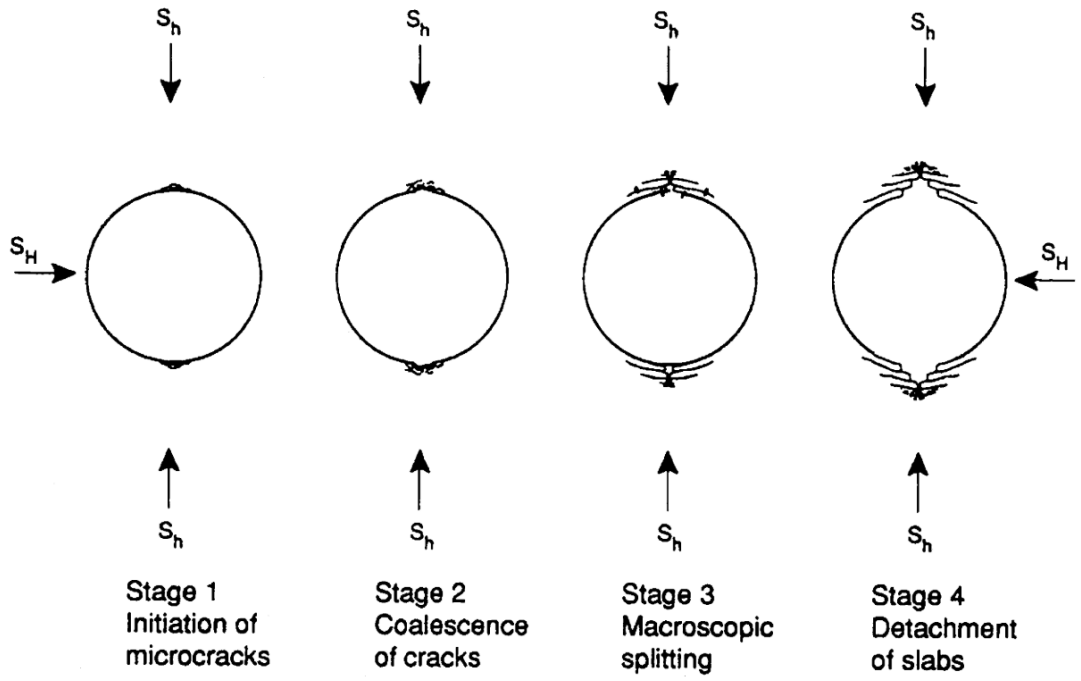

Figure 3.15: Borehole breakout development in a vertical borehole (Amadei and Stephansson, 1997).

The stress concentration in the borehole walls amplifies the difference between the principal stresses (Haimson and Herrick, 1986). In 1964, E. R. Leeman stated that the breakouts developed parallel to the minor principal stress in the plane perpendicular to the borehole axis (Amadei and Stephansson, 1997). This can be seen in Figure 3.15 where the principal stresses are in the vertical and horizontal planes. Since borehole breakouts occur at several 100 meters of depth (in Sweden, they are usually not found above a 1000 m depth), it is reasonable to

assume that σ_V, σ_H and σ_h are principal stresses (Ljunggren et al., 2003). As mentioned in Section 2.3.5, the principal stresses approach horizontal and vertical orientations with increasing overburden.

A camera, a dipmeter, an acoustic televiewer or an electric microscanner can be used to characterise breakouts. A dipmeter consists of pads that are pressed against the borehole wall to measure rock resistivity. An acoustic televiewer consists of a transducer that produces an ultrasonic acoustic pulse to provide an image of the wall. The electric microscanner consists of 16 electrode buttons and produces a high-resistivity image or map where the breakouts will appear as dark patches (Amadei and Stephansson, 1997).

Borehole breakout analysis is generally used as an indicator of principal stress orientations. Nevertheless, the width and depth of breakouts have been found to be related to the magnitude of the horizontal stresses in vertical boreholes. There have been developed approaches where magnitudes of these stresses are estimated from breakout geometry (Haimson and Herrick, 1986). However, both Amadei and Stephansson (1997) and Ljunggren et al. (2003) stated that this must be done with caution. Breakouts can be enlarged by other factors than stress, such as weathering of the borehole wall, intensity of the drilling, drilling method and by the diameter of the borehole (Amadei and Stephansson, 1997).

3.3.2 Drilling-induced-fractures

Another naturally occurring borehole failure type, is drilling-induced-fractures (DIF). These fractures occur when the stress concentration around a borehole goes into tension that exceeds the tensile strength of the rock. DIFs are narrow fractures like the fractures in Figure 3.11 and will, like in the Figure, develop parallel to the major horizontal stress in vertical boreholes (Zoback and Zoback, 2002). DIFs are identified in the same was as borehole breakouts with either a camera, a dipmeter, a televiewer or a microscanner (Ask et al., 2015).

DIFs can also be used to indicate if the borehole is located in a principal stress direction by looking at the orientation of the fractures. If the DIFs are almost parallel with the borehole axis, the borehole axis is parallel with a principal stress. However, if the DIFs are inclined towards the borehole axis, the borehole axis is not parallel with a principal stress (Ask et al.,

2015).

3.3.3 Strengths and weaknesses

There was not found much information about DIFs, so only strengths and weaknesses of borehole breakout analysis will be discussed. Borehole breakout analysis is a fairly quick method that provides reliable estimates of the minor principal stress orientation (Ljunggren et al., 2003; Amadei and Stephansson, 1997). In addition, borehole breakouts analysis provides data from depths of several kilometres where the measurement methods are inapplicable (Zoback and Zoback, 2002).

On the other hand, borehole breakout analysis is only applicable if breakout occurs. This can be a problem at shallow depths where the stresses often can be lower than the compressive strength of the rock mass. Borehole breakouts also require rock mass of a certain quality for the hole to not collapse. While anisotropic rock masses may disturb the breakout location, which will lead to incorrect results. Another weakness with borehole breakout analysis, is that it is mainly suitable for determination of stress orientation and not magnitudes (Ljunggren et al., 2003). It may also be difficult to separate borehole breakouts from other drilling related phenomena (Fejerskov et al., 2000).

3.4 Focal Mechanism

Earthquake focal mechanism, also called fault-plane solution (Amadei and Stephansson, 1997, 79), is an estimation method that utilises earthquake records to determine stress directions and relative stress magnitudes (Cronin, 2010). Earthquakes occur in regions that undergo deformation when accumulated strain exceeds the strength of the rock mass. The stress field that deformed that region can be analysed if enough seismographs recorded the earthquake (Lee and Stewart, 1981). The basic P-wave first motion method for fault-plane solution will be described in this section.

3.4.1 P-wave first motion

P-wave first motion is used to identify fault geometry, and fault geometry can be used to find stress directions and relative magnitudes. The fault geometry is determined by relative stress magnitude of the horizontal stresses with respect to the vertical stress (Stein and Pelayo, 1991). When an earthquake occurs, energy is partly released by vibration of seismic waves. The first seismic wave to reach the seismographs, is the P-wave (Lee and Stewart, 1981).

The first direction of motion of the vertical P-wave component is recorded by seismographs and is related to the direction of slip on the fault. If the first motion is upwards (left in Figure 3.16), it is an compressional P-wave and the fault is moving towards the seismograph. Whereas if the first motion is downwards (right in Figure 3.16), it is a dilatational P-wave and the fault is moving away from the seismograph. When the first motion is weak, it can often be difficult to determine direction of first motion (Cronin, 2010).

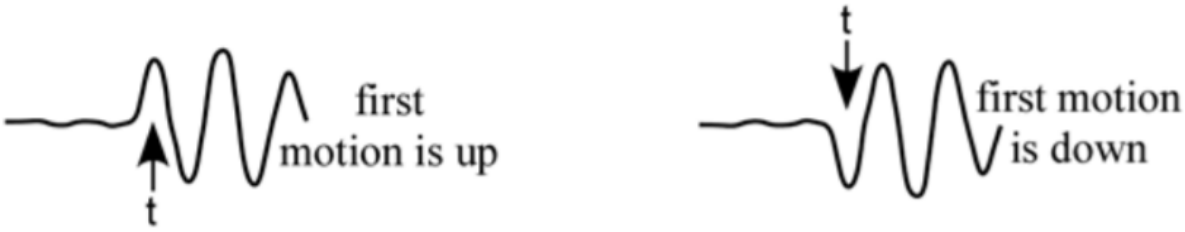

Figure 3.16: First motion of an earthquake is either up (left) or down (right) (Cronin, 2010).

The area surrounding the earthquake focus can be divided into four quadrants as illustrated in Figure 3.17. The colours of the quadrants indicate first motion of the P-wave. The black quadrants represent compression, while the white quadrants represent dilation. The quadrants are separated by two planes, which are called nodal planes (Yeats et al., 1997). Along the nodal planes, the P-wave motion is zero (Lee and Stewart, 1981). For the nodal planes to be located, seismographs at different locations must record first motion (Yeats et al., 1997).

One of the nodal planes will be the fault plane that generated the earthquake (in Figure 3.17, the horizontal plane is the fault plane), but field observations are required to determine which one (Cronin, 2010). However, there will only be one unique pair of σ_1–σ_3 for the two nodal planes. The pressure axis will be in the white quadrants, and the tension axis will be located in the black quadrant. These axes will be approximately 45° from the nodal planes, and are equal

σ_1 and σ_3. σ_2 will be located perpendicular to the nodal planes (Yeats et al., 1997).

Since faulting geometry is related to the horizontal stress magnitudes in relation to the vertical stress magnitude, relative magnitude of the three stresses can be found (see Figure 1.2 and Table 4.1). As discussed in Section 2.1.1, the principal stresses in the Earth's crust will approach horizontal and vertical orientation with increasing depth. The principal stresses will therefore most likely be σ_V, σ_H and σ_h for focal mechanism data that is applicable at about depth from 5 to 50 km (Stein and Pelayo, 1991; Zoback and Zoback, 2002). The relative magnitude between the principal stresses can therefore be found with focal mechanism.

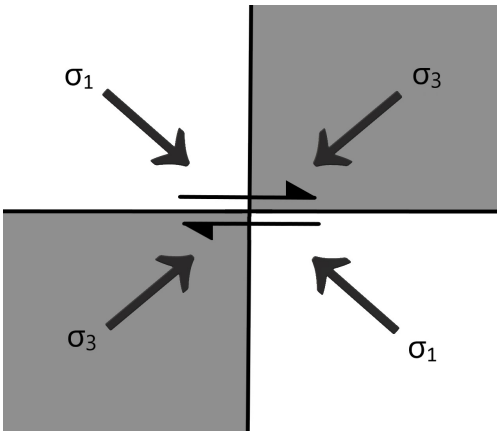

Figure 3.17: Quadrants and nodal planes around an earthquake focus. Horizontal plane = fault plane.

Beachball diagram

A common way to represent focal mechanism, is by beachball diagrams. A beachball diagram is a projection on lower-hemisphere stereographs that shows the four quadrants around an earthquake centre in black and white, separated by the nodal planes. The beachball diagrams for the main fault types are presented in Figure 3.18. From the Figure it can be seen that only three of the quadrants are be visible for normal and reverse faulting, which are pure dip-slip. It is also clear from the Figure that Figure 3.17 shows a strike-slip fault (Cronin, 2010).

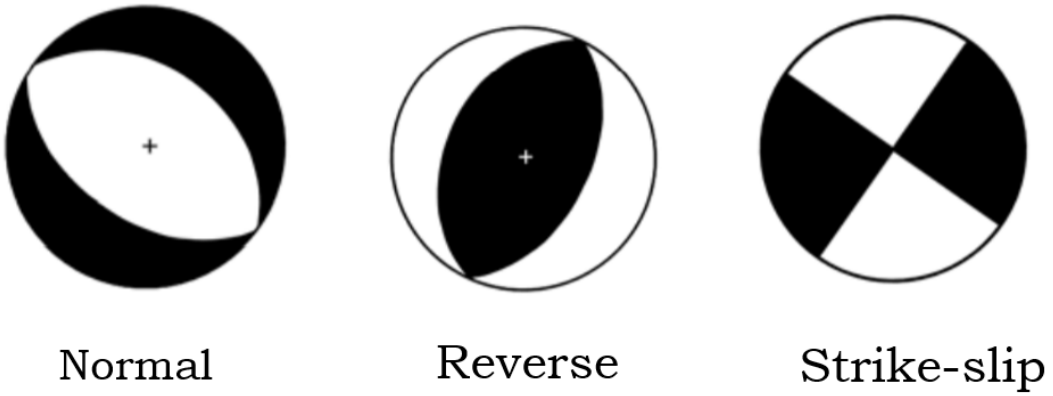

Figure 3.18: Beachball diagram presentation of the main fault types. Black represents compression and white represents dilation. Modified after Cronin (2010).

3.4.2 Strengths and weaknesses

A major strength with the focal mechanism method, it that it provides data from mid crustal depths from about 5–50 km, which no other stress determination method does (Ljunggren et al., 2003). Another strength, is that focal mechanism can be used to determine relative stress magnitude from fault geometry (Stein and Pelayo, 1991).

On the other hand, the focal mechanism method does not provide information about absolute stress magnitudes (Ljunggren et al., 2003). Another weakness with focal mechanism, is that stress directions can reflect the orientation of a weakness plane rather than the regional stresses. This happens when earthquake occurs along a pre-existing fault (Stein and Pelayo, 1991). σ_1 and σ_3 will then not have the same orientation as the tension and pressure axis, which is assumed in the p-wave first motion method (Amadei and Stephansson, 1997). The first motion observation may also be in wrong quadrant due to either wrongful assignment by the algorithm or wrongful location of the earthquake (Li, 2015).

3.5 Comparison of the Methods

Table 3.1 presents a comparison of the stress determination methods presented in this chapter. Due to the limited information about DIF, this method is excluded from Table 3.1.

The crosses in parenthesis in Table 3.1 symbolise that the statement is true under certain conditions. As described in Section 3.1.1, 2D overcoring can be used to find the 3D stress field if carried out in a special way. Hydraulic fracturing has been performed down to depths of 5000 m (Myrvang, 2001), but SINTEF only performs measurements to about 300 m (Larsen, 2017). HTPF requires a jointed rock mass, but as mentioned in Section 3.2.3 the rock mass cannot be too jointed. While the CSIR triaxial cell does generally not provide continuously monitoring of data or testing in wet boreholes, but some of the modified versions like the Borre probe do (Myrvang, 2001).

Table 3.1: **Comparison of different stress determination methods**. Doorstopper = the Doorstopper method, USBM = overcoring with the USBM gauge, CSIR triaxial = overcoring with the trxiaxial CSIR cell, HF = hydraulic fracturing, HTPF = hydraulic test of pre-existing fracture, BO = borehole breakout analysis and FM = focal mechanism. (x) = true under certain conditions.

Description		**Method**							
		Doorstopper	USBM	CSIR triaxial	CSIRO HI	HF	HTPF	BO	FM
Method type	Measurement	x	x	x	x	x	x		
	Estimation							x	x
Mode	2D	x	x			x		x	x
	3D	(x)	(x)	x	x		x		
Provide	Stress orientation	x	x	x	x	x	x	x	x
	Stress magnitude	x	x	x	x	x	x		
Depth range	≤ 1000 m	x	x	x	x	x	x		
	≈ 1–4 km					(x)		x	
	5–40 km								x
Performed in	New borehole	x	x	x	x	x	x	x	
	Existing borehole					x	x	x	
	Wet borehole			(x)	x	x	x	x	
	No borehole								x
Work in	High stress conditions	x					x	x	x
	Jointed rock mass	x					(x)		
Measure stress directly						x	x		
Require knowledge of rock properties		x	x	x	x				
Continuously reading during testing			x	(x)	x	x	x		
Longtime monitoring		x							
Borehole does not have to be in a principal stress direction				x	x	x			

Chapter 4

Updated Norwegian In Situ Rock Stress Database

There has not been collected in situ rock stress data from the Norwegian region in a database since the 1990s (see Section 1.3). Combined with the importance of in situ stresses knowledge for engineering purposes, as well for geophysicists and geologists (see Section 1.1), there is need for an updated Norwegian in situ rock stress database. The database presented in this thesis will be composed of existing rock stress data from 1990 until present time. The purpose of the database is to provide as much information about the stress state in Norway as possible. The database will therefore be comprised of both data from shallow measurement methods and from deeper estimation methods. This chapter presents the structure of the database, introduces the parameters that constitute the database and presents the data collected graphically.

4.1 Database Structure

The database has been created in Microsoft Access, which is a database creation program and a management tool developed by Microsoft. Access can store large amounts of data in tables consisting of columns and rows, similar to Microsoft Excel spreadsheets. Each column is a field with specific properties that determines what data type that can be added. Each row contains a unique data record. The data in the tables can be edited and viewed in other database objects

such as forms, queries and reports (Ojango, J. M. K.). This section will present the tables and forms that make up the database. Queries and reports were not used in the database and will therefore not be presented.

4.1.1 Tables in database

The database is comprised of four tables, where one contains information about the in situ stress field and serves as the main table. This table also contains description of location and of the bedrock. Two of the other tables contain test data from rock stress measurements, one table for overcoring and one for hydraulic fracturing. The last table was created for data uncertainty data. The structure of the database allows new tables for other stress determination methods to be integrated if necessary.

In Microsoft Access, tables can be linked to each other by creating relations between the tables. By creating relations, ease of access of the information is enhanced and the possibility of identical input fields in several tables is eliminated (Ojango, J. M. K.). The relations between the four tables in the database are shown in Figure 4.1. The input fields for each table are also visible in the Figure.

The table called *RockStressData* is the main table and the three other tables are connected to this table. The test data tables, *Overcoring* and *HydraulicFracturing*, are connected to the main table by a one-to-many relation (1–∞). While the data uncertainty table *MeasurementUncertainty* has a one–to–one (1–1) relation with the main table. A 1–∞ relation means that each record in the main table can be connected to many in the test data tables, but not the other way around. A 1–1 relationship means that one record in the main table can only be connected to one in the data uncertainty table. A one-to-one relation is used to stop duplicates from being created.

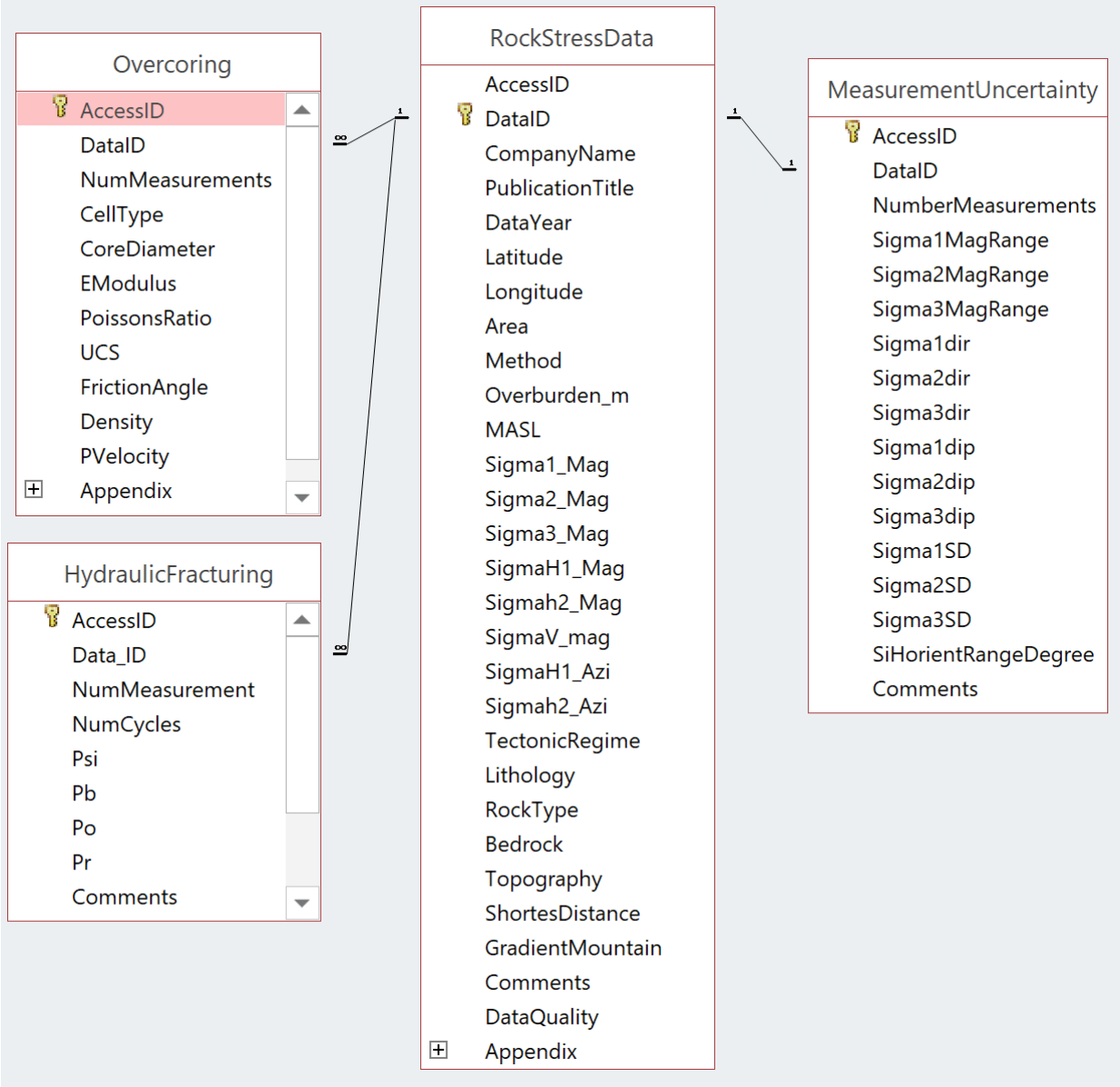

Figure 4.1: The database tables and their relation in Microsoft Access.

4.1.2 Data entry forms

Forms are used to enter, edit and display data, and are bound to one or more tables where the data is stored. When data is added or edited in forms, the connected table(s) will be updated accordingly. Data can be added or edited directly in tables, but forms are often used because they can be made more user-friendly. When a form is created, it is optional what input fields from the source table(s) to include. In addition to fields from tables, forms can contain pictures or buttons that opens objects, move between records or search in the data (Ojango, J. M. K.).

Figure 4.2 shows the main entry form in the database. This form opens automatically when the database file is opened. The form is a compilation of the four tables and their input fields. The input fields from the data uncertainty table has been included as a subform, while overcoring and hydraulic fracturing are separate forms. These forms were not included as subforms due to space limitations, but can be accessed by pressing the buttons called "Overcoring" and "Hydraulic fracturing". The goal with the main form was to have one form where all fields from the four tables would be accessible. By having this, knowledge of only one form, and none of the tables, would be required when adding data. This was wanted to make the database easy to use for people with little experience in Microsoft Access.

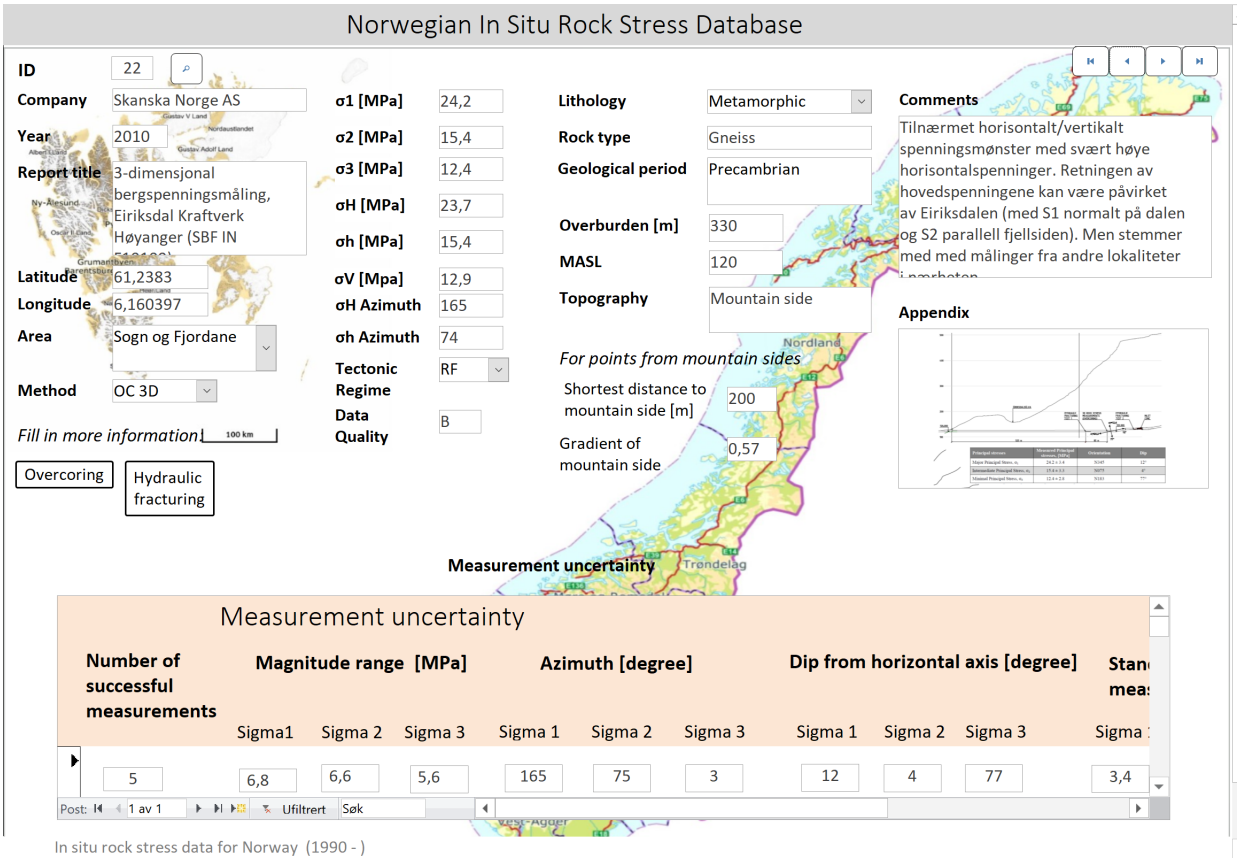

Figure 4.2: Database main entry form with data added in Microsoft Access.

Data uncertainty form

In Figure 4.2 only part of the data uncertainty form is visible. Figure 4.3 shows the complete form. The ID field to the right is the link to the connected record in the main form. The field is grey because ID is added automatically and the field is not editable.

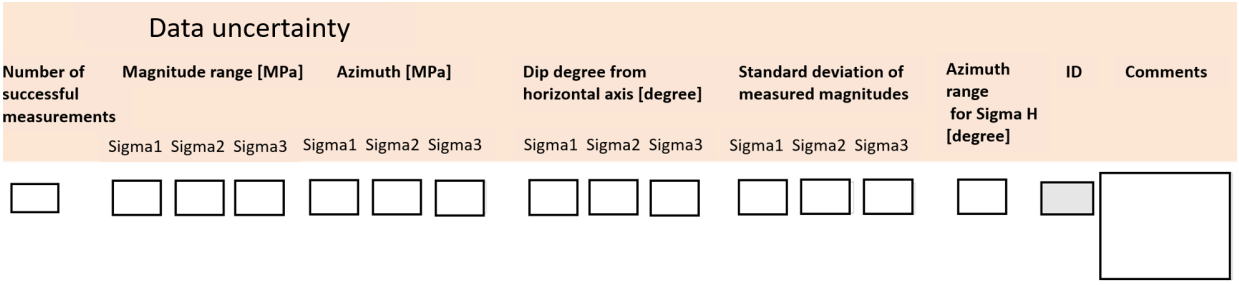

Figure 4.3: Database data uncertainty form in Microsoft Access.

Test data forms

When the buttons named "Overcoring" and "Hydraulic fracturing" in Figure 4.2 are pressed, the forms shown in Figure 4.4 and 4.5 will open. Unlike the data uncertainty form, the ID fields are not grey and this means that ID has to be added manually.

Overcoring form

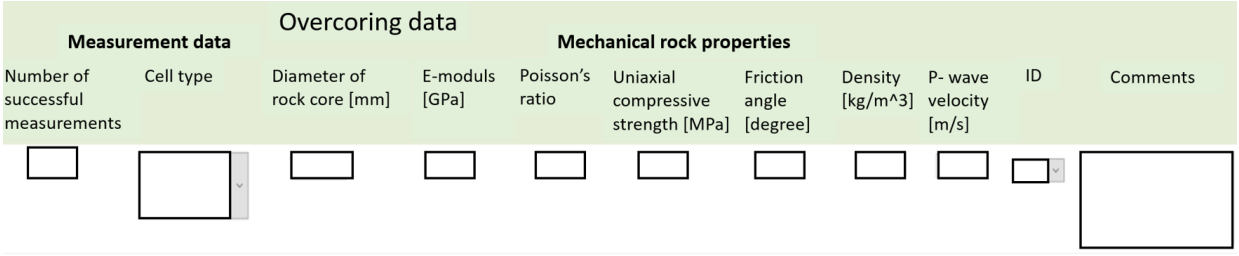

Figure 4.4: Overcoring entry form in Microsoft Access.

Hydraulic fracturing form

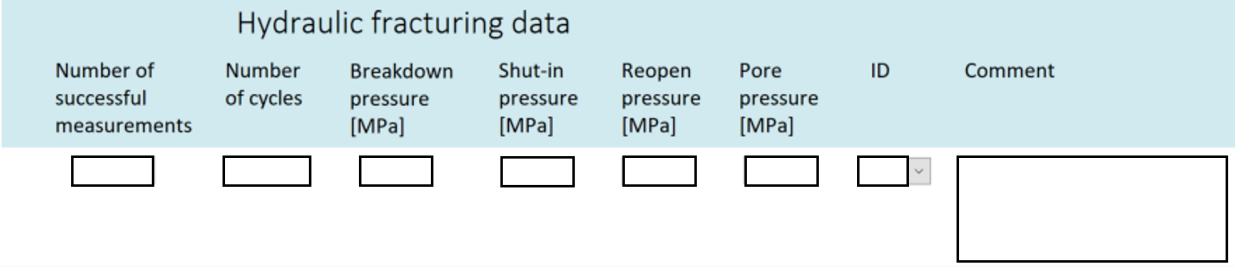

Figure 4.5: Hydraulic fracturing entry form in Microsoft Access.

4.1.3 Form overview

There has also been created a form that presents an overview of the four forms from Section 4.1.2. The form is presented in Figure 4.6. It is not necessary to use this form when adding or editing data, but it gives easy access to the forms without having to open the main entry form. Desired form is selected from the bar, which is indicated by the red box in Figure 4.6.

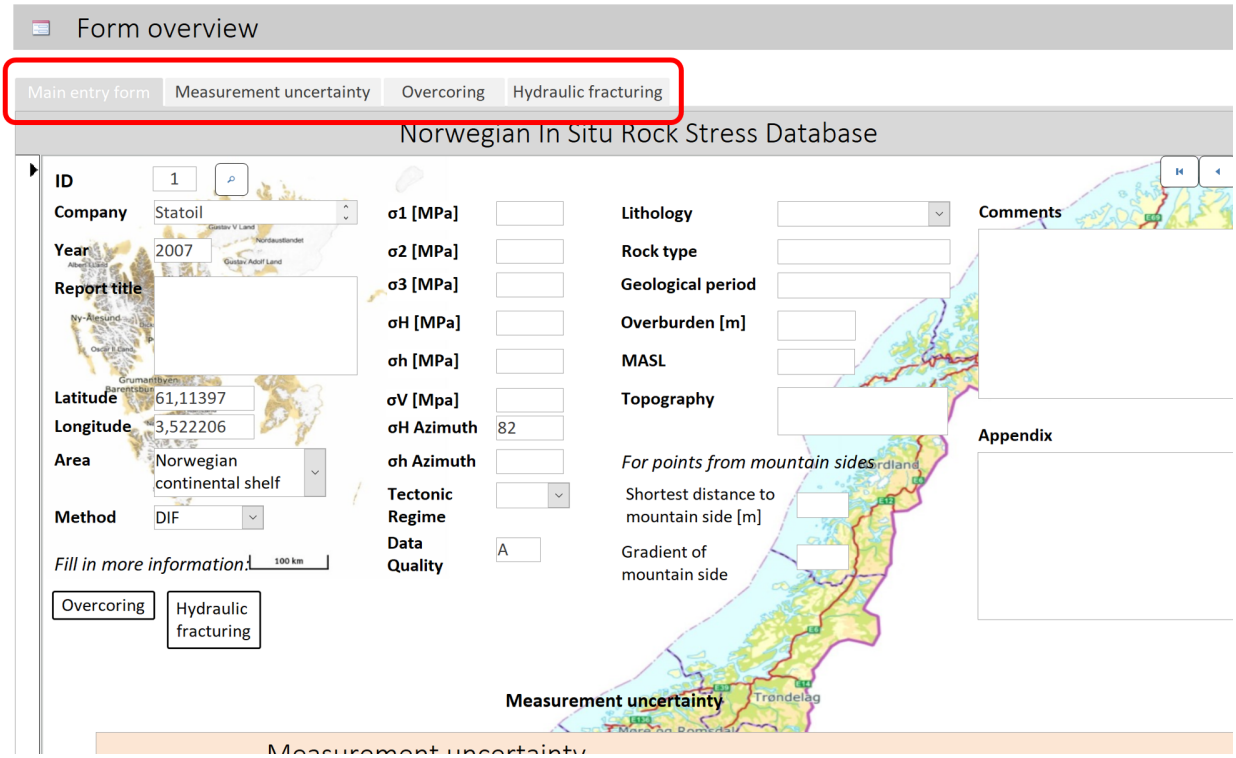

Figure 4.6: Database form overview in Microsoft Access.

4.2 Database Parameters

Figure 4.1 shows the tables in the database and their input fields, which make up the parameters in the database. As mentioned in Section 4.1, the tables consist of information about the in situ stress field, description of location and geological information, as well as test data and data uncertainty. The parameters are presented in form format in Figure 4.4, 4.5 and 4.3. This section will describe each parameter in the database and explain why these parameters have been included.

4.2.1 General information

General information consists of the following input fields:

- ID number
- Company name
- Year
- Report title

Every data point must be assigned a unique ID-number for the data record to be easy traceable. The name of the company that owns the data must also be included. In the year field, the year of each records is given. The database will only consist of data from from 1990 and newer. Lastly, the title of the document the data record is obtain from should be given. This is the data source and will allow users to cross-check the data. Common document types for in situ rock stress data are reports, conference papers and PowerPoint presentations. Name of conference will also be given when the data is from a conference.

4.2.2 Geographical position

Geographical position consists of the following input fields:

- Coordinates
- Area

Position of the data records will be given by coordinates and area. A coordinate system is a set of mathematical rules that specifies how coordinates are related to a point, while a geodetic datum is a reference specification for a measurement system. The European Reference Frame (EUREF)89 is the official geodetic Cartesian datum for Europe and Norway. The data points in the database are given by EUREF89 as geographical coordinates (latitudes and longitudes) (Statens kartverk, 2009). Area is described by county if the data record is from mainland Norway, or as Norwegian continental shelf, Svalbard or Atlantic Ocean.

4.2.3 Stress determination method

Stress determination method for each data point must be specified in the database. The method is selected from a drop-down list consisting of the acronyms for following methods (the methods are presented in Chapter 3):

- 2D and 3D overcoring (2D OC, 3D OC and 2&3D OC)
- Hydraulic fracturing (HF)
- Hydraulic testing of pre-existing fractures (HTPF)
- Borehole breakout (BO)
- Drilling-induced tensile fractures (DIF)
- Focal mechanism (FM)

Stress determination method is included as a parameter because it tells what kind of data each record is and what type of information each data record should contain. Different information is expected from different methods, depth of data point is for instance dependent on method (see Table 3.1).

Test data from the measurement methods is also included in the database. It was decided to include this because all stress determination methods are based on manual interpretation, and test data can be used for reinterpretation when new software tools are developed (Myrvang, 1996). Data from the estimation methods came in Excel spreadsheets with no test data, and no measurement were done with HTPF, so these methods do therefore not have their own

forms or tables. However, if test data from other methods is collected in the future, new parameters can easily be added to the database. There is space intentionally left blank in the main form to include buttons for other stress determination methods (Figure 4.7).

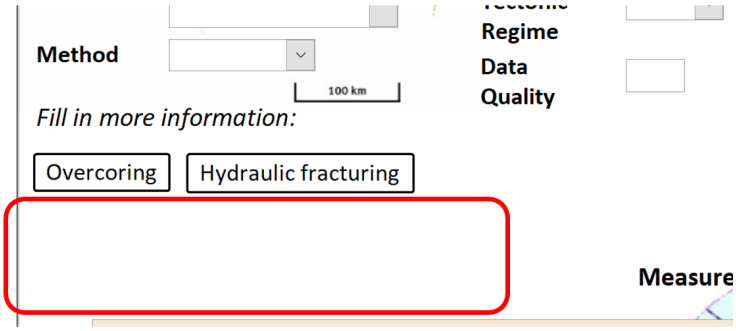

Figure 4.7: Space intentionally left blank for future addition of stress determination methods in database.

Overcoring test parameters

The overcoring test parameters can be seen in Figure 4.4 and can be divided into two main categories:

- Test data
  - Number of successful measurements
  - Cell type
  - Rock core diameter
- Mechanical rock properties
  - E-modulus
  - Poisson's ratio
  - Uniaxial compressive strength (UCS)
  - Friction angle
  - Density

Cell type is chosen from a drop-down list consisting of the cells presented in Section 3.1. It is however allowed to add other cell types if needed. Rock core diameter is the diameter of the cores obtained from the test hole. After removal, these cores are used in laboratory to determine mechanical rock properties. As described in Section 3.1, strain and not stress is measured during overcoring. To calculate stress from strain Hooke's law is applied (Appendix A.2.1), which requires knowledge the elastic rock properties E-modulus and Poisson's ratio. In addition to E-modulus and Poisson's ratio, uniaxial compressive strength, friction angle, density of rock core and P-wave velocity are common rock properties to test, and input fields for them are therefore included.

Hydraulic fracturing test parameters

Hydraulic fracturing test parameters can be seen in Figure 4.5 and consist of following:

- Number of successful measurements
- Number of cycles
- Average pressure for:
  - Breakdown pressure (P_b)
  - Shut-in pressure (P_{si})
  - Reopening pressure (P_r)
  - Pore pressure (P_o)

A test consists of several single measurements that may be successful or not, and each single measurement consists of a number of cycles. As stated in Section 3.2.1, each measurement should have at least three cycles, but that is not always possible. The number of cycles during a test may also vary for the measurements, and can be an interval. The pressures that are shown in Figure 3.13 are be included as they are the basis for the in situ stress values.

4.2.4 In situ rock stress

In situ rock stress consists of the following input fields:

- Principal stress magnitudes
- Horizontal and vertical stress magnitudes
- Horizontal stress orientations
- Tectonic stress regime

In situ stress field

As stated in Section 2.1.1, a stress field can be completely specified by the magnitude and orientation of the principal stresses σ_1, σ_2 and σ_3. Since the principal stresses are usually in the horizontal and vertical plane in the Earth's crust, the stress field can be fully described by orientation of either σ_H or σ_h and the magnitudes of σ_H, σ_h and σ_V. Due to topographical effects, geological features, anisotropy, discontinuity and/or heterogeneity of the rock mass, the principal stresses can be reoriented (discussed in Section 2.3). σ_H, σ_h and σ_V will then become components of the principal stresses, rather than principal stresses. It is therefore important to separate σ_1, σ_2 and σ_3 from σ_H, σ_h and σ_V in the database. Additionally, some stress measurements only provide information about either principal stresses or horizontal/vertical stresses.

Magnitude is given in megapascal [MPa] and orientation is given by azimuth. Azimuth is the angle between an object and the true north. When the vertical stress has not been measured, the theoretical vertical gravitational stress (Equation 2.2 in Section 2.2.1) can be given if wanted. Measurements done by NTNU/SINTEF at more than 250 locations indicate that the vertical stress usually coincide with the theoretical gravitational stress in Norway (Hanssen, 1997). However, when theoretical gravitational stress is given instead of measured stress, a T will be given after the number to specify that the value is theoretical.

Tectonic stress regime

Focal mechanism data provides information about relative stress magnitude, but not about principal stress magnitudes. Relative stress magnitude has therefore been included as a parameter in the database. The tectonic stress regime in an area is determined by the relative stress magnitude between the vertical and horizontal stresses. See Section 1.3.1 for a more detailed presentation of tectonic stress regimes. Figure 2.4 and Table 4.1 show how relative stress magnitude is related to tectonic stress regimes, where tectonic stress regimes are expressed by faulting types.

Table 4.1: Tectonic stress regimes defined by relative principal stress magnitudes in a vertical/horizontal stress field. σ_V = vertical stress, σ_H = major horizontal stress and σ_h = minor horizontal stress.

Faulting type	Relative stress magnitude
Normal faulting (NF)	$\sigma_V > \sigma_H > \sigma_h$
Revers faulting (RF)	$\sigma_H > \sigma_h > \sigma_V$
Strike-slip faulting (SS)	$\sigma_H > \sigma_V > \sigma_h$
Normal faulting with strike-slip component (NS)	$\sigma_V \approx \sigma_H > \sigma_h$
Revers faulting with strike-slip component (RS)	$\sigma_H \gg \sigma_V \approx \sigma_h$

Normal fault with strike-slip component or reverse with strike-slip component are called transitional regimes. Transitional regimes are regimes that are transition between two stress regimes where two of the stresses are about equal in magnitude (Zoback, 1992, 11711).

4.2.5 Bedrock

Bedrock consists of the following input fields:

- Lithology
- Rock type
- Geological period

Lithology is chosen from a drop-down list where the rock mass can be categorised as either igneous, sedimentary or metamorphic. This was added since Zang et al. (2012) concluded that

K from Equation 2.3 was dependent on lithology. He found that K deviated for igneous/metamorphic and sedimentary rocks. To provide more detailed information on the rock mass, rock type can be added if known. In Section 2.4 it is stated that rock masses from specific geological periods show higher, or lower, stresses than average in Norway. Therefore, geological period categorised after Appendix A.3 is also included in the database.

4.2.6 Location

Location consists of the following input fields:

- Overburden
- meters above sea level (MASL)
- Topography
- Shortest distance to and gradient of the mountain side

Overburden, MASL and a short description of topography have been added to describe location of the data points. The location of data point has been included as a parameter to have more information about the point, and because local features can affect the in situ stress field (see Section 2.3.5). Overburden can also be used to calculate the theoretical gravitational in situ stresses.

As discussed in Section 2.3.5, local effects that often cause deviating in situ stress are high mountains and deep valleys. Mid-Norway is characterised by high altitude mountains and Western Norway by high mountains and deep fjords (Myrvang, 2001). Myrvang (2001) concluded that these topographic features influenced the near surface stress measurements very much. For data points from measurements located in areas dominated by high mountains and deep valleys/fjords, shortest distance to the mountain side from the data point and gradient of the mountain side should be given if possible. This information could be used to analyse to what extent the stress field is affected by topography by comparing distance to the mountain side, gradient and overburden with stress magnitudes and orientations for different records. However, it is important to be aware that the values will be calculated from elevation profiles and are not accurate.

4.2.7 Data uncertainty

Data uncertainty consists of the following input fields:

- Magnitude range for σ_1, σ_2 and σ_3
- Azimuth for σ_1, σ_2 and σ_3
- Dip degree from horizontal axis σ_1, σ_2 and σ_3
- Standard deviation of measured magnitudes σ_1, σ_2 and σ_3
- Azimuth range of σ_H

Expect for orientation range, all the input fields are for σ_1, σ_2 and σ_3 and not σ_H, σ_h and σ_V. The principal stresses σ_1, σ_2 and σ_3 are calculated from test results and the vertical and horizontal stresses are calculated based on these values. The uncertainties of the vertical and horizontal stresses are therefore directly related to the uncertainties of the principal stresses.

Magnitude range is the interval from the lowest measured stress magnitude to the highest. Dip degree from horizontal axis is will be a degree in the interval from 0 - 90 °, where 0 ° is along the horizontal axis and 90 ° along the vertical. Standard deviation is calculated from DISO for overcoring (discussed in Section 3.1.2), while it has to be calculated manually for hydraulic fracturing. Orientation range for σ_H is the interval from the lowest measured azimuth to the highest for σ_H.

4.2.8 Data quality

Section 1.3.1 presents the quality ranking scheme utilised by the WSM project. The parts of the quality ranking scheme that concerns the methods presented in Chapter 3, can be seen in Table A.1 and A.2 in Appendix A.4. From the Tables, it is evident that there is little focus on stress magnitudes, and that the scheme favours deep records (WSM project mainly focuses on regional stress patterns, see Section 1.3.1). The WSM quality ranking scheme is therefore unfit to use in this database since local stress fields and stress magnitudes are equally important as stress orientations and regional stress patterns.

The quality will be ranked from A to E where A is the best quality. If the quality is unknown, an U for unknown can be given. The data from estimation methods was already assigned quality from A–E by the companies that had done the estimations. It is unsure exactly what those companies have based the ranking on. For data from measurement methods, it was decided to rank the data based what was written in the source reports and the data uncertainty information (Section 4.2.7).

The measurement conditions described in the reports will be an important factor when assigning quality. Measurement conditions are dependent on rock mass quality (for instance presence of joins or heterogenity caused by varying mineral grain size or composition), borehole orientation and proximity to geological features like faults. The number of measurements in each test will also be considered, where few measurements will give lower quality than many measurements. Due to the different theory behind the methods, it is normally done more measurements for hydraulic fracturing than overcoring. The methods are therefore not compared with each other, but with other records by same method.

In some cases, there can be done manual interpretation of some parameters when they are missing/not calculated in the reports. For instance, the orientation for σ_H may be set equal to that of σ_1 or σ_2 if dip degree is less than 10°. For hydraulic fracturing, σ_1 can be calculated from Equation 3.1 when not given. While if orientation of σ_H orientation is only presented on maps in the reports, it can be read from the map if north is indicated. This will however reduce the quality of the data.

Table 4.2 shows a summary of the quality assignment that will be used for hydraulic fracturing and overcoring. Number of measurements is based on what SINTEF (2014) recommends. The quality may deviate from the Table in some cases where the data is considered better/worse than what the Table indicates.

Table 4.2: Quality ranking for measurement records

Requirements	Quality				
	A	B	C	D	E
Measurement conditions	Good	Good	Good	Middle	Bad
No. of measurements	For OC ≥ 5 For HF ≥ 15	For OC ≥ 3 For HF ≥ 10	For OC ≥ 2 For HF ≥ 5	For OC 1 For HF ≥ 1	For OC 1 For HF 1
Geological features in proximity to test location	None	None	None big	Yes	Yes
Cross-checked with other results	Yes	No	No	No	No
Manual interpretation of parameters*	None	None	Yes	Yes	Yes

* Manual interpretation of one or more parameters that was not given in the source reports for the data record

4.3 Collected In Situ Rock Stress Data

Throughout the fall of 2017 and spring of 2018, 115 in situ stress data records have been collected from onshore Norway, offshore Norway and Svalbard. Data from the estimation methods makes up 64 % of the data, while 36 % is from measurement methods. The distribution of stress determination method is presented in Figure 4.8. This section presents the data collected graphically with focus on different database parameters. Microsoft Excel 2016 was used to create graphs and the maps have been created in ArcMap 10.6. Due to the difficulty to assign comparable and reliable data quality, quality has been ignored.

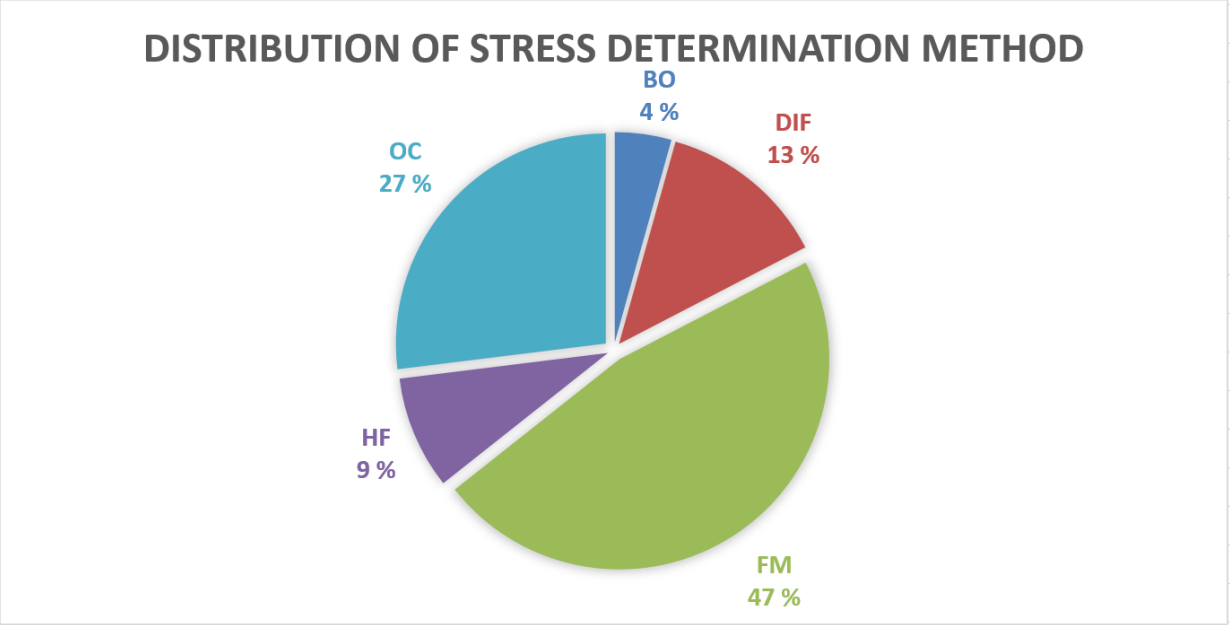

Figure 4.8: Distribution of stress determination method in database. BO = borehole breakout analysis, DIF = drilling-induced fractures, FM = focal mechanism, HF = hydraulic fracturing and OC = overcoring.

4.3.1 Geographical position of data points

Of the 115 data points, 51 % were located onshore in Norway, 38 % offshore and 11 % of the data points were on Svalbard. Figure 4.9 shows geographical location of the data points with symbols and colours that represent stress determination method.

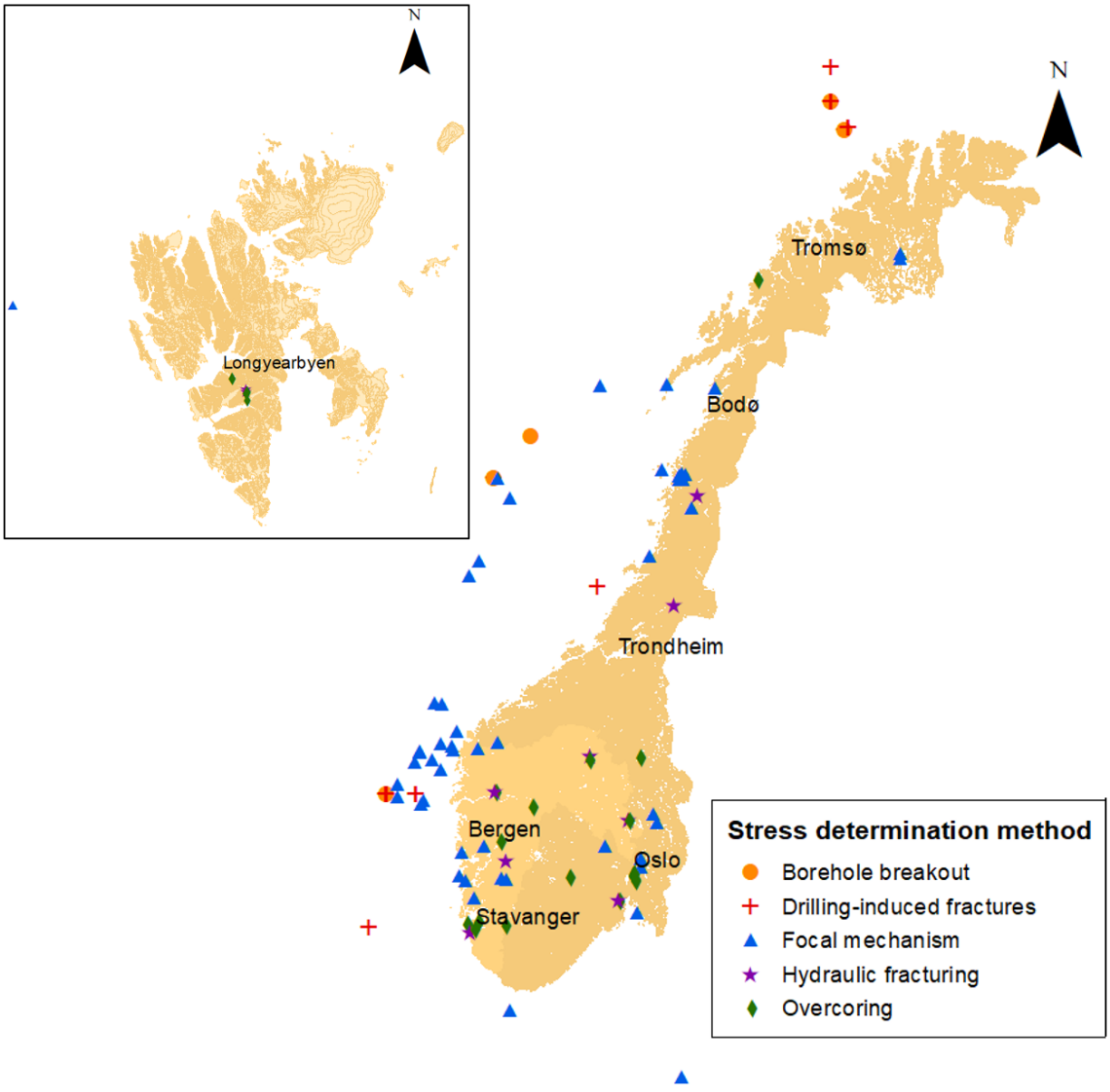

Figure 4.9: Geographical position and stress determination method of data points in database.

4.3.2 Stress orientations

106 out of 115 records had information about σ_H orientation. Figure 4.10 and 4.11 show σ_H orientation for the data points. The colour of each record indicates stress determination method.

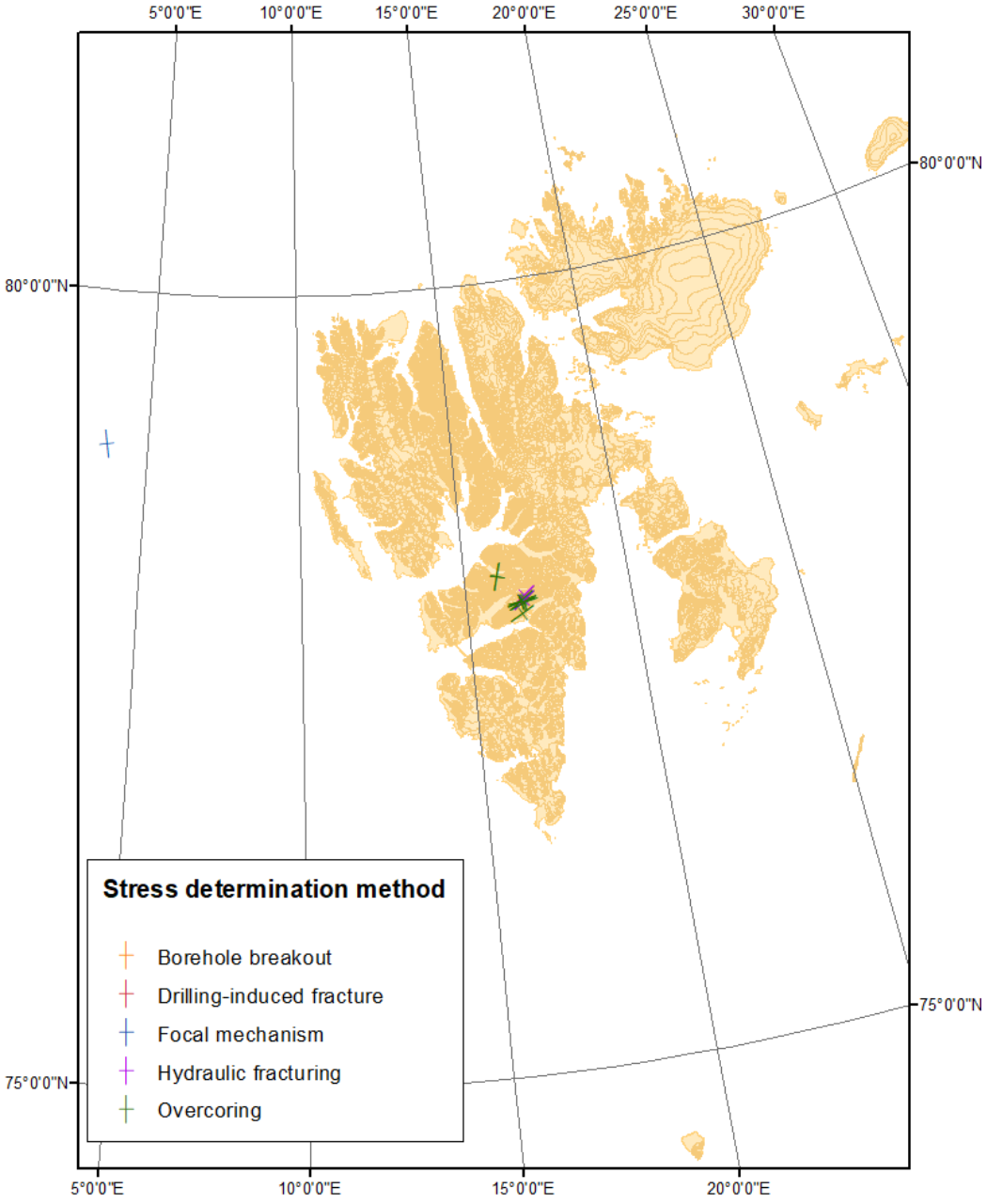

Figure 4.10: σ_H orientation for Svalbard.

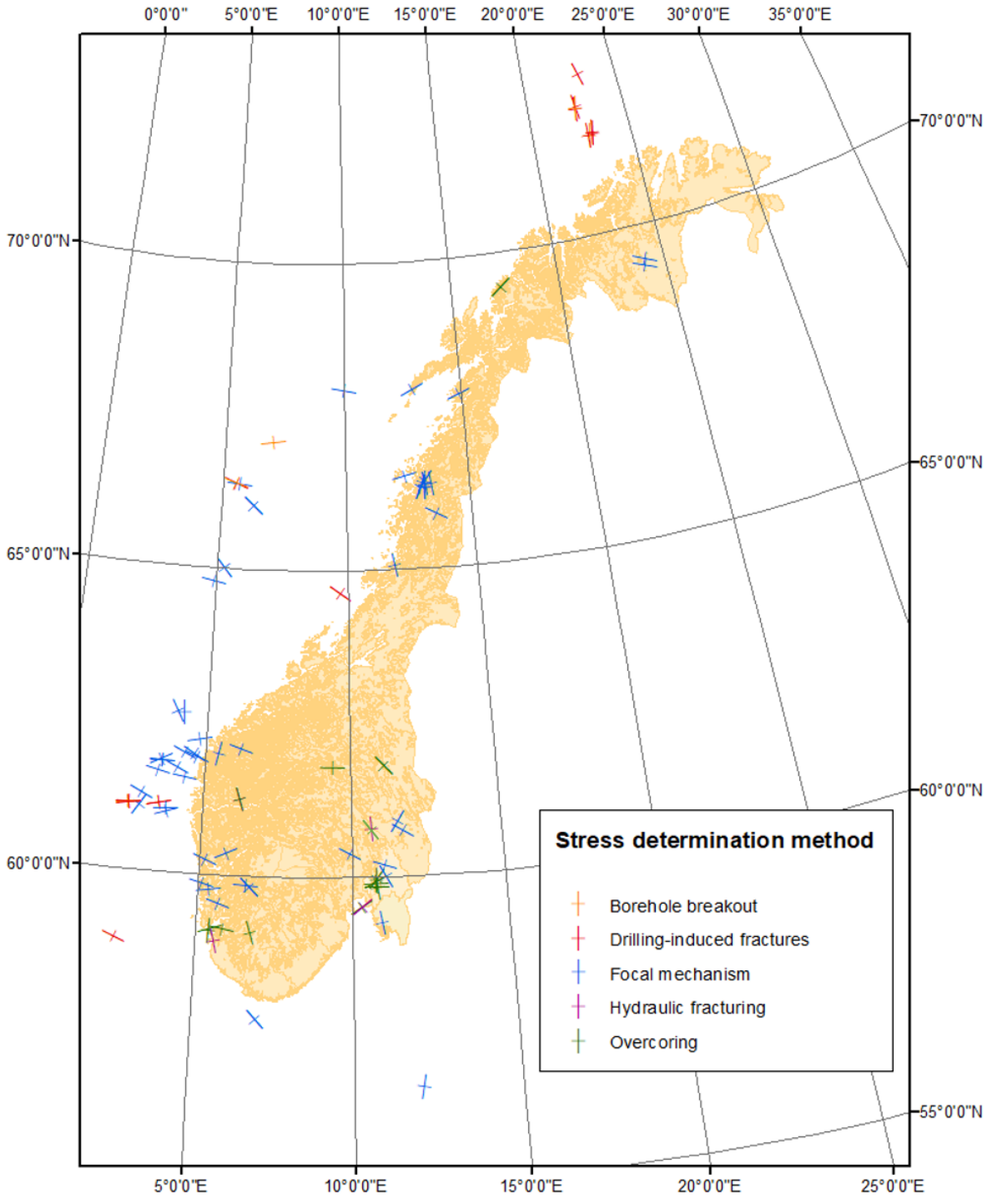

Figure 4.11: σ_H orientation for Norway.

4.3.3 Relative stress magnitudes

Out of the 115 data records, 70 had information about both σ_H orientation and relative stress magnitude of the horizontal stresses with respect to the vertical stress. These points are presented in Figure 4.12 and 4.13. In the Figures, relative stress magnitudes are expressed by tectonic stress regimes (see Figure 1.2 and Table 4.1 for classification). Overburden for records obtained with measurement methods ranged from 11–700 m, while the estimation records were located at depths of 5–50 km. The data points were therefore classified as either deep estimations or shallow measurements in the Figures.

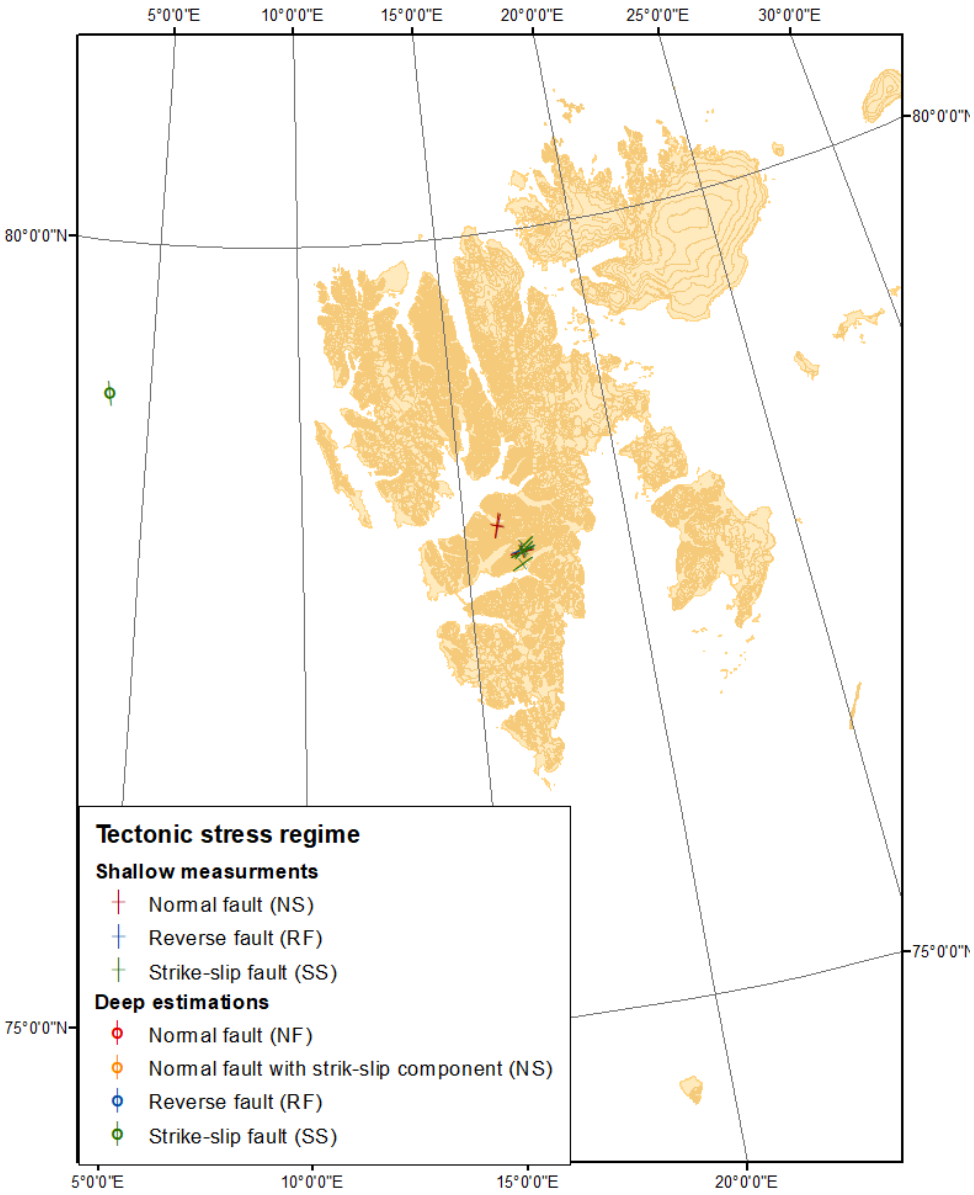

Figure 4.12: Tectonic stress regime and σ_H orientations for Svalbard.

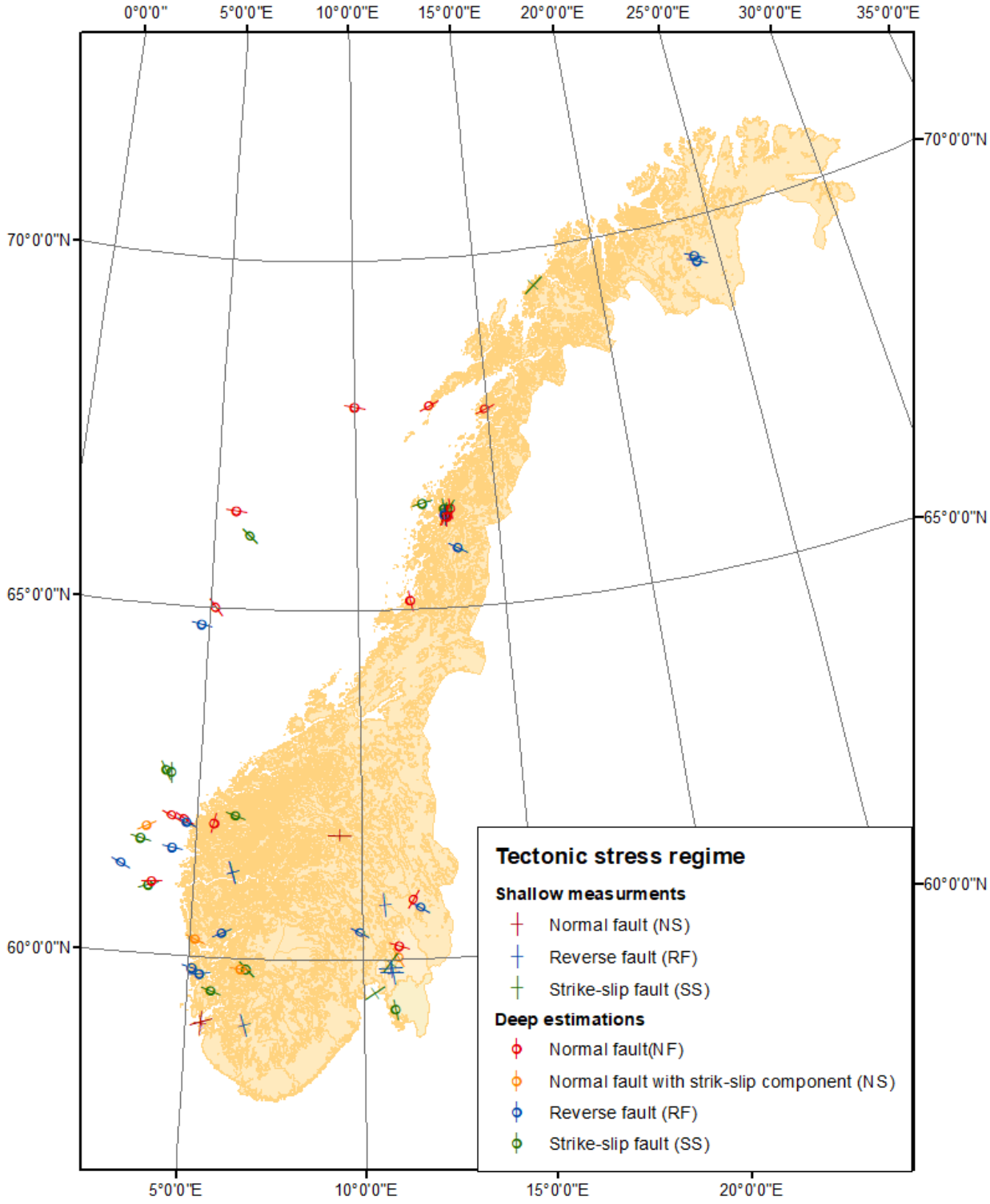

Figure 4.13: Tectonic stress regime and σ_H orientation for Norway.

4.3.4 Stress magnitudes

Principal stress magnitudes are plotted against overburden in Figure 4.14. The stress magnitudes increased with increasing depth and the stress gradients for these points were 0.045 for σ_1, 0.029 for σ_2 and 0.023 for σ_3. In Appendix A.6.1, the stress ratios for the principal stresses are plotted. From the graphs following ratios were calculated: $\frac{\sigma_2}{\sigma_3}$ = 1.45, $\frac{\sigma_1}{\sigma_2}$ = 1.44 and $\frac{\sigma_1}{\sigma_3}$ = 1.90.

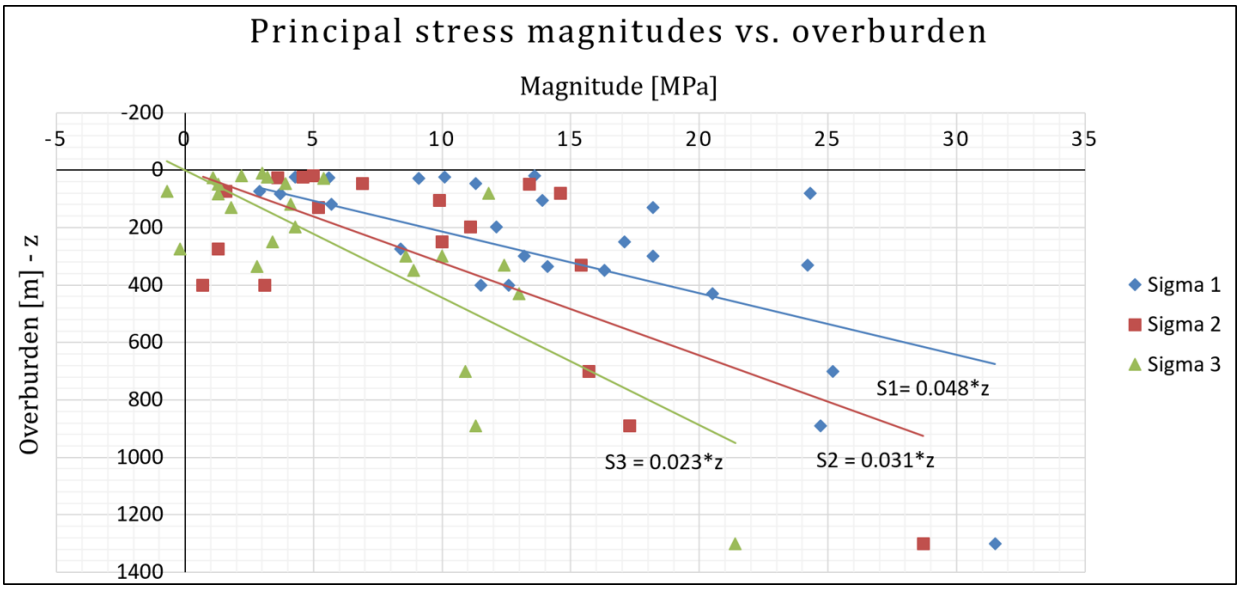

Figure 4.14: Principal stress σ_1 (S1), σ_2 (S2) and σ_3 (S3) magnitudes plotted against overburden.

In Figure 4.15, principal stress magnitudes are plotted against the average value of the principal stress magnitudes rather than overburden. It can be seen that Figure 4.15 has less scatter than Figure 4.14.

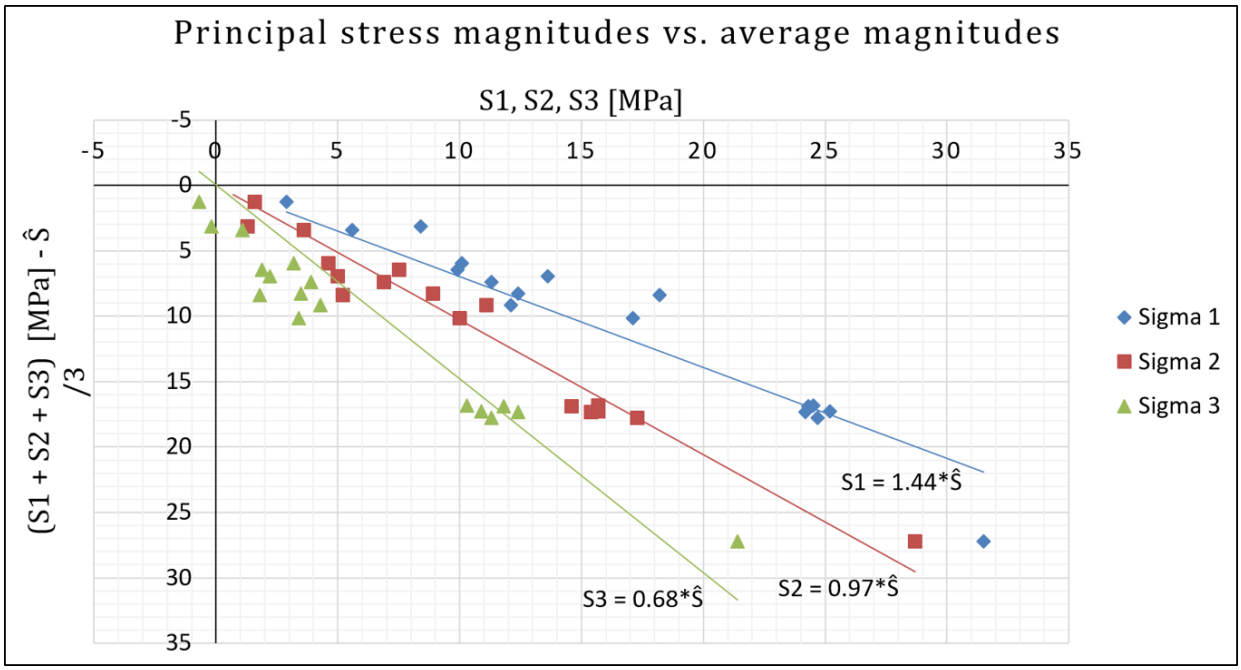

Figure 4.15: Principal stress σ_1 (S1), σ_2 (S2) and σ_3 (S3) magnitudes plotted against average magnitude of the three stresses.

Figure 4.16 shows the horizontal and vertical stresses plotted against overburden. From the Figure it can be seen that $\sigma_H > \sigma_V > \sigma_h$. The stress magnitudes increased with increasing depth and the gradients calculated from these points were 0.057 for σ_H, 0.038 for σ_H and 0.032 for σ_h. In Appendix A.6.1, the stress ratios for the horizontal and vertical stresses are plotted. From the graphs following ratios were calculated: $\frac{\sigma_H}{\sigma_V} = 1.2$, $\frac{\sigma_h}{\sigma_V} = 0.75$ and $\frac{\sigma_h}{\sigma_H} = 0.46$.

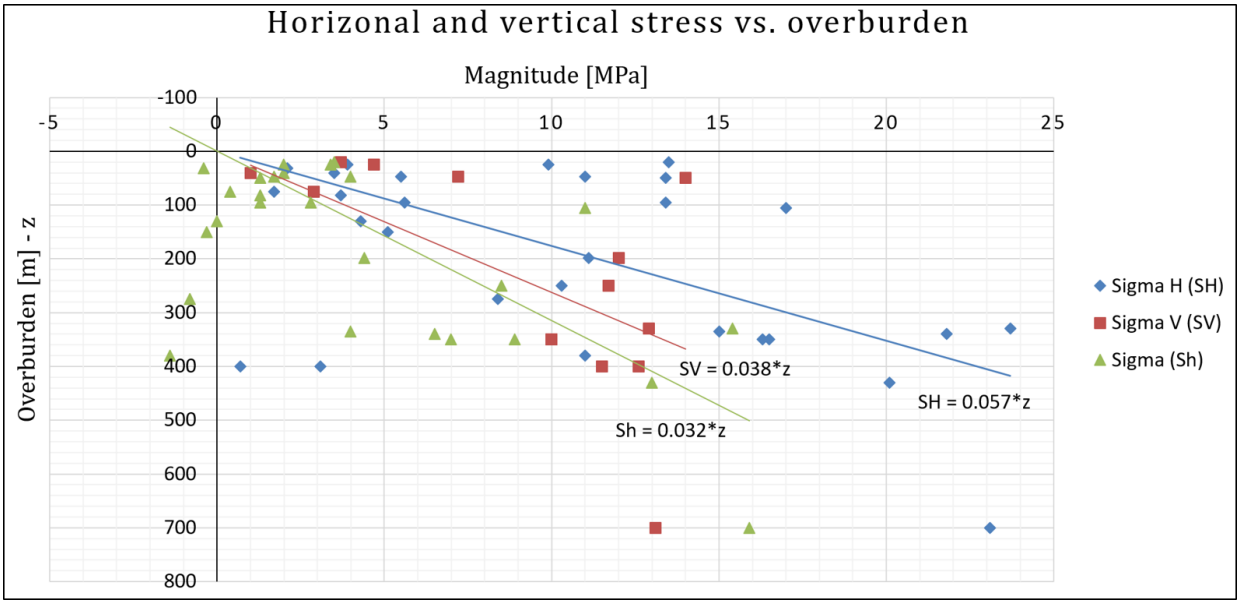

Figure 4.16: Horizontal and vertical stress σ_H (SH), σ_V (SV) and σ_h (Sh) magnitudes magnitudes plotted against overburden.

Lithology

Figure 4.17 shows principal stress magnitudes plotted against overburden where the data points are separated according to lithology as either sedimentary or igneous and metamorphic rocks. There was not created any trend line for σ_3 in sedimentary rock because there were only three records with this information. From the Figure it can be seen that the points in sedimentary rocks show higher stresses than those in igneous and metamorphic rocks. In Appendix A.6.1, the stress ratios for the principal stresses are plotted. From the graphs, the $\frac{\sigma_1}{\sigma_2}$ ratio for sedimentary rocks was 2.06. Following principal stress ratios were calculated igneous and metamorphic rocks $\frac{\sigma_2}{\sigma_3}$ = 1.42, $\frac{\sigma_1}{\sigma_2}$ = 1.36 and $\frac{\sigma_1}{\sigma_3}$ = 1.86.

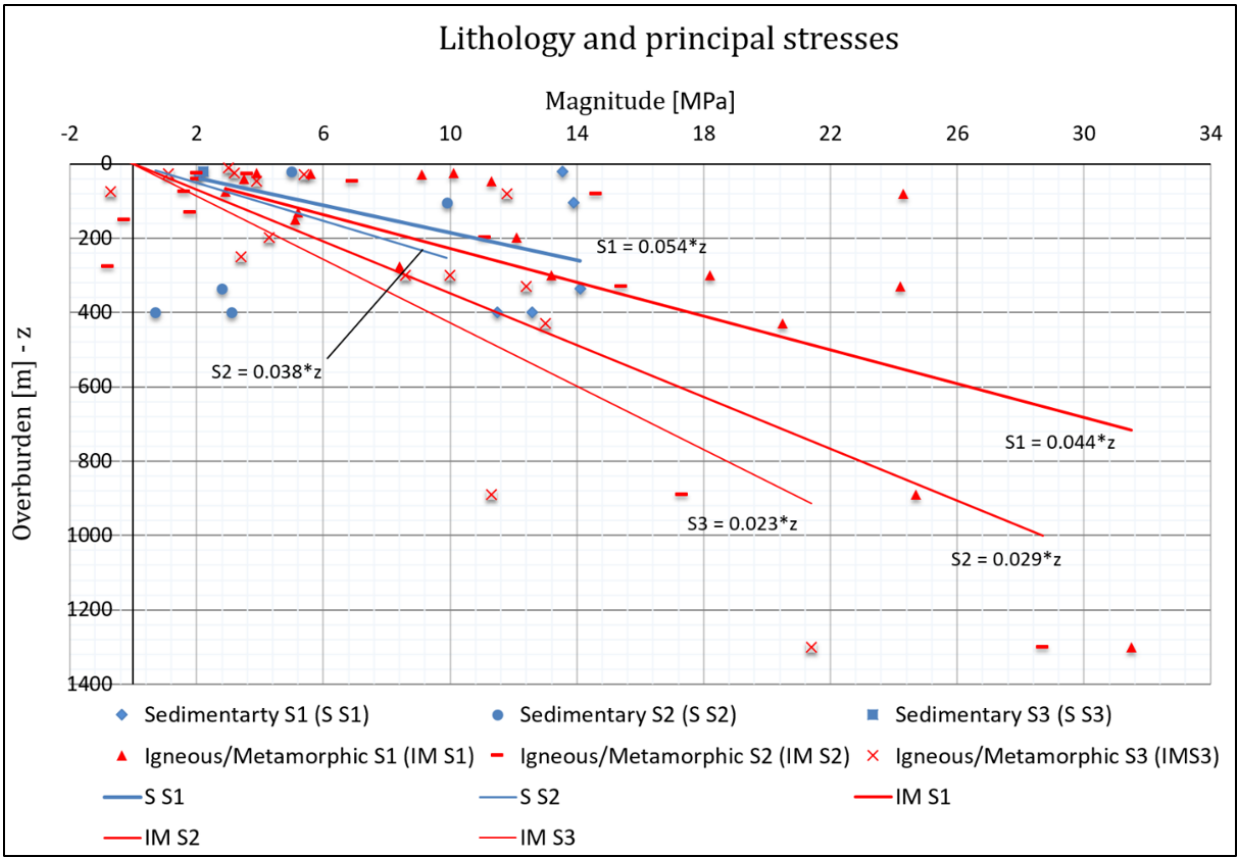

Figure 4.17: Principal stress σ_1 (S1), σ_2 (S2) and σ_3 (S3) magnitudes plotted against overburden. Data points are separated by lithology as either sedimentary or igneous and metamorphic rocks.

Geological period

Figure 4.18 shows principal stress magnitudes plotted against overburden where the data points are separated according to geological age of the rocks. The geological timescale is presented in Appendix A.3. There was only one data point in Permian rock with principal stress magnitudes and is was therefore not included. From the Figure it can be seen that the Precambrian rocks have higher stress magnitudes than the Cambrian-Silurian rock masses. From Appendix A.6.1 following principal stress ratios were calculated rocks of Cambrian-Silurian age: $\frac{\sigma_2}{\sigma_3}$ = 1.78, $\frac{\sigma_1}{\sigma_2}$ = 1.46 and $\frac{\sigma_1}{\sigma_3}$ = 2.24. Following ratios were calculated for rocks of Precambrian age: $\frac{\sigma_2}{\sigma_3}$ = 1.36, $\frac{\sigma_1}{\sigma_2}$ = 1.35 and $\frac{\sigma_1}{\sigma_3}$ = 1.80.

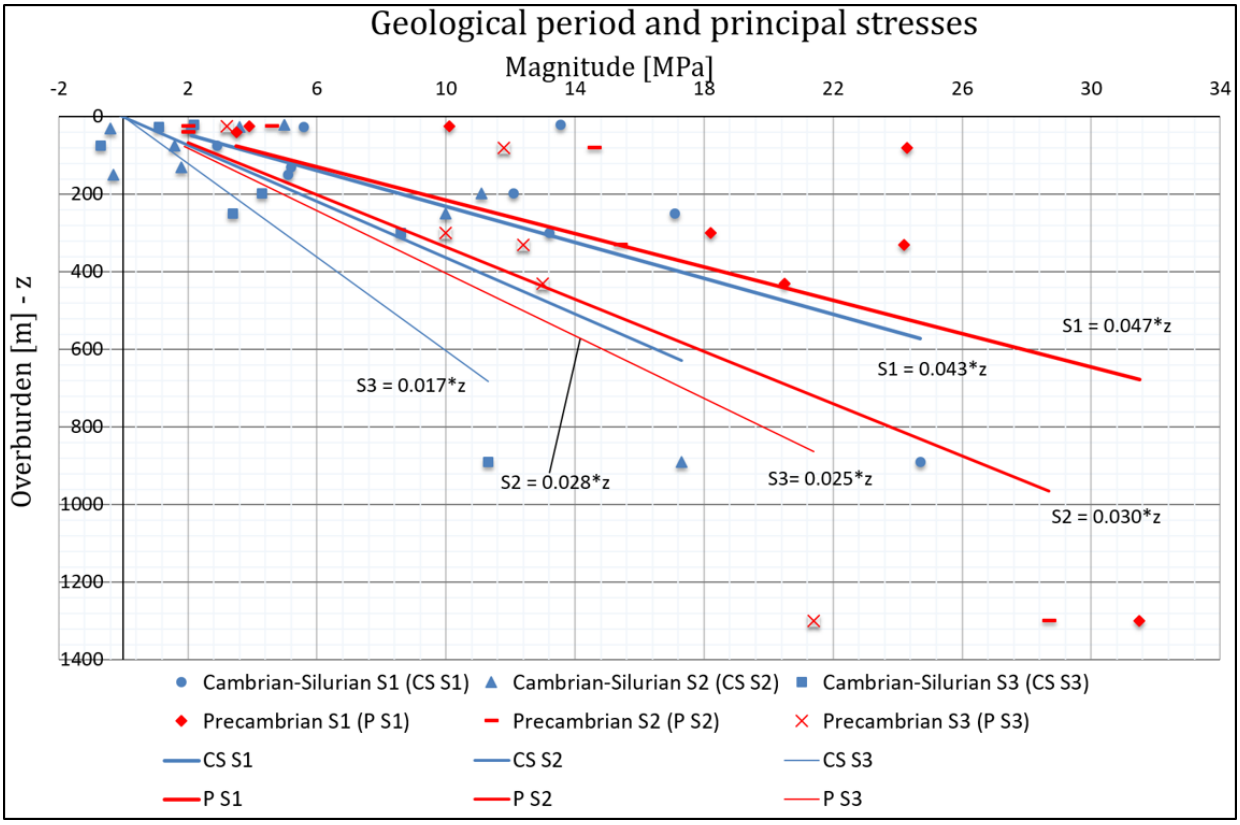

Figure 4.18: Principal stress σ_1 (S1), σ_2 (S2) and σ_3 (S3) plotted against overburden. The data points are separated by geological age of the rock mass.

Chapter 5

Discussion

This chapter contains a discussion of the database structure, σ_H orientations, stress magnitudes, lithology and geological age and the effect of topography on the in situ stress field. The data records have been assigned quality, but the quality ranking differs based on stress determination method since the borehole breakout, DIF and focal mechanism data were assigned quality by Statoil and NORSAR. This made the records incomparable with each other, and quality has therefore not been discussed.

5.1 Database Structure

The current database is made up of four tables and four forms, where one is the main form and is a compilation of the four tables. The database consists of parameters that cover the in situ stress state, geological information, location of data points in relation to depth and topography, test data and measurement uncertainty. However, the database could be structured differently. This section discusses alternative database structures and database parameters.

An alternative structure is to structure the database based on stress determination method. The data obtained with different methods would then be separated in different tables. An advantage with this structure is that all information for each record would be accessible from only one table or form. The way the database is structured at the present time, one data record

can have information in up to three different table. That information is spread over multiple tables may make it more difficult to find information or to collect all information from one record. From the data collected (presented in Appendix A.6.2) it also seems that the amount of blank input fields is dependent on stress determination method. The number of blank input fields could be reduced by creating separate tables for the different stress determination methods.

By structuring the database according to stress determination methods, the usefulness of forms may be reduced and forms could be excluded from the database. To remove the forms would decrease the number of database objects that the user must handle. If there is one form for each table, these forms may end up so similar to the tables that they may be considered redundant. However, there are some advantages with forms. Forms make it is easier to focus on one record at a time, they can display objects like pictures or maps and forms can contain buttons that automates tasks. Forms may also be made more user-friendly than tables (Ojango, J. M. K.).

A disadvantage by separating data according to stress determination method, is that only the test data input fields would be unique for the different tables. All the other input fields would be identical and this will make it difficult create a main form similar to that presented in Figure 4.2. Another disadvantage is that it would take longer time to carry out analyses that are independent on method. This can for instance be analyses of stress magnitudes in relation to depth or principal stress ratios.

The number of empty input fields can alternatively be reduced by only collecting measurement data. The data records from the measurement methods were the only methods that had enough information to fill every input field. However, the measurement and estimation covers different depth ranges (evident from Table 3.1). The only way to obtain knowledge about the in situ stress state at depths below $\approx$ 1000 m is by estimation methods.

Another possible way to reduce the number of blank fields will be to reduce the number of input fields. From Table A.3 and A.4, it can be seen that the input fields that describe location often are blank. However, by removing these input fields it would be more difficult to estimate to what extent the data records in these areas are affected by the topography. Relative stress

regime is another input field that may be considered redundant because this information can be found from other input fields (σ_1, σ_2, σ_3 and σ_H, σ_h σ_V). However, the focal mechanism data has information about the relative stress magnitudes, but not about stress magnitudes. By removing this input field, the focal mechanism data would have no information about stress magnitudes. There are some records that have information in every input field, and by removing any field, some information would be lost.

It seems that the most fitting database structure is dependent on the intended use of the data. As stated in Chapter 4 the goal with creating this database is to provide as much information about the in situ stress field in Norway as possible. Therefore, it would not be a good idea to remove any of the input fields. Neither would it be a good idea be to only collect measurement data, because there would be little information about the in situ stresses below $\approx$ 1000 m. However, to separate the data records by stress determination method would decrease the number of blank input fields. It would also be easier to find all information for each record. On the other hand, it would be difficult to create one form where all data could be added like in Figure 4.2.

5.2 Orientation of the Major Horizontal Stress

Section 2.4 briefly summarises the major horizontal stress σ_H orientations for onshore and offshore Norway found by Fejerskov et al. (2000). This section will present the stress trends identified by Fejerskov et al. (2000) in more detail and compare them with the data in Figure 4.10 and 4.11, which is presented in rosette plots in Figure 5.1 and 5.2. The stress map created by Fejerskov et al. (2000) is presented in Figure A.4 in Appendix A.5.1.

Fejerskov et al. (2000) found that the Barents Sea and northern Norway displayed a consistent N–S σ_H orientation. According to Fejerskov and Lindholm (2000), the N–S orientation in the Barents Sea could be caused by a combination of the ridge push effect from the mid-Atlantic ridge and the density contrast at the continental margin. The mid-Atlantic ridge and the continental margin are shown in Figure A.5 and A.6 in Appendix A.5.2. The ridge push effect creates compressional stresses that act perpendicular to the crest of the ridge (see Section 2.2.2). Whereas there will be a density contrast at the continental margin since the continental

crust is lighter and thicker than the oceanic crust. The contrast creates horizontal stresses that will act perpendicular to the margin. These stresses are tensional in the continental crust and compressional in the oceanic crust (Fejerskov and Lindholm, 2000).

In Figure 4.11 and to the left in Figure 5.1, the N–S σ_H orientation that Fejerskov et al. (2000) found can be identified. The borehole breakout and DIF data records all have N–S to NNW–SSE σ_H orientation. From Figure A.5 it can be seen that the ridge push effect acts NNW–SSE in the Barents Sea, whereas the tensional horizontal stress caused by the density contrast acts E–W in the continental shelf. Combining these two forces results in compressive horizontal stresses acting approximately N–S. The stresses in the Barents Sea can therefore be a result of these forces. However, since some of the points have NNW–SSE orientation (see Figure 5.1), the ridge push effect may affect the stress field more than the density contrast.

In the continental shelf in the Norwegian Sea and from 62°– 70° North in Norway, Fejerskov et al. (2000) identified a rotation of σ_H towards a NW–SE to WNW–ESE orientation. They concluded that this rotation was mainly caused by the rotation of the mid-Atlantic ridge and the associated ridge push effect. In Figure 5.1, a WNW–ESE trend can be seen in the Norwegian Sea. This orientation coincides with the findings of Fejerskov et al. (2000). A coast-perpendicular compressive σ_H orientation also agrees with sedimentary loading on the continental shelf. Sediment loading creates compressional horizontal stresses beneath the load that act perpendicular to the coast (Fejerskov and Lindholm, 2000). According to (Fejerskov and Lindholm, 2000), the sediment rate in the Norwegian Sea in Pliocene (see Appendix A.3 for geological timescale) may have been high enough to create bending stresses. Onshore from 62°– 70° North, left in Figure 5.2, the data is scattered and there is difficult to identify any trends.

According to Fejerskov et al. (2000), σ_H orientations were more scattered in western Norway and northern North Sea (58°– 62° North). Still, they identified a WNW–ESE σ_H trend. In Figure 5.1, two different trends can be identified between 59°–62° North in the North Sea: a W–E and a WNW–ESE orientation. A WNW–ESE orientation in the continental shelf correlates both with the direction of the ridge push and of sediment loading in the continental shelf. However, the sedimentation rate here has been lower than in the Norwegian Sea and the effect is more unclear (Fejerskov and Lindholm, 2000).

By comparing the rosettes in Figure 5.2, it looks like the σ_H orientations onshore in eastern western, mid and eastern Norway are dependent on the depth of the data points. In the middle of Figure 5.2, data from these areas obtained with focal mechanism a depths of 5–50 km are presented and a WNW–ESE σ_H trend can be seen. To the right in Figure 5.2, only data with overburdens of 25–700 m are presented and there is no WNW–ESE trend. Instead, there is a N–S trend in western Norway and a E–W trend around Oslo (see Figure 4.11). This may indicate that the stress field at depths down to ≈ 1000 m is affected by local factors like topography or geological structures, but with increasing depth the stress field is more a result of tectonic stresses. The WNW–ESE orientation correlate with the ridge push effect. However, by comparing Figure 5.2 and 5.1, it can be seen that the data is more scattered onshore than the offshore data which could increase the uncertainty of the trends identified.

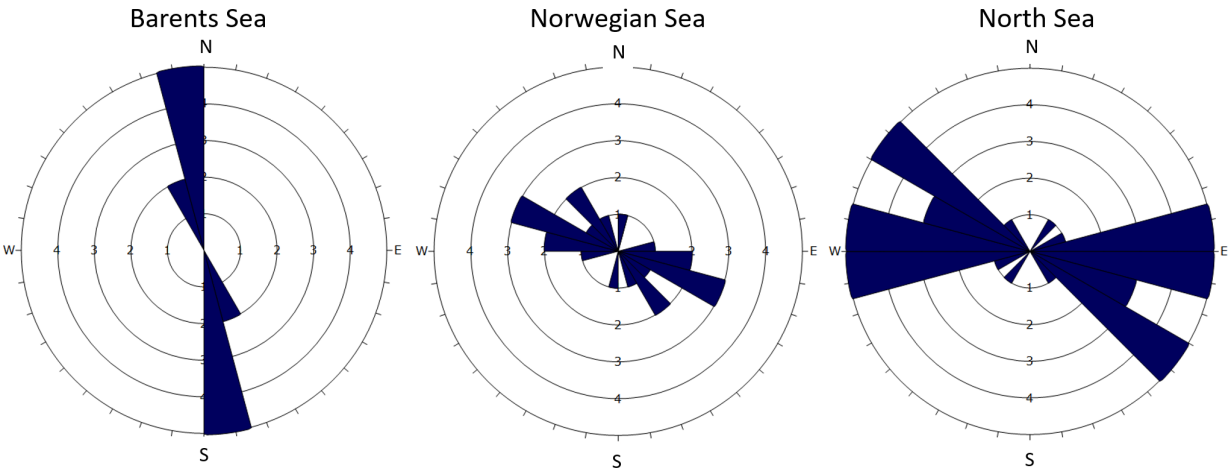

Figure 5.1: σ_H orientations from the Norwegian continental shelf presented in rosette plots. One arc segment has a width of 15° and each circle represents one data point (created in Dips 7.0).

On Svalbard (Figure 4.10) a trend of SW–NE σ_H orientation can be identified. From Figure A.6 it can be seen that the mid-Atlantic ridge east of Svalbard has N–S direction, but NE–SW north of Svalbard. The continental margin is rotated the same way, but has E–W direction north of Svalbard. This rotation makes it difficult to identify mechanisms that can explain the stress orientations. Furthermore, the data from Svalbard is from a small geographical area with mining activity, and may not be representative for larger areas. The data point from the Atlantic Ocean west of Svalbard has N–S σ_H orientation.

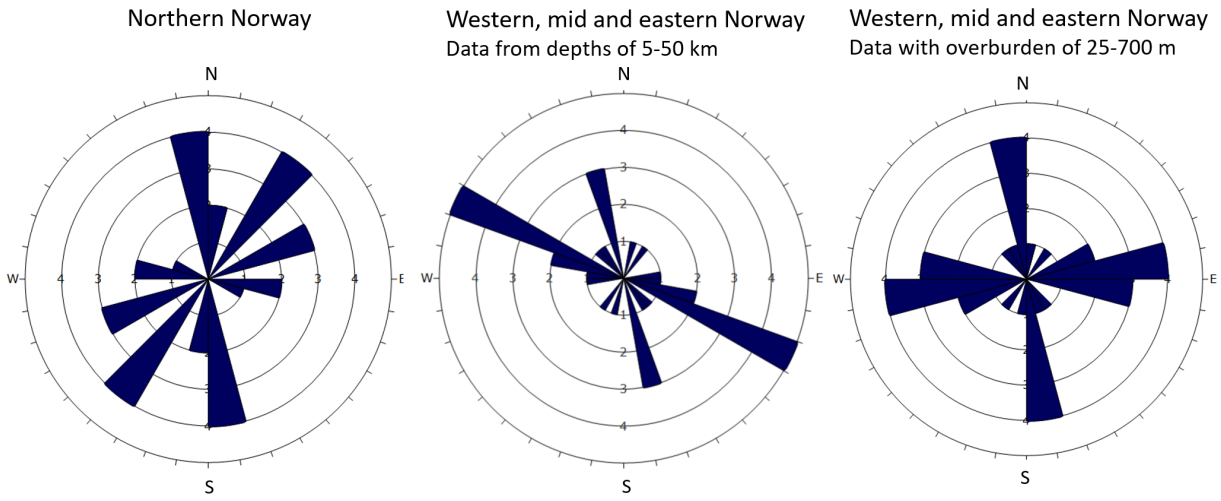

Figure 5.2: σ_H orientations from onshore Norway presented in rosette plots. One arc segment has a width of 15° and each circle represents one data point (created in Dips 7.0).

5.3 Stress Magnitudes

This section presents a discussion of stress magnitudes. This involves a discussion of the magnitude of the vertical stress in relation to the horizontal stress, of tectonic stress regimes and of principal stress ratios. Finally, lithology or age of the rock mass will be discussed in relation to the in situ stress state.

5.3.1 Vertical versus horizontal stress

As stated in Section 2.2.1, the stress state is mainly a result of gravitational stress only if the vertical stress increases linearly with depth with a stress gradient between 0.025 and 0.033 MN/m^3. This interval is based on the unit weigh of rocks since gravitational stress is given by this weight multiplied with overburden and gravitational acceleration (Equation 2.2). The stress gradient of σ_V derived from the data collected in the database is 0.038 (plot is shown in Figure 4.16). This suggests that the in situ stress state is a result of more than the weight of the overlying rock mass.

Table 5.1 supports this statement since $\frac{\sigma_H}{\sigma_V}$ = 1.2, the major horizontal stress is larger than the vertical. If the in situ stress field was purely gravitational, σ_H would be lower than σ_V (evident from Equation 2.3). That σ_H in general exceeds σ_V in the Norwegian region can also

be seen by looking at the tectonic stress regimes in Figure 4.12 and 4.13. Reverse and strike-slip faulting, faulting styles where $\sigma_H > \sigma_V$, make up 64 % of the data records. These results are in opposition to the measurement data also based on focal mechanism data, which covers a greater depth range than the values from Figure 4.16 and Table 5.1. In their work, Fejerskov (1996) and Hanssen (1997) concluded that the tectonic stresses generated by the ridge push effect was likely the main source for the high horizontal stresses observed in the Norwegian region.

However, 36 % of the data records have normal faulting which implies that σ_V is the major stress. Furthermore, the scatter of data is high both when magnitudes are plotted against depth and when the major horizontal stress is plotted against the vertical (Figure 4.16 and Figure A.15 in Appendix A.6.1). Still, the results correlate well with other data from the Norwegian region that has been analysed by Myrvang (1996), Myrvang (2002), Fejerskov (1996) and Hanssen (1997). The high amount of data scatter might reduce the reliability of the values found, but it is probable that the horizontal stress in general exceeds the vertical stress in the Norwegian region.

5.3.2 Tectonic stress regimes

Based on Figures 4.12 and 4.13, it is difficult to identify trends related to tectonic stress regimes. However, from Figure 4.13 it seems that normal faulting is the dominating faulting regime offshore and along the coast of Nordland from 65°– 68° North. This implies that $\sigma_V > \sigma_H > \sigma_h$ in this area. Bungum et al. (2010) stated that sedimentary loading caused by recent erosion has taken place along the coast of Nordland. As mentioned in Section 2.2.2, this creates bending stresses in the crust. These will be located perpendicular to the coast, and are tensional close to the coast and at the continental margin (Fejerskov and Lindholm, 2000). By comparing Figure 4.13 and A.5, it is evident that the points are located at the coast or close to the margin, with σ_H orientation perpendicular to the coast.

Since the ridge push effect works in the same direction as the tensional bending stresses, but have compressional horizontal stresses, the combined effect reduces σ_H. This could explain why $\sigma_V > \sigma_H > \sigma_h$ in this area. However, this trend is based on a limited data amount which

may be too low to state that this is a general trend for the area. Furthermore, in order to conclude that there exists a trend for an area, the depths of the data records have to be considered. In general, the vertical stress exceeds the horizontal stress with increasing depth (Amadei and Stephansson, 1997). The points that have normal faulting are located at depths from 10–20 km, whereas the deepest point has strike-slip faulting and is located at a depth of 30 km. It can therefore not be seen any clear correlation between stress regime and depths in this area.

Hanssen (1997) investigated tectonic stress regimes for western Fennoscandia and observed a trend based on his data. In the upper 1000 m of the crust, reverse faulting was observed. This was followed by strike-slip faulting and then normal faulting deeper in the Earth's lithosphere. This trend is not observed from the 70 records in the database with information about relative stress magnitudes between the horizontal stresses and the vertical. On the contrary, the deepest records from focal mechanism have reverse faulting.

5.3.3 Stress ratios

Table 5.1 presents the ratio between the principal stresses. These ratios are taken from Figure A.7, A.8 and A.9 in Appendix A.6.1. The ratios coincide well with the values found by Hudson (2010). Hudson (2010) presented a table of mean principal stress ratios from different countries (Australia, Chile, UK and Finland). The ratios from the different countries gave similar values where the average values were: $\frac{\sigma_2}{\sigma_3}$ = 1.6, $\frac{\sigma_1}{\sigma_2}$ = 1.5 and $\frac{\sigma_1}{\sigma_3}$ = 2.6. From Appendix A.6.1, it also looks like the data points are quite clustered around the trend line with about equal amount of scatter for the three graphs.

The consistency of the in situ rocks stress data from different countries is according to Hudson (2010) caused by the fractured rock mass. Since the rock mass to a degree is fractured, it can only sustain certain stress ratios. Harrison et al. (2007) concluded that this consistency supports the hypothesis that the Earth's crust is in a limiting state of equilibrium (Harrison et al., 2007). Harrison et al. (2007, 676) also stated that the reduction of scatter in Figure 4.15 (principal stress magnitudes against average magnitude of the principal stresses) compared with Figure 4.14 (principal stress magnitudes against overburden), implied that there is control on the principal stress magnitudes within the Earth's crust at any given point.

The graphs for $\frac{\sigma_H}{\sigma_V}$, $\frac{\sigma_h}{\sigma_V}$ and $\frac{\sigma_h}{\sigma_H}$ (Appendix A.6.1) show more scatter and the data points are less clustered around the trend line than the graphs for $\frac{\sigma_2}{\sigma_3}$, $\frac{\sigma_1}{\sigma_2}$ and $\frac{\sigma_1}{\sigma_3}$. Out of the graphs with horizontal and vertical stresses, the graph showing $\frac{\sigma_h}{\sigma_H}$ has the least amount of data scatter. It is also the graph with most data points. Zang et al. (2012) presented similar results for horizontal and vertical stress ratios, and found that the $\frac{\sigma_h}{\sigma_H}$ ratio also seemed to be independent on lithology. They concluded that this correlation was caused by σ_H's direct relationship with σ_h. According to Zang et al. (2012), σ_h is determined from field measurements and σ_H is then often derived from direct correlation with σ_h.

Table 5.1: Mean stress ratios.

Principal stresses			Horizontal and vertical stresses		
$\frac{\sigma_2}{\sigma_3}$	$\frac{\sigma_1}{\sigma_2}$	$\frac{\sigma_1}{\sigma_3}$	$\frac{\sigma_H}{\sigma_V}$	$\frac{\sigma_h}{\sigma_V}$	$\frac{\sigma_h}{\sigma_H}$
1.5	1.4	1.9	1.2	0.8	0.5

5.3.4 Lithology and geological age

Table 5.2 presents a summary of stress gradients and ratios calculated from the data collected in the database separated according to lithology and geological period. The stress gradients are from Figures 4.17 and 4.18, while the ratios are from Figures A.10, A.11, A.12, A.13 and A.14 in Appendix A.6.1. There are only three data points in sedimentary rock with σ_3 magnitude, thus calculations involving σ_3 have not been carried out for sedimentary rocks.

Table 5.2: Different stress gradients and ratios separated by lithology and geological age.

Stress ratio	**All entries***	**Lithology**		**Geological period**	
		Sedimentary	Igneous/Metamorphic	Cambrian-Silurian	Precambrian
σ_1/z	0.047	0.054	0.044	0.043	0.047
σ_2/z	0.031	0.038	0.029	0.028	0.030
σ_3/z	0.023		0.023	0.017	0.025
σ_2/σ_3	1.45		1.42	1.78	1.36
σ_1/σ_2	1.44	2.06	1.36	1.46	1.35
σ_1/σ_3	1.90		1.86	2.24	1.80

*All entries also include the records without information about lithology and/or geological period

Lithology

From Figure 4.17 it is evident that the sedimentary data points have higher stresses than those from igneous and metamorphic rocks. From Table 5.2 it can be seen that the stress gradients for all data entries (sedimentary, igneous, metamorphic and data points without information about lithology) for σ_1, σ_2 and σ_3 are 0.045, 0.029 and 0.023. The gradients for igneous and metamorphic rocks are 0.044, 0.029 and 0.023, about equal to those for all data entries. For sedimentary rocks the gradients for σ_1 and σ_2 are 0.054 and 0.038 σ_2.

That the sedimentary rocks have higher stress gradients than igneous and metamorphic rocks is opposite of what Zang et al. (2012) found in their analysis that was based on 1278 data records. A possible explanation for the contradictory results can be the number of data points and location of these points. Only six data points in the database have information about principal stress magnitudes and are in sedimentary rocks. These six points could be affected by local factors and may therefore not be representative for larger areas.

Additionally, four of the six points are from the same area on Svalbard. Figure 5.3 shows σ_H and σ_h for Svalbard and Norway plotted against overburden. To compare horizontal stresses rather than principal stresses was chosen because there are more data points with information about horizontal stresses than principal stresses on Svalbard (13 and 11 compared with seven and five). There are only three data points with σ_V magnitude from Svalbard, so it was therefore not included.

From Figure 5.3 it can be seen that the data points from Svalbard have higher σ_H and σ_h magnitudes than those from mainland Norway. σ_H has a stress gradient of 0.058 on Svalbard compared with 0.047 in Norway and 0.032 compared with 0.029 for σ_h. The sedimentary rocks can therefore have higher stresses because the in situ stresses in general are higher on Svalbard than in Norway. However, the difference in stress magnitude is small for σ_h. To state with more certainty if the stresses are higher on Svalbard, more data is needed. It would also be useful to compare the principal stresses σ_1, σ_2 and σ_3.

Another reason why the results conflict with those found by Zang et al. (2012), could be the overburdens of the data points. It can be seen from Figure 4.17 that the igneous and metamorphic rocks cover a greater depth range than the sedimentary rocks. The deepest point in

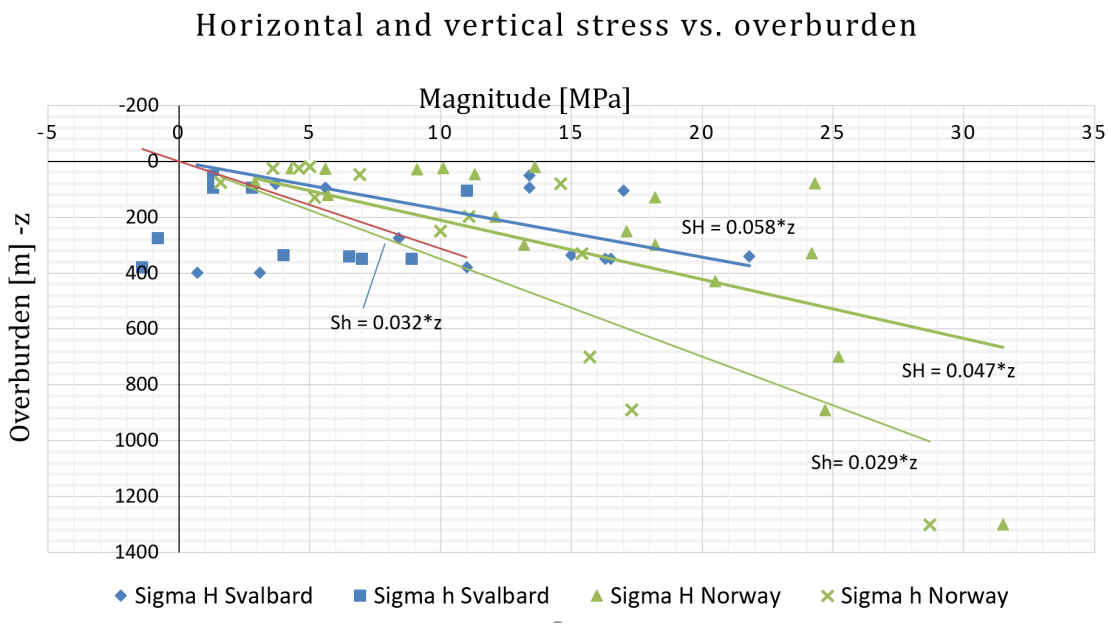

Figure 5.3: Horizontal and vertical stress magnitudes plotted against overburden where data entries are separated by Svalbard and Norway (created in Microsoft Excel).

igneous or metamorphic rocks has an overburden of 1300 m, whereas the deepest point located in sedimentary rock has an overburden of 400 m. Variation of stress gradients related to overburden will be discussed in more detail later in this section.

The $\frac{\sigma_1}{\sigma_2}$ stress ratio for sedimentary rocks is one of the ratios that deviates most compared with for all entries in Table 5.2 (a value of 2.06 compared with 1.44). A ratio of 2.06 for sedimentary rocks means that σ_1 in average is about twice as big as σ_2 for sedimentary rocks. This ratio is higher than all the $\frac{\sigma_1}{\sigma_2}$ ratios Hudson (2010) presented for Australia, Chile, UK and Finland. The sedimentary data points are located in sandstone, limestone and claystone. These rocks are layered sedimentary rocks and in Section 2.3.1 it is stated that these rock types show distinct anisotropy. That the rocks are anisotropic may contribute to a more anisotropic stress field.

The principal stress ratios for igneous and metamorphic rocks are $\frac{\sigma_2}{\sigma_3}$ = 1.42, $\frac{\sigma_1}{\sigma_2}$ = 1.36 and $\frac{\sigma_1}{\sigma_3}$ = 1.86. This is close to the ratios for all entries for $\frac{\sigma_2}{\sigma_3}$ and $\frac{\sigma_1}{\sigma_3}$, and slightly below for $\frac{\sigma_1}{\sigma_2}$. The data points also seem to be quite clustered around the trend lines for all three ratios, which could improve the reliability of the results. That the igneous and metamorphic ratios are closer to the ratios of all entries, may be a related to number of data points. There are 23 data points in igneous and metamorphic rocks compared to 35 for all entries and six in

sedimentary rocks.

The $\frac{\sigma_1}{\sigma_2}$ ratio for igneous and metamorphic rocks is 1.42, which is slightly below the ratio for all entries. The data points are located in gneiss (mica, granite, tonalite and not specified), granite, basalt, greenstone and rhyolite. Mica gneiss is a metamorphic rock type known to have foliation, and should therefore show distinct anisotropy (see Section 2.3.1). However, there is only one data record located in this rock type and none of the other rock types are known to show distinct anisotropy. The lower degree of stress anisotropy compared with sedimentary rocks may reflect that these rocks are more isotropic than the sedimentary rocks.

Geological age

Myrvang (1996) stated that Precambrian rocks and Permian intrusion in general have higher stresses than average in Norway, while Cambrian-Silurian rock types have lower stresses than average (see section 2.4). There is only one point located in Permian rocks with principal stress magnitudes, but the stress gradients for Precambrian rocks give stress gradients for σ_1, σ_2 and σ_3 of 0.047, 0.03 and 0.025. The rocks of Cambrian-Silurian age give stress gradients of 0.043, 0.028 and 0.017 for σ_1, σ_2 and σ_3. The values are presented in Figure 4.18 and Table 5.2.

The σ_1, σ_2 and σ_3 stress gradients for all data entries are 0.045, 0.029 and 0.023. All entries are made up of points from Cambrian-Silurian, Precambrian, Carboniferous-Permian, Paleogene-Neogene (see Appendix A.3 for geological time scale) and points without information about age. The gradients for Precambrian rocks are slightly higher than these values, whereas the Cambrian-Silurian rocks are slightly below. Thus, the stress gradients found for Precambrian and Cambrian-Silurian rocks support Myrvang (1996)'s statements.

However, these results are only based on ten points in Cambrian-Silurian rocks and 13 in Precambrian rocks, compared with 35 for all entries. This limited amount of data may give unreliable results. An illustration of this can be seen in Figure 5.4 where the two deepest points for each geological period are removed and the stress gradients increase significantly. The lowest increase in stress gradient is 1.5 times for σ_3 in Cambrian-Silurian rocks and the highest increase is 2.5 times for σ_2 in Precambrian rocks. That all the stress gradients are higher at more shallow depths may indicate that the shallower points are more affected by local factors.

It is also stated in Section 2.3.1 that anisotropy decreases with increasing depth. Since most of the data points have overburdens of less than 500 m, the results may only be representative for the stress state at shallow depths. Based on the results from Figure 5.4, it seems that the stress gradients would be lower if there are more points located deeper. However, the rocks of Precambrian age still have higher gradients than those of Cambrian-Silurian.

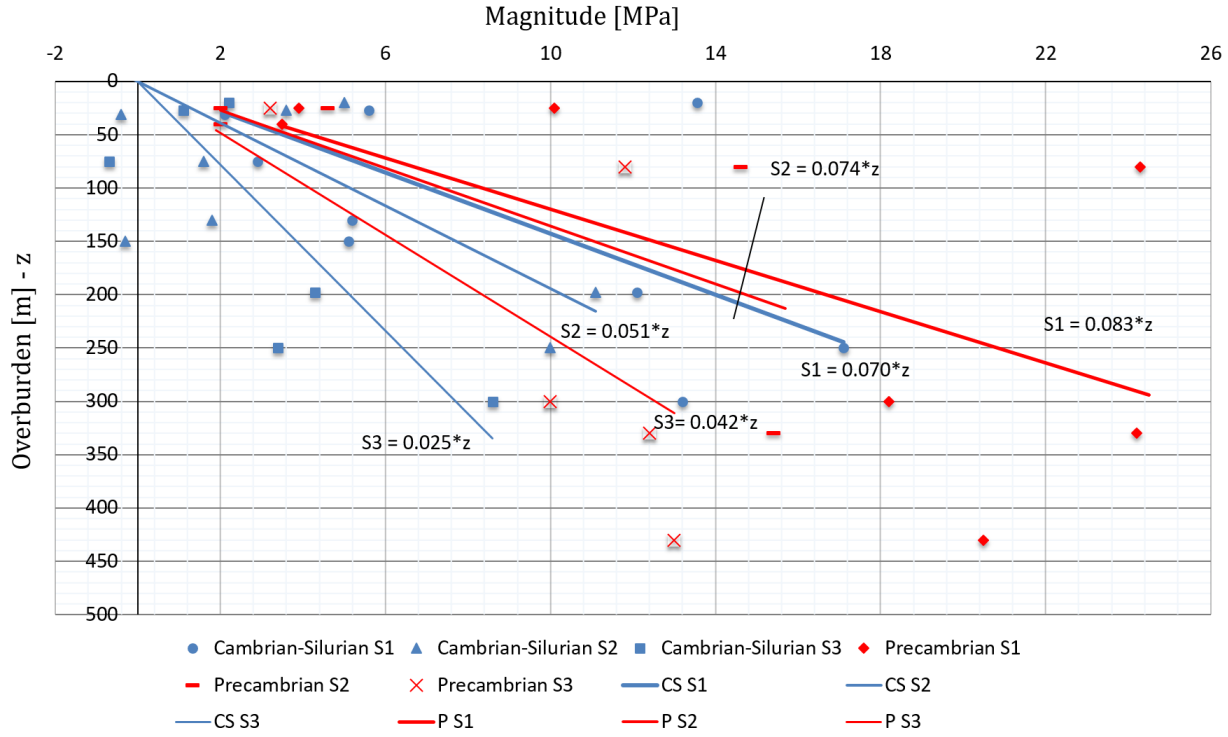

Figure 5.4: Principal stress σ_1 (S1), σ_2 (S2) and σ_3 (S3) magnitudes separated according to geological age of rocks plotted against overburden. The deepest points for each geological period are removed (created in Microsoft Excel).

The principal stress ratios $\frac{\sigma_2}{\sigma_3}$, $\frac{\sigma_1}{\sigma_2}$ and $\frac{\sigma_1}{\sigma_3}$ for Cambrian-Silurian rocks are found to be 1.78, 1.46 and 2.24. This is higher than those for all data entries for $\frac{\sigma_2}{\sigma_3}$ and $\frac{\sigma_1}{\sigma_3}$, although the values for $\frac{\sigma_1}{\sigma_2}$ and $\frac{\sigma_1}{\sigma_3}$ coincide well with those found by Hudson (2010). The rocks of Cambrian-Silurian age are granite, mica schist, limestone, mica gneiss, amphibolitic augen gneiss, greenstone and phyllite. This is a combination of sedimentary, igneous and metamorphic rock types. The stress ratio of $\frac{\sigma_1}{\sigma_2}$ for Cambrian-Silurian rocks is in between the ratio for sedimentary and for igneous and metamorphic rocks. This might support the statement that rock anisotropy affects relative stress magnitudes. Still, as stated when looking at the principal stress gradients, the data amount is small and it might be difficult to draw reliable conclusions from the data.

For Precambrian rocks, all the ratios are lower than average with values of 1.36, 1.35 and 1.8 for $\frac{\sigma_2}{\sigma_3}$, $\frac{\sigma_1}{\sigma_2}$ and $\frac{\sigma_1}{\sigma_3}$. The ratios are close to those obtained from igneous and metamorphic rocks. The amount of scatter in the graphs is also about equal that of the graphs for igneous and metamorphic rocks presented in Appendix A.6.1. The rocks of Precambrian age are gneiss (granite, tonalite and not specified), granite and rhyolite. These rock types are all either igneous or metamorphic, which means that the calculations are based on the same data.

The $\frac{\sigma_2}{\sigma_3}$ ratio for rocks of Cambrian-Silurian age is one of the ratios that deviates most from the ratios for all entries in Table 5.2. This could be related to other factors than rock type. Possible explanations could include location, position or overburden range for the data points. The results might be affected by local factors if the points are from the same area, or by topography if the points are shallow or in area with mountains and fjords. Out of the Cambrian-Silurian data points, 40 % are from mountain sides. Four of the points are from Rogaland, two from Oslo, one in Nordland, Hordaland, Hedmark and Oppland. Overburden for the Cambrian-Silurian rocks ranges from 20 m to 890 m. Whereas 12 % of all the data entries in the database are from mountain sides. If only looking at onshore data, the percentage increases to 34 %. The onshore data covers an overburden range from 11 to 1300 m.

The percentage of data located in mountain sides is similar when only comparing onshore data. The data of Cambrian-Silurian age is mainly located in western and eastern Norway, but it is spread over multiple counties. The overburden range is smaller than for all onshore data points. The deepest point from all onshore data, located in Precambrian rock, has an overburden of 300 m more than the deepest in Cambrian-Silurian rocks. As mentioned, it seems that the stress gradients decrease if more data with overburden of more than 500 m is added (seen from Figure 5.4). However, even though the stress gradients may be affected by overburden range, it is not certain that the ratios would change. For the $\frac{\sigma_2}{\sigma_3}$ ratio to decrease, σ_2 must be more affected by the change in overburden range than σ_3. This seems to be the case in Figure 5.4, but there are too few points to state that this generally is the case. Thus, it is difficult to identify any trends that can explain why some of the stress ratios deviate from the values found for all entries, which possibly can be related to the small data amount as well.

5.4 Topographical Effects

As discussed in Section 2.3.5, topography can affect the stress field by redistributing the principal stresses. In areas with mountains and fjords/valleys, the topography often forces the stresses to align with the fjords or valleys (Fejerskov et al., 2000). Four points that are located in such areas that have information about stress magnitudes and overburden will be discussed in this section. The points that will be discussed are marked by the circles in Figure 5.5.

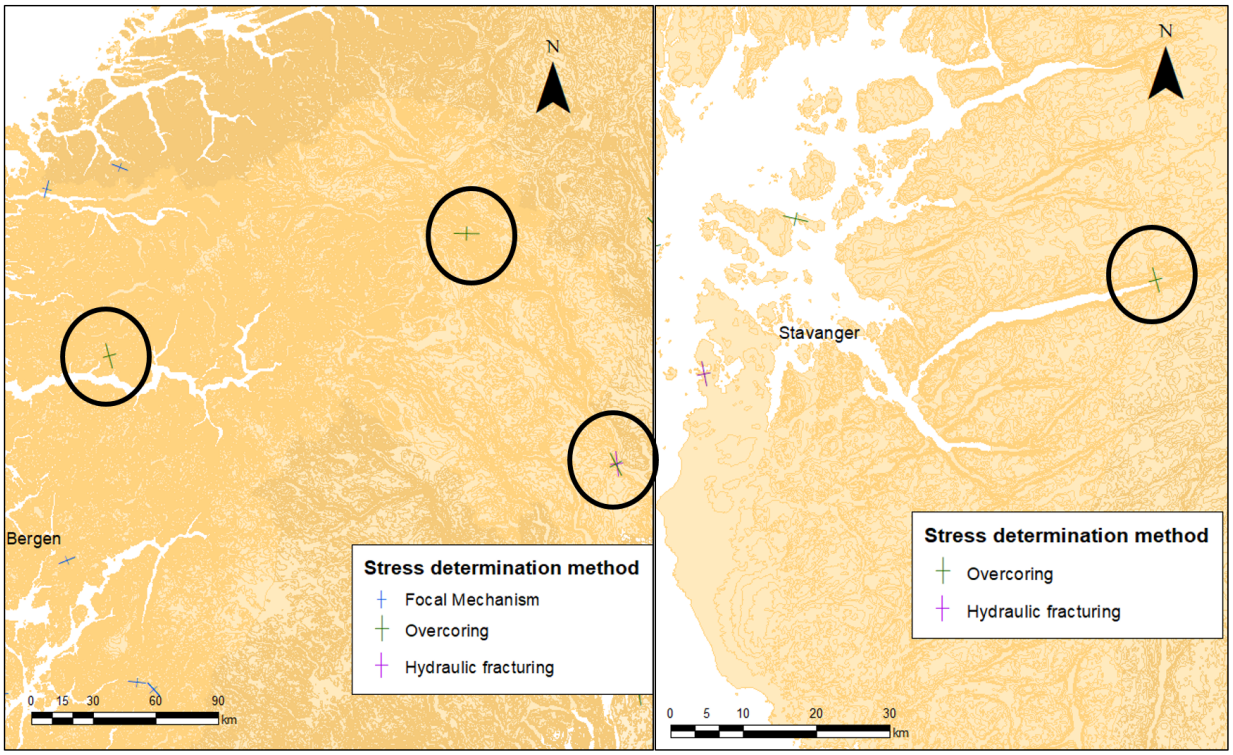

Figure 5.5: Points marked by circle from left to right: Eiriksdal hydropower plant, Nedre Otta hydropower plant, Gøvik olympiske fjellhall and Lysebotn 2 hydropower plant. The symbols show σ_H orientation (created in ArcMap 10.6).

Figure 5.6 shows the data point from Eiriksdal hydropower plant. Overcoring has been carried out at this location with an overburden of about 330 m. The distance to and gradient of the mountain side have been estimated to be around 230 m and 0.57. Figure 5.6a shows σ_1 orientation given by azimuth, whereas Figure 5.6b shows the profile of the mountain side where Eiriksdal hydropower plant is located. The point is not precisely located.

From Figure 5.6a it can be seen that σ_1 is orientated perpendicular to the mountain side. σ_1 has the same orientation as σ_H and dips 12° from the horizontal plane, σ_2 and σ_3 dips 4° and

77° from the horizontal plane. The principal stress field is thus located approximately in the horizontal and vertical plane where $\sigma_1 \approx \sigma_H$ and $\sigma_3 \approx \sigma_V$. According to Section 2.3.5, σ_1 will be either parallel or perpendicular to the slope if it is affected by the topography. σ_1 will be parallel with the slope if $\sigma_H > \sigma_V$. This disagrees with the stress field presented in Figure 5.6a since $\sigma_1 \approx \sigma_H$ and perpendicular to the slope. The distance to the mountain side of ≈ 230 m implies that the point is not located close to the slope surface (can also be seen in Figure 5.6b). Therefore, the effect of topography may be lower which could explain why σ_1 is not oriented parallel with the slope.

The magnitudes of σ_1, σ_2 and σ_3 are 24.2, 15.4 and 12.5 MPa. These magnitudes are higher than what Equations 2.2 and 2.3 give for gravitational stress, which means that the stress state is affected by more than the overlying weight. As previously mentioned, it is likely that the mid-Atlantic plate spreading contributes to high horizontal stresses in the Norwegian region. Still, the horizontal stresses measured at Eiriksdal hydropower plant are quite high. The measurement point is located at the same level as the bottom of the fjord. This is in proximity to point 1 in Figure 2.8. In Section 2.3.5 it is stated that the bottom of fjords or valleys will have horizontal stress concentration. The high stresses measured can therefore be a combination of both tectonic stresses and stress concentration caused by the topography.

Figure 5.7 shows the measurement point from Nedre Otta hydropower plant. Overcoring has been carried out at this location with an overburden of about 250 m. The distance to and gradient of the mountain side have been estimated to be around 170 m and 0.9. Figure 5.7a shows the orientation of σ_1 given by azimuth, whereas Figure 5.7b shows the profile of the mountain side where Nedre Otta hydropower plant is located. The point is however not precisely located.

From Figure 5.6a it can be seen that σ_1 is perpendicular to the mountain side. σ_1, σ_2 and σ_3 dips 51°, 6° and 39° from the horizontal axis, which implies that $\sigma_V > \sigma_H$. This is confirmed by the measured magnitudes σ_V = 11.7 MPa and σ_H = 10.3 MPa. Unlike in Figure 5.6a, σ_1 is orientated downhill parallel with the slope surface. This σ_1 orientation coincides well with the theory presented in Section 2.3.5, which states that σ_1 will be parallel with the slope surface if $\sigma_V > \sigma_H$ when affected by topography. Compared with Figure 5.6b, this point is located closer to the slope surface and it therefore seems likely that the stress state will be more affected by

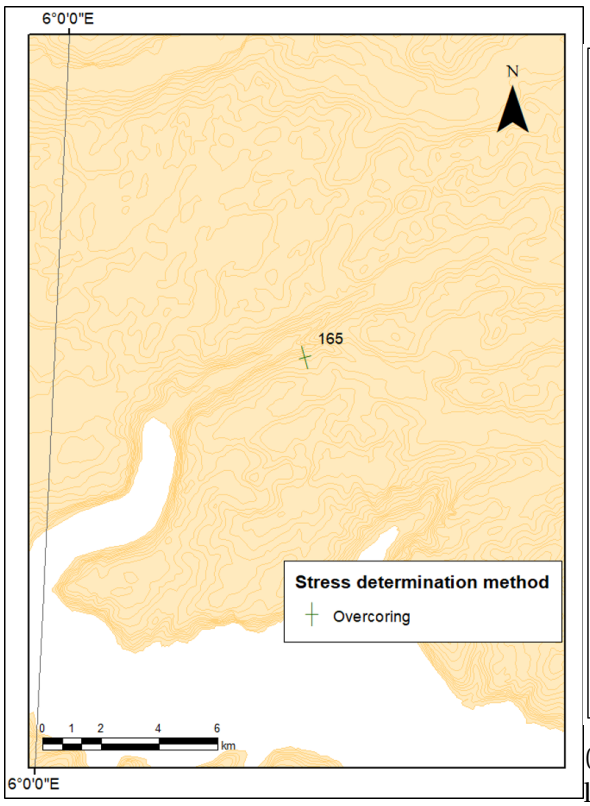

(a) Map with σ_1 orientation and azimuth (created in ArcMap 10.6).

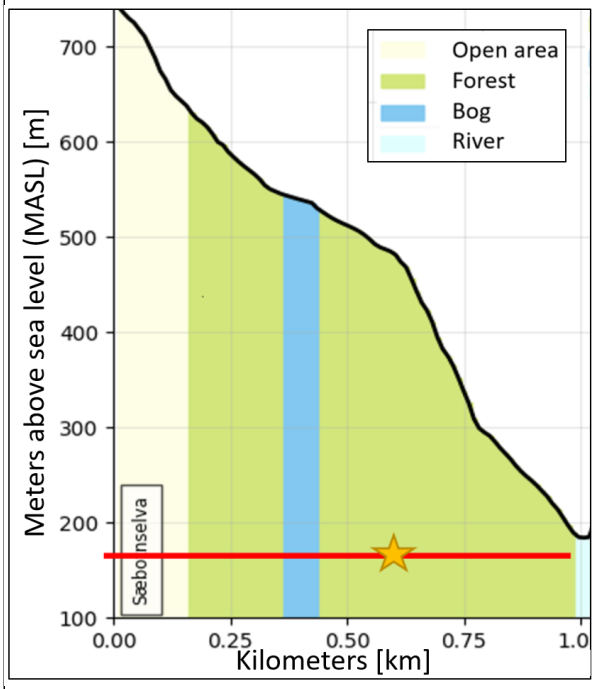

(b) Profile of mountain side, measurement point location is indicated by star. Colours represent surface terrain (created at kartverket.no).

Figure 5.6: In situ rock stress data point from Eiriksdal hydropower plant, Sogn og Fjordane.

the topography. In addition, the gradient of the mountain side is higher which means that this slope is steeper. A steep mountain side may affect the stress orientation more than a gentler mountain side.

Figure 5.8 shows two measurement points from Gjøvik olympiske fjellhall, one with hydraulic fracturing and one with overcoring. Hydraulic fracturing was carried out with an overburden of 40 m and overcoring with 25 m. The gradient of the mountain side is 0.3. The distance to mountain side was not possible to estimate due to the inaccurate position of the measurement point.

In Figure 5.8, σ_H orientations are presented since the orientations of σ_1 are unknown. From the Figure it can be seen that the σ_H orientations are oriented parallel with the mountain side. These orientations agree with the theory presented in Section 2.3.5 since the horizontal stresses are slope-parallel. However, the mountain side gradient indicates that it is more a hill side than a mountain side. This may limit the topographical effect on the in situ stress field.

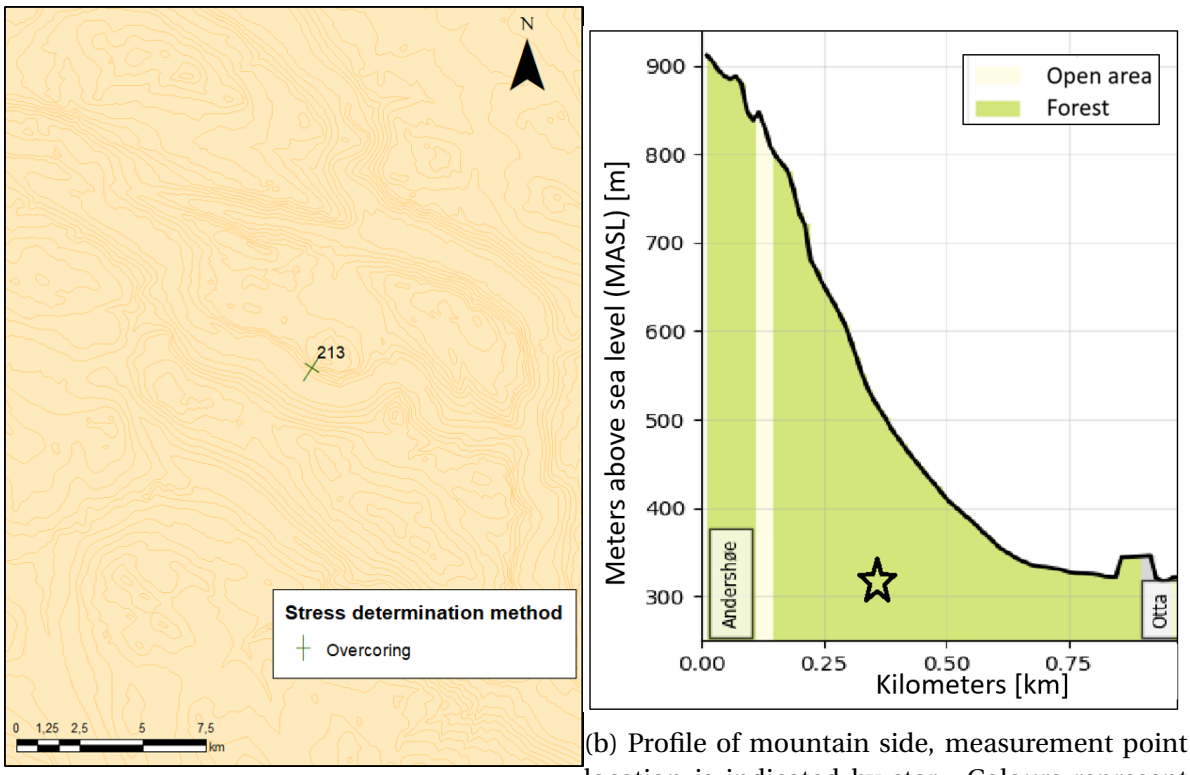

(a) Map with σ_1 orientation and azimuth (created in ArcMap 10.6).

(b) Profile of mountain side, measurement point location is indicated by star. Colours represent surface terrain (created at kartverket.no).

Figure 5.7: In situ rock stress data point from Nedre Otta hydropower plant, Oppland.

Still, based on the overburdens of 40 m and 25 m it could be assumed that the measurement points are located relatively close to the slope surface. The measurement points may therefore be affected by the slope, which the σ_H orientations indicate.

Figure 5.9 shows the measurement point from Lysebotn 2 hydropower plant. Overcoring has been conducted with an overburden of about 700 m. It was not possible to determine either gradient of or distance to the mountain side since position of the point is uncertain. From the Figure it can be seen that σ_1 orientation for Lysebotn hydropower plant is perpendicular to the mountain side. σ_1 dips 23° from the horizontal plane, whereas σ_2 and σ_3 dips 6° and 66° from the horizontal plane. σ_H has same orientation as σ_1, which differs from the theory presented in Section 2.3.5 in same way as the point from Eiriksdal hydropower plant does. Due to the unknown location of the measurement point, it was not possible to create a profile of the mountain side. However, the point has an overburden of 700 m and is located -50 MASL (50 m below sea level). It can therefore be possible that the point lies deep enough so that the stress orientation will not be affected by the slope surface.

The magnitudes of σ_H, σ_h and σ_V are 23.1, 15.9 and 13.1 MPa. The vertical stress is lower than the theoretical gravitational (Equation 2.2), while the horizontal stresses are higher (Equation 2.3). The magnitude of the horizontal stresses can be a result of the stress concentration caused by topography if the measurement point is located close to point 1 in Figure 2.8. The exact position of the measurement point is as stated unknown, so it is uncertain if it is close enough to point 1 in Figure 2.8 for the topography to affect the stress field. If it is not, the high horizontal stresses will be a result of other factors than topography. A possible factor could be tectonic stresses related to the ridge push effect as previously discussed.

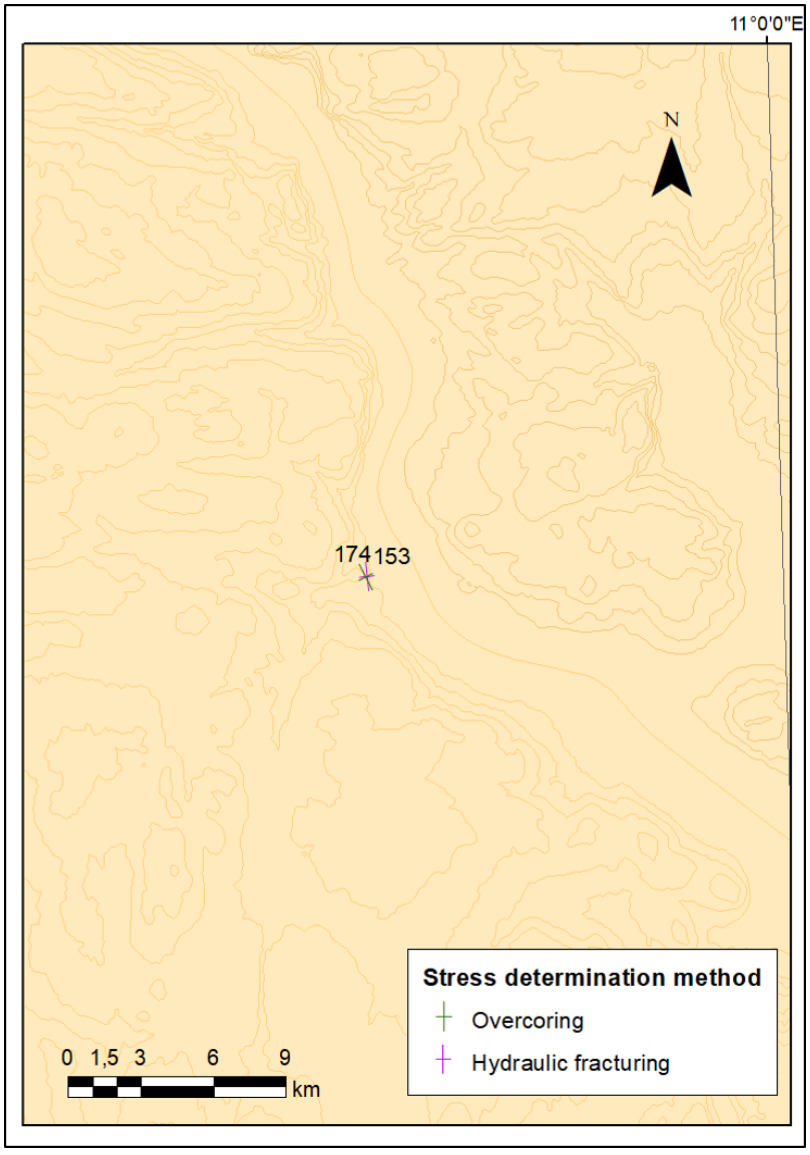

Figure 5.8: Map with σ_H orientation and azimuth for Gjøvik olympiske fjellhall, Oppland (created in ArcMap 10.6).

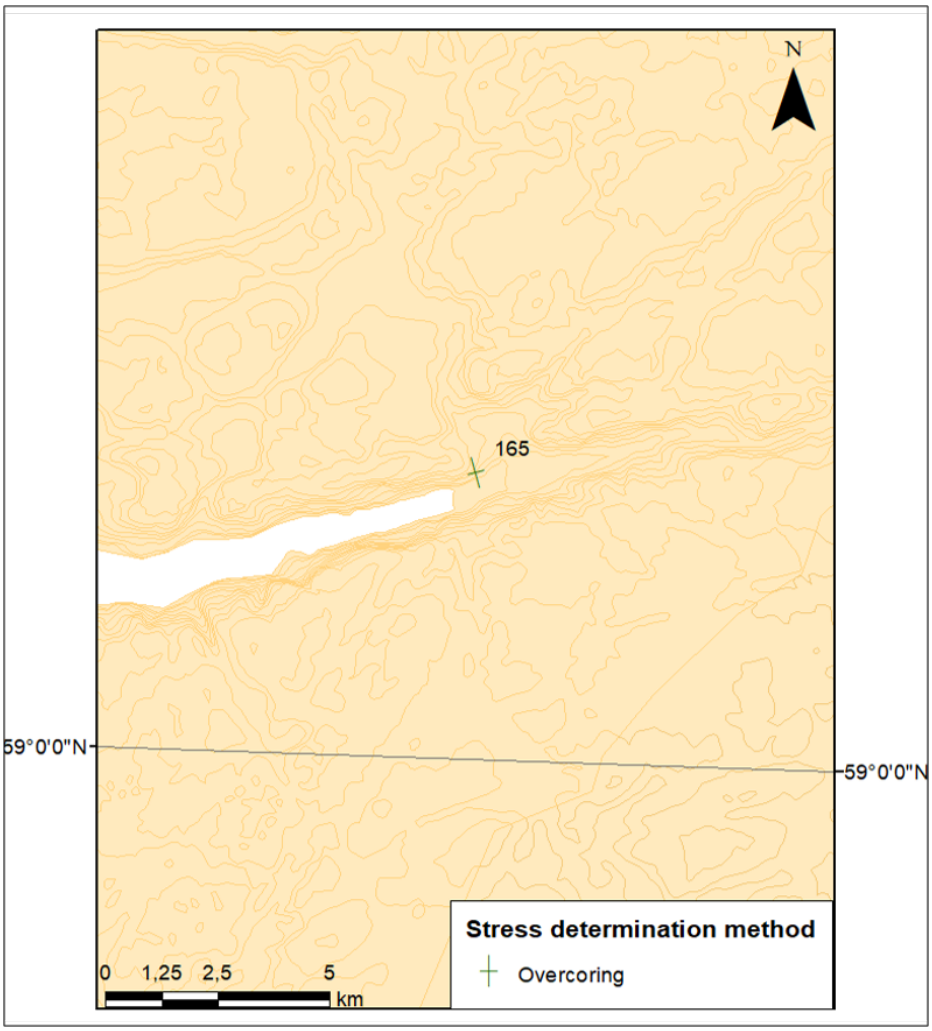

Figure 5.9: Map with σ_1 orientation and azimuth for Lysebotn hydropower plant, Rogaland (created in ArcMap 10.6).

Chapter 6

Conclusion

The main objectives of this thesis have been to develop an updated Norwegian in situ rock stress database and to collect existing in situ rock stress data to fill the database. The database consists of four tables where one serves as the main table. The main table contains information about the in situ stress field, description of locations with focus on overburden and topography and information regarding bedrock. The other tables contain test data from rock stress measurements and data uncertainty. There have been collected 115 data records that have been obtained with borehole breakout analysis, drilling-induced-fractures, focal mechanism, hydraulic fracturing and overcoring. From the analysis of this data, following conclusions have been made:

- There was much scatter in the data; especially for onshore stress orientations and stress magnitudes. For stress magnitudes, the amount of scatter was reduced when the principal stresses were plotted against each other and against the average value of the three principal stresses.
- Offshore, the main σ_H orientation trends were N–S and WNW–ESE. These trends were consistent with the ridge push effect from the mid-Atlantic ridge. However, the orientations also coincided with other mechanisms; the density contrast at the continental margin in the Barents Sea and the sediment loading on the continental shelf in the Norwegian Sea.
- Onshore, the σ_H orientations seemed to depend on depth in western, central and east-

ern Norway. Data from depths of 5–50 km mainly had a WNW–ESE σ_H orientation, while the data with overburdens of 25–1300 m exhibited a NE–SW orientation around Oslo and a N–S orientation in western Norway. A WNW–ESE σ_H orientation agrees with the ridge push effect, while the shallow orientations could be the results of local features like topography and geological structures.

- The horizontal stress generally exceeded the vertical, which can be seen by $\frac{\sigma_H}{\sigma_V} = 1.2$ and that 64 % of the data had reverse or strike-slip faulting. Tectonic stresses from the mid-Atlantic ridge could be the reason for this, since $\sigma_H > \sigma_V$ is not possible in a purely gravitational stress field.

- Sedimentary rocks had higher stress gradients than igneous and metamorphic rocks, which was unexpected. It seemed that the gradients were dependent on the overburden of the data points and decreased with increasing overburden. All the sedimentary points were located at shallow depths and the high gradients could be a consequence of this. The sedimentary rocks also had more stress anisotropy than igneous and metamorphic rocks. This may indicate that stress anisotropy is positively correlated to rock anisotropy, since the sedimentary rocks were layered rock known to show distinct anisotropy. However, the calculations were based on small data sets which reduces the reliability of these results.

- Rocks of Precambrian age had higher stress gradients than rocks of Cambrian-Silurian age. This was expected based on Myrvang (1996)'s statements. However, these calculations were also based on small data sets.

- The effect of topography on the in situ stress field was evaluated by studying four data points located in mountain sides. It seemed that the effect topography had on the principal stress orientations decreased inwards in the rock mass. There were also indications of high horizontal stresses beneath the valleys, which corresponds to known theory.

Overall, a larger amount of data with more information about stress magnitudes would have been advantageous because it could have improved the reliability of the results. More data with σ_H orientation from central, southern and northern Norway would also be desirable since there were few points from these areas.

Chapter 7

Further Work

The results presented in this thesis show the need for more data both in relation to stress orientations and stress magnitudes. Further work will therefore involve collecting more in situ rock stress data from the Norwegian region. In addition, expansion of the database might be necessary if data from other stress determination methods than borehole breakout analysis, drilling-induced-tensile fractures, focal mechanism, hydraulic fracturing and overcoring is compiled. This can be done by creating tables and forms for new methods, and include them in the main form. If testing data for borehole breakouts and drilling–induced fractures is obtained, testing tables must be created for these methods as well. Finally, a quality ranking scheme that makes the data obtained with different methods comparable with each other should be developed.

Bibliography

Amadei, B., Savage, W. Z., and Swolfs, H. S. (1987). Gravitational stresses in anisotropic rock masses. *International Journal of Rock Mech., Min. Sci.& Geomech. Abstracts*, 24(1):5–14.

Amadei, B. and Stephansson, O. (1997). *Rock Stress and Its Measurements*. Chapman & Hall, Cambridge, 1 edition.

Ask, M. V. S., Ask, D., Elvebakk, H., and Olesen, O. (2015). Stress Analysis in Boreholes Drag Bh and Leknes Bh, Nordland, North Norway. *Rock Mechanics and Rock Engineering*, 48(4):1475–1484.

Brown, E. T. and Hoek, E. (1978). Trends in relationship between measured in situ stresses and depth. *International Journal of Rock Mech., Min. Sci.& Geomech. Abstracts*, 14:211–215.

Bungum, H., Olesen, O., Pascal, C., Gibbons, S., Lindholm, C., Vestol, O., Pascal, C., Stewart, I. S., and Vermeersen, B. L. A. (2010). To what extent is the present seismicity of Norway driven by post-glacial rebound? *Journal of the Geological Society, London*, 167(2):373–384.

Carafa, M. M. C. and Barba, S. (2013). The stress field in Europe: optimal orientations with confidence limits. *Geophysical Journal International*, 193(2):531–548.

Cronin, V. (2010). *A primer on focal mechanism solutions for geologist*. Baylor University, Texas.

Fejerskov, M. (1996). *Determination of in-situ rock stress related to petroleum activities on the Norwegian Continental Shelf*. PhD thesis, Norwegian University of Science and Technology, Trondheim.

Fejerskov, M. and Lindholm, C. (2000). Crustal stress in and around Norway – an evaluation of

stress generating mechanisms. In Nøttvedt, A., editor, *Dynamics of the Norwegian Margin*, volume 167, pages 451–467. Geological Society, London, Special Publications, Bath.

Fejerskov, M., Lindholm, C., Myrvang, A., and Bungum, H. (2000). Crustal stress in and around Norway – a compilation of in situ stress observations. In Nøttvedt, A., editor, *Dynamics of the Norwegian Margin*, volume 167, pages 441–449. Geological Society, London, Special Publications, Bath.

Haimson, B. C. and Cornet, F. H. (2003). ISRM Suggested Methods for rock stress estimation—Part 3: hydraulic fracturing (HF) and/or hydraulic testing of pre-existing fractures (HTPF). *International Journal of Rock Mechanics and Mining Sciences*, 40:1011–1020.

Haimson, B. C. and Herrick, C. G. (1986). Borehole breakouts - a new tool for estimating in situ stress? In *International Symposium on Rock Stress and Rock Stress Measurements*, pages 271–281, Stockholm. Centek Publisher.

Hanssen, T. H. (1997). *Investigations of some rock stress measuring techniques and the stress field in Norway*. PhD thesis, Norwegian University of Science and Technology, Trondheim.

Harrison, J. A., Hudson, J. P., and Carter, J. N. (2007). Is there a relation between the in situ principal stress magnitudes in rock masses? In *Proceedings of the 1st Canada-US Rock Mechanics Symposium – Rock Mechanics Meeting Society's Challenges and Demands*, volume 1, pages 675–682, Vancouver.

Harrison, J. P. and Hudson, J. A. (2000). *Engineering Rock Mechanics, Part 1 - An Introduction to the Principles*. Elsevier Science Ltd., Kidlington.

Harrison, J. P. and Hudson, J. A. (2001). *Engineering Rock Mechanics: Part 2: Illustrative Worked Examples*. Elsevier Science Ltd., The Netherlands.

Heidbach, O., Tingay, M., Barth, A., Reinecker, J., Kurfeß, D., and Müller, B. (2010). Global crustal stress pattern based on the World Stress Map database release 2008. *Tectonophysics*, 482(1):3–15.

Hillis, R. R., Enever, J. R., and Reynolds, S. D. (1999). In situ stress field of eastern Australia. *Australian Journal of Earth Sciences*, 46:813–825.

Hudson, J. A. (2010). Stresses in rock masses: A review of key points. In *EUROCK 2009 -Rock Engineering in Difficult Ground Conditions – Soft Rocks and Karst*, pages 61–72, Dubrovnik. ISRN.

Hyett, A. J. (1990). *The potential state of stress in a naturally fractured rock mass*. PhD thesis, Imperial College, University of London.

Jaeger, J. C., Cook, N. G. W., and Zimmerman, R. W. (2007). *Fundamentals of rock mechanics*. Blackwell Publishing Ltd, Singapore, 4 edition.

Larsen, T. E. (2017). E-mail. Private Communication. 04 December 2017.

Lee, W. H. K. and Stewart, S. W. (1981). Methods of data analysis. In *Principles and Applications of Microearthquake Networks*. Academic Press Inc., USA.

Leeman, E. R. (1969). The 'Doorstopper' and triaxial rock stress measuring instruments developed by the C.S.I.R. *Journal of the South African Institute of Mining and Metallurgy*, 69(7):305–339.

Li, C. C. (2015). *Applied Rock Mechanics*. Norwegian University of Science and Technology, Trondheim.

Ljunggren, C. (1990). *New Developments in Hydrofracturing Stress Measurement Techniques and a Comparison to the HTPF Method*. PhD thesis, Luleå University of Technology, Luleå.

Ljunggren, C., Chang, Y., Janson, T., and Christiansson, R. (2003). An overview of rock stress measurement methods. *International Journal of Rock Mechanics and Mining Sciences*, 40(7-8):975–989.

Myrvang, A. (1996). *Bergmekanikk*. Norwegian University of Science and Technology, Trondheim.

Myrvang, A. (2001). *Bergmekanikk*. Norwegian University of Science and Technology, Trondheim.

Myrvang, A. (2002). Hvordan står det til med bergspenningene i Norge? In *Bergmekanikkdagen 2002*, pages 411–421, Oslo. Norsk forening for Fjellsprengningsteknikk and Norsk Bergmekanikkgruppe.

Nilsen, B. and Broch, E. (2012). *Ingeniørgeologi-berg grunnkurskompedium*. Institutt for geologi og bergteknikk, Norwegian University of Science and Technology, Trondheim.

Ojango, J. M. K. *A basic introduction to Microsoft Access*. Egerton University and International Livestock Research Institute, Kenya. Accessed: 04 April 2018.

SINTEF (2014). *In-situ rock stress measurements and numerical modelling: Brief description of methods applied by SINTEF*. SINTEF Building and Infrastructure, Rock Engineering, Trondheim.

Sjöberg, J., Christiansson, R., and Hudson, J. A. (2003). ISRM Suggested Methods for rock stress estimation—Part 2: overcoring methods. *International Journal of Rock Mechanics and Mining Sciences*, 40:999–1010.

Sjöberg, J. and Klasson, H. (2003). Stress measurements in deep boreholes using the *Borre* (SSPB) probe. *International Journal of Rock Mechanics and Mining Sciences*, 40:1205–1223.

Statens kartverk (2009). *Koordinatbaserte referansesystem: datum, koordinatsystem, transformasjon, konvertering og avbildning*. Statens kartverk Geodesi, Hønefoss.

Stein, S. and Pelayo, A. (1991). Seismological Constraints on Stress in the Oceanic Lithosphere. *The Philosophical Transactions of the Royal Society*, 337(1645):53–69.

Stephansson, O., Ljunggren, C., and Jing, L. (1991). Stress measurements and tectonic implications for Fennoscandia. *Tectonophysics*, 189(1):317–322.

Stephansson, O., Myrvang, A. M., and Särkkä, P. (1986). State of stress in Fennoscandia. In *International Symposium on Rock Stress and Rock Stress Measurements*, pages 21–33, Stockholm. Centek Publisher.

The geological society of America (2012). *GSA geological time scale*. `https://www.geosociety.org/GSA/Education_Careers/Geologic_Time_Scale/GSA/timescale/home.aspx`. Accessed: 19 April 2018.

World Stress Map (2017). *World Stress Map Project - A Service for Science and Earth System Management*. `http://www.world-stress-map.org/`. Accessed: 11 October 2017.

Worotnicki, G. (1993). CSIRO triaxial stress measuring cell. In Hudson, J., editor, *Comprehensive Rock Engineering- Principles, Practice & Projects*, volume 3, pages 329–395. Pergamont Press, Great Britain.

Yeats, R. S., Sieh, K., and Allen, C. R. (1997). *The Geology of Earthquakes*. Oxford University Press, New York, USA.

Zang, A., Stephansson, O., Heidbach, O., and Janouschkowetz, S. (2012). World Stress Map Database as a Resource for Rock Mechanics and Rock Engineering. *Geotechnical and Geological Engineering*, 30:625–646.

Zoback, M. D. and Zoback, M. L. (2002). Stress in the Earth's lithosphere. In James, D. E., editor, *Geophysics*, pages 1221–1232. Springer US, Boston.

Zoback, M. L. (1992). First- and second-order patterns of stress in the lithosphere: The World Stress Map Project. *Journal of Geophysical Research: Solid Earth*, 97:11703–11728.

Zoback, M. L., Zoback, M. D., Adams, J., Assumpção, M., S., B., Bergman, E. A., Blümling, P., Brereton, N. R., Denham, D., Ding, J., Fuchs, K., Gay, N., Gregersen, S., Gupta, H. K., Gvishiani, A., Jacob, K., Klein, R., Knoll, P., Magee, M., Mercier, J. L., Müller, B. C., Paquin, C., Rajendran, K., Stephansson, O., Suarez, G., Suter, M., Udias, A., Xu, Z. H., and Zhizhin, M. (1989). Global patterns of tectonic stress. *Nature*, 341(6240):11703–11728.

Acronyms

2D Two-dimensional. 26–28, 35, 36, 49

3D Three-dimensional. 29, 30, 35, 40, 41, 49

CSIR Council for Scientific and Industrial Research. 26, 27, 30–35, 49

CSIRO Commonwealth Scientific and Industrial Research Organization. 26, 33–35

DIF drilling-induced-fractures. 42, 44, 45, 48, 79, 82

DISO Determination of In-Situ Stress by Overcoring. 31, 65

EUREF European Reference Frame. 59

FRSDB Fennoscandian Rock Stress Database. 2, 3, 6, 7, 25

HI Hollow Inclusion. 26, 33–35

HTPF hydraulic testing of pre-existing fractures. 36, 40–42, 49, 59

MA Million years. 21, 22

MASL meters above sea level. 64, 96

NTH Norwegian Institute of Technology. 30

NTNU Norwegian University of Science and Technology. 1, 6, 27, 30, 31, 62

SINTEF The Foundation of Technical and Scientific Research. 27, 28, 30, 31, 38, 49, 62, 66

SSPB Swedish State Power Board. 32

USBM US Bureau of Mines. 26, 28–30, 33–35

WSM World Stress Map. 2–5, 7, 25, 65

Appendices

This chapter consists of following appendices:

A.1 Fennoscandian Rock Stress Database Stress Map

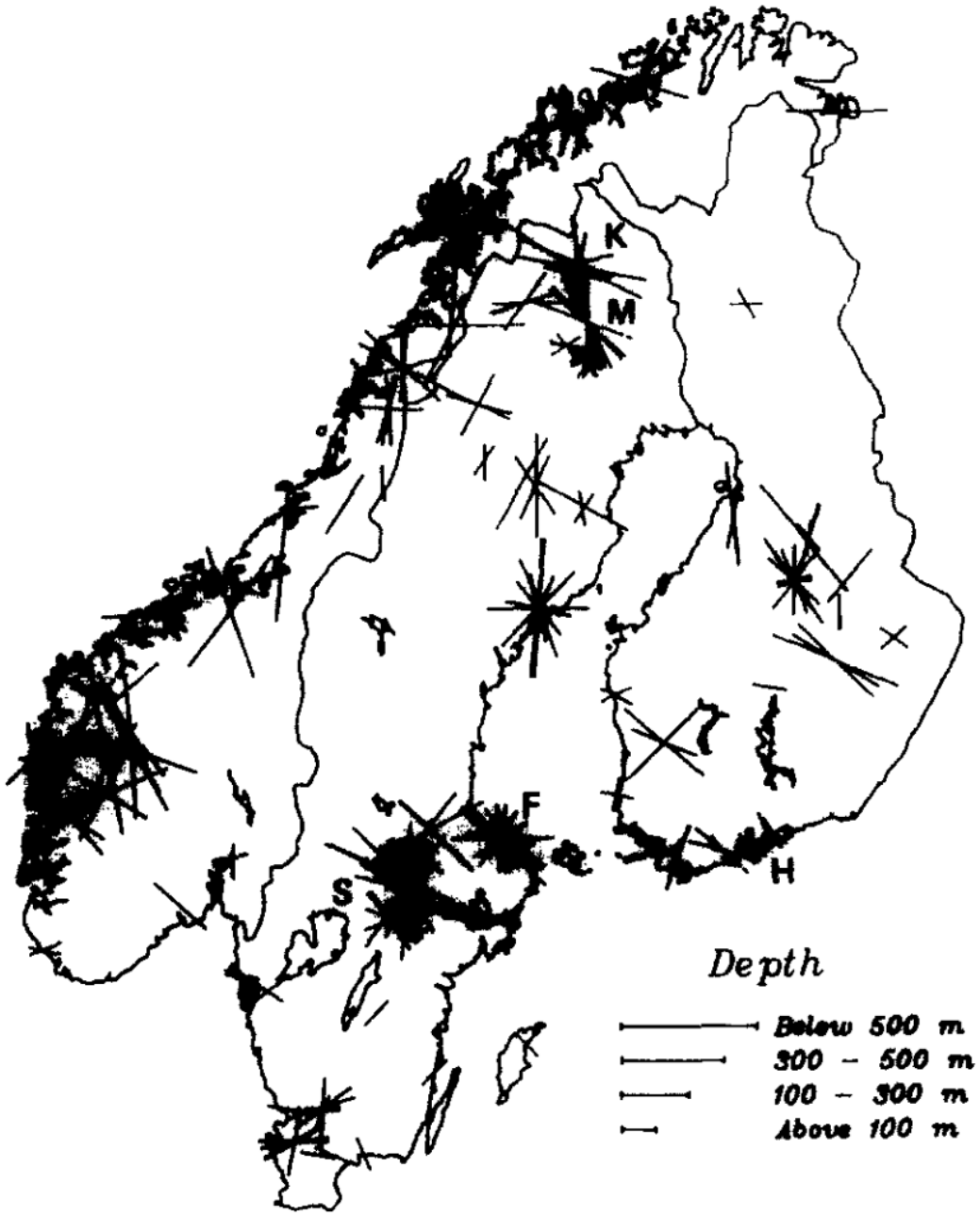

Figure A.1: FRSDB map with σ_H stress trends at different depths (Stephansson et al., 1986).

A.2 Equations

A.2.1 Hooke's law

For elastic materials, Hooke's law states that there is a linear relationship between axial stress σ_z and strain ϵ_z (Li, 2015, 2-2):

$$\sigma_z = E \cdot \epsilon_z \tag{A.1}$$

Where E is the elastic modulus, expresses the material's deformation ability (Myrvang, 1996).

Hooke's law for plane stress state

According to (Li, 2015) and (Myrvang, 1996), Poisson's ratio ν for an isotropic material is defined as:

$$\nu = -\frac{\epsilon_x}{\epsilon_z} = -\frac{\epsilon_y}{\epsilon_z} \tag{A.2}$$

The negative sign is used to make ν positive (Myrvang, 1996).

Total strain in x-direction:

$$\epsilon_x = \frac{\sigma_x}{E} - \nu \cdot \frac{\sigma_z}{E} = \frac{1}{E} \cdot (\sigma_z - \nu\sigma_x) \tag{A.3}$$

Total strain in z-direction:

$$\epsilon_z = \frac{\sigma_z}{E} - \nu \cdot \frac{\sigma_x}{E} = \frac{1}{E} \cdot (\sigma_x - \nu\sigma_z) \tag{A.4}$$

Hooke's law for plane stress state expressed in term of stresses:

By solving Equation A.3 and A.4 with respect to stress give following expressions:

$$\sigma_x = \frac{E}{1-\nu^2} \cdot (\epsilon_z + \nu\epsilon_z), \qquad \sigma_z = \frac{E}{1-\nu^2} \cdot (\epsilon_z + \nu\epsilon_x) \tag{A.5}$$

Hooke's law for three dimensions

Hooke's law for three dimension expressed by the three principal stresses σ_1, σ_2 and σ_3 after Myrvang (1996) and (Li, 2015):

$$\epsilon_1 = \frac{\sigma_1}{E} - \nu\frac{\sigma_2}{E} - \nu\frac{\sigma_3}{E} = \frac{1}{E} \cdot [\sigma_1 - \nu(\sigma_2 + \sigma_3)] \tag{A.6}$$

$$\epsilon_2 = \frac{1}{E} \cdot [\sigma_2 - \nu(\sigma_1 + \sigma_3)] \tag{A.7}$$

$$\epsilon_3 = \frac{1}{E} \cdot [\sigma_3 - \nu(\sigma_1 + \sigma_2)] \tag{A.8}$$

Hooke's law for three dimensional stress state expressed in term of stresses:

By solving Equation A.6, A.7 and A.8 with respect to stress give following expressions:

$$\sigma_1 = \frac{E}{1+\nu} \cdot (\frac{\nu e}{1-2\nu} + \epsilon_1), \qquad \sigma_2 = \frac{E}{1+\nu} \cdot (\frac{\nu e}{1-2\nu} + \epsilon_2), \qquad \sigma_3 = \frac{E}{1+\nu} \cdot (\frac{\nu e}{1-2\nu} + \epsilon_3), \tag{A.9}$$

Where $e = \epsilon_1 + \epsilon_2 + \epsilon_3$

A.2.2 Secondary principals stresses for overcoring with USBM gauge

According to Myrvang (2001), diametrical change u can be realted to the secondary principal stresses as follows:

$$u = \frac{a}{E} \cdot [(\sigma_1 + \sigma_2) + 2 \cdot (\sigma_1 - \sigma_2) \cdot 2\theta)] \tag{A.10}$$

Where a = diameter of borehole

E = E-modulus

θ = angle between σ_1 and the direction u is measured in

θ, σ_1 and σ_2 can be found by following Equations by measuring the diametrical change in three directions u, u' and u" (Myrvang, 2001):

$$\sigma_1 + \sigma_2 = \frac{E}{2a} \cdot (u' + u'') \tag{A.11}$$

$$\sigma_1 - \sigma_2 = \frac{E}{a\sqrt{2a}} \cdot \sqrt{(u' - u'')^2 + (u'' - u''')^2} \tag{A.12}$$

$$\tanh 2\theta = \frac{2u' - (u' + u''')}{u' - u'''} \tag{A.13}$$

A.2.3 Kirch's Equations

Kirch's Equations are derived from the theory of elasticity and give magnitude of secondary stress components for a circular opening in an isotropic rock mass (Li, 2015). Figure A.2 illustrates stresses around circular opening. Kirch's Equations are following:

$$\sigma_r = \frac{\sigma_1 + \sigma_3}{2} \cdot (1 - \frac{a^2}{r^2}) + \frac{\sigma_1 - \sigma_3}{2} \cdot (1 - \frac{4a^2}{r^2} + \frac{3a^4}{r^4}) \cos 2\theta \tag{A.14}$$

$$\sigma_\theta = \frac{\sigma_1 + \sigma_3}{2} \cdot (1 + \frac{a^2}{r^2}) - \frac{\sigma_1 - \sigma_3}{2} \cdot (1 + \frac{3a^4}{r^4}) \cos 2\theta \tag{A.15}$$

$$\tau_{r\theta} = -\frac{\sigma_1 - \sigma_3}{2} \cdot (1 + \frac{2a^2}{r^2} - \frac{3a^4}{r^4}) \sin 2\theta \tag{A.16}$$

Where σ_r = radial stress at given point

σ_θ = tangential stress

$\tau_{r\theta}$ =shear stress

σ_1 = the in situ major principal stress

σ_3 = the in situ minor principal stress

a = radius of circular tunnel

r = distance from tunnel centre to point

θ = angle between radius and x-axis

When σ_1 and σ_3 are not zero, the maximum tangential stress will be located at θ = 90, 270 and the minimum tangential stress will be located at θ = 0, 180 in Figure A.2. Along the tunnel perimeter, a will be equal to r. This give following expressions for the major and minor tangential stress at tunnel perimeter (Li, 2015):

$$\sigma_{\theta max} = 3\sigma_1 - \sigma_3 \tag{A.17}$$

$$\sigma_{\theta min} = 3\sigma_3 - \sigma_1 \tag{A.18}$$

From Figure A.2, it is evident that the major tangential stress $\sigma_{\theta max}$ will be located parallel with σ_3 and the minor tangential stress $\sigma_{\theta min}$ will be located parallel with σ_1.

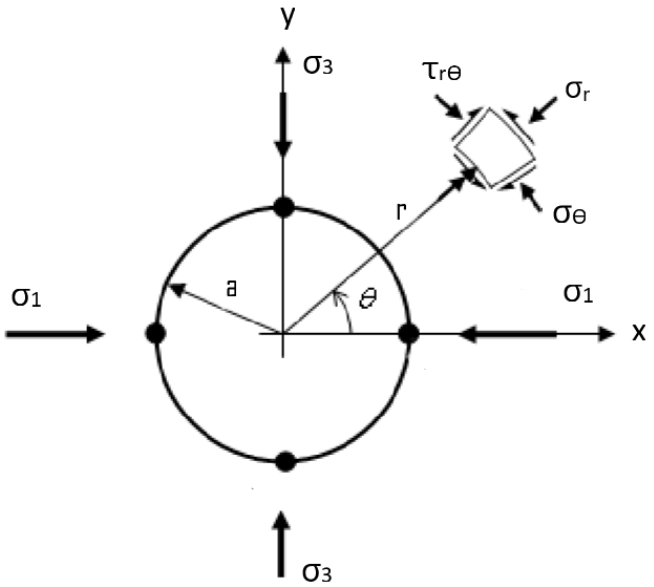

Figure A.2: Stress distribution around a circular opening. Modified after (Li, 2015).

A.3 GSA Geological Timescale

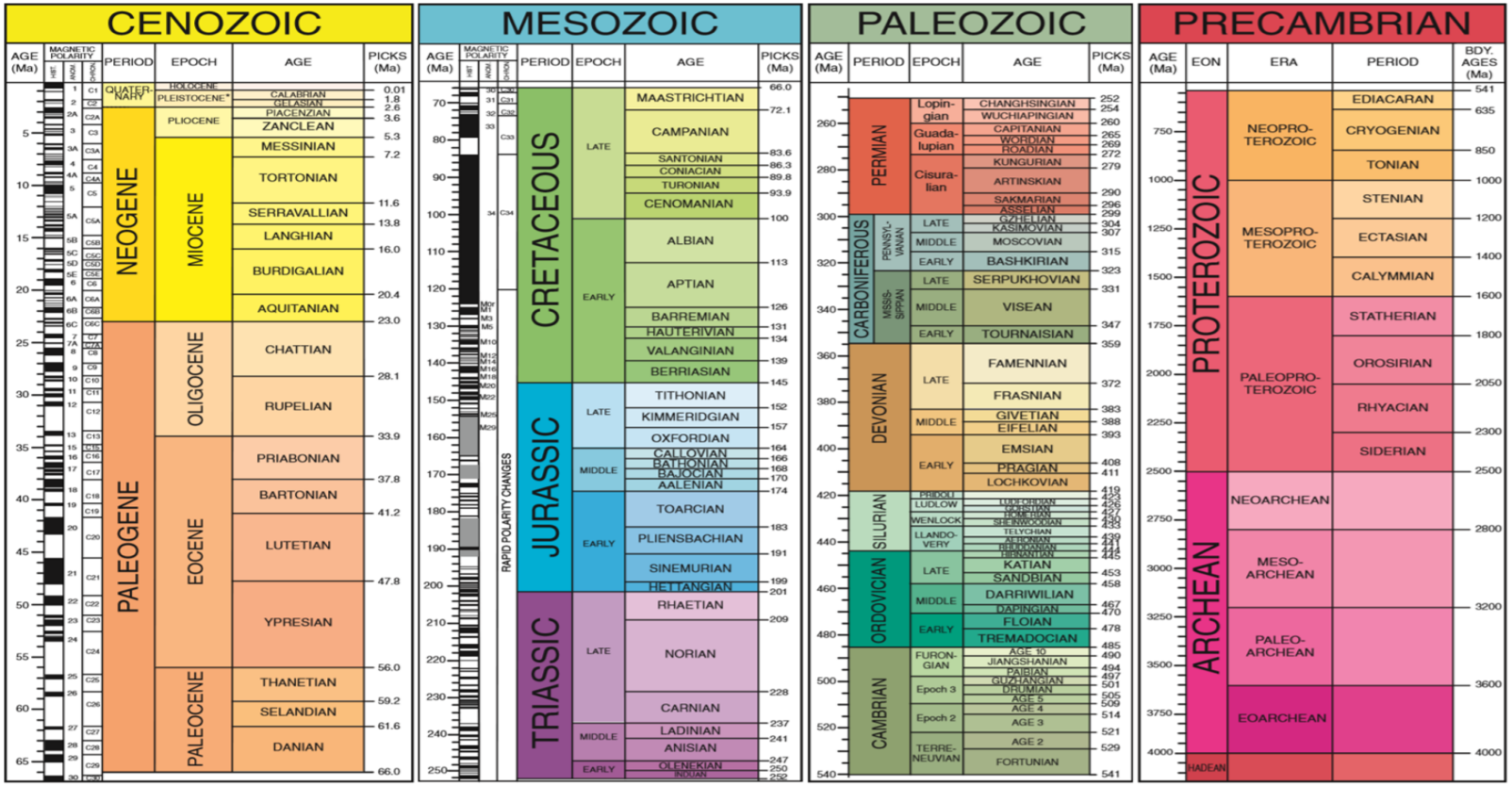

Figure A.3: GSA Geological timescale (The geological society of America, 2012).

A.4 World Stress Map (WSM) Quality Ranking Scheme

Table A.1: World Stress Map quality ranking scheme for some stress determination methods. Shows requirements for A–C quality

Method	Quality		
	A σ_H within ±15°	B σ_H within ±15 – 20°	C σ_H within ±20 – 25°
Overcoring (OC)	≥ 11 measurements depth ≥ 300 m s.d. ≤ 12°	≥ 8 measurements depth ≥ 100 m s.d. ≤ 20°	≥ 5 measurements depth ≥ 30 m s.d. ≤ 25°
Hydraulic fracturing (HF)	≥ 5 fracture orientations in a single well with s.d. ≤ 12° depth ≥ 300 m distributed over a depth range ≥ 300 m	≥ 4 fracture orientations in a single well with s.d. ≤ 20° depth ≥ 100 m distributed over a depth range ≥ 200 m	≥ 3 fracture orientations in a single well with s.d. ≤ 25° depth ≥ 30 m distributed over a depth range ≥ 100 m
Borehole breakouts (BO) - caliper logs	≥ 10 distinct fractures and combined length ≥ 300 m in a single well with s.d. ≤ 12°	≥ 6 distinct fractures and combined length ≥ 100 m in a single well with s.d. ≤ 20°	≥ 4 distinct fractures and combined length ≥ 30 m s.d. ≤ 25°
Borehole breakouts (BO) - image logs	≥ 10 distinct fractures and combined length ≥ 100 m in a single well with s.d. ≤ 12°	≥ 6 distinct fractures and combined length ≥ 40 m in a single well with s.d. ≤ 20°	≥ 4 distinct fractures and combined length ≥ 20 m s.d. ≤ 25°
Drilling-induced fractures (DIF)	≥ 10 distinct fractures and in a single well with a combined length ≥ 100 m and s.d. ≤ 12°	≥ 6 distinct fractures and in a single well with combined length ≥ 40 m and s.d. ≤ 20°	≥ 4 distinct fractures and in a single well with combined length ≥ 20 m and s.d. ≤ 25°
Focal mechanism Single (FMS)			Well constrained single event solution M ≥ 2.5
Focal mechanism Formal inversion (FMF)	Formal inversion of ≥15 well constrained single event solutions in close geographic proximity and s.d or misfit angle ≤ 12°	Formal inversion of ≥8 well constrained single event solutions in close geographic proximity and s.d or misfit angle ≤ 20°	
s.d = standard deviation			

Table A.2: World Stress Map quality ranking scheme for some stress determination methods. This table shows requirements D–E quality

Method	Quality	
	D Questionable orientation, σ_H ($\pm 25 - 40°$)	E No reliable orientation ($> \pm 40°$
Overcoring (OC)	≥ 2 measurements depth ≥ 10 m S.D ≤ 40°	≤ 2 measurements or depth ≤ 10 m or s.d. > 40 °
Hydraulic fracturing (HF)	Single hydrofrac orientation	Only stress magnitudes are measured no information on orientation
Borehole breakouts (BO) - caliper logs	≤ 4 distinct breakouts and combined length ≤ 30 m s.d. ≤ 40°	Wells without reliable breakouts or s.d. > ° s.d. > 40°
Borehole breakouts (BO) - image logs	≤ 4 distinct breakouts and combined length ≤ 20 m s.d. ≤ 40°	Wells without reliable breakouts or s.d. > ° s.d. > 40°
Drilling-induced fractures (DIF)	≤ 4 distinct fractures and in a single well with combined length ≤ 20 m and s.d. ≤ 40°	Wells without fractures and s.d. > 40°
Focal mechanism Single (FMS)	Well constrained single event solution M < 2.5	Mechanism with P, B, T axes all plunging $25° - 40°$ Mechanism with P and T axes both plunging $40° - 50°$
Focal mechanism Formal inversion (FMF)		
s.d = standard deviation		

A.5 Figures referred to in discussion

A.5.1 Stress Map by Fejerskov et. al (2000)

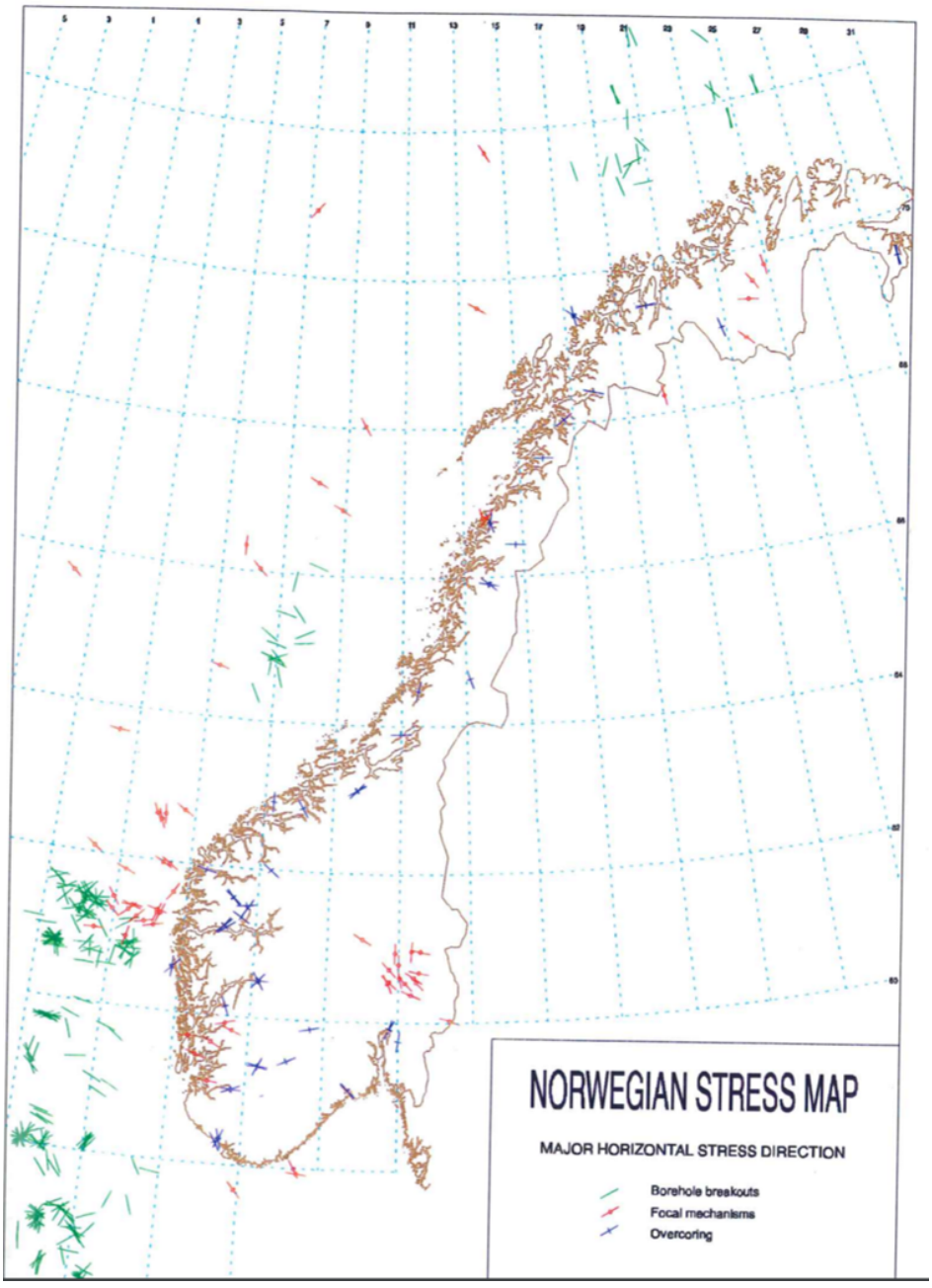

Figure A.4: Stress map (Fejerskov et al., 2000).

A.5.2 Mid–Atlantic ridge

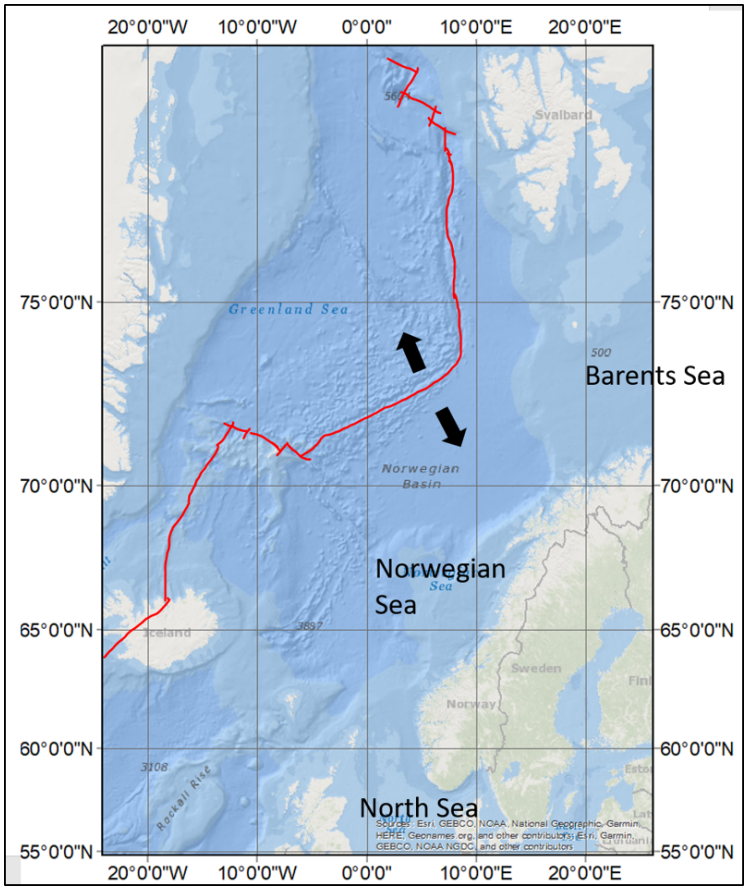

Figure A.5: Map of the mid-Atlantic ridge from Iceland to Svalbard. The arrows represent tectonic plate movement and the red line indicates the mid-Atlantic ridge (created in ArcMap 10.6).

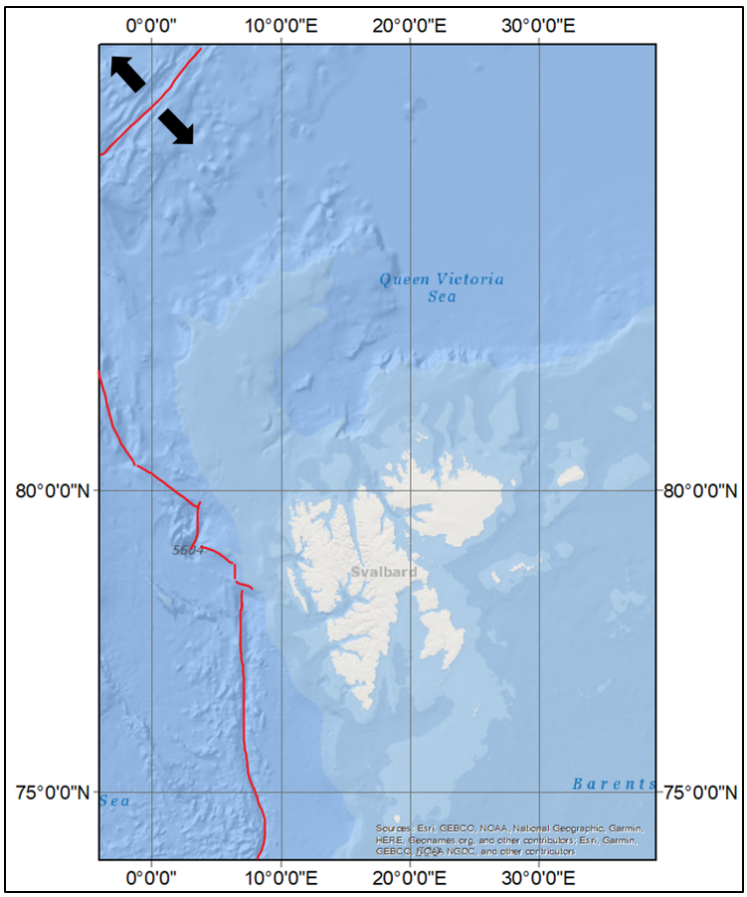

Figure A.6: Map of the mid-Atlantic ridge and continental margin around Svalbard. The arrows represent tectonic plate movement and the red line indicates the mid-Atlantic ridge (created in ArcMap 10.6).

A.6 Collected In Situ Rock Stress Data

A.6.1 Graphs

Principal stress ratios

Figure A.7, A.8 and A.9 show principal stress ratios $\frac{\sigma_2}{\sigma_3}$, $\frac{\sigma_1}{\sigma_2}$ and $\frac{\sigma_1}{\sigma_3}$ for all data entries. Figure A.10, A.11, A.12, A.13 and A.14 show principal stress ratios $\frac{\sigma_2}{\sigma_3}$, $\frac{\sigma_1}{\sigma_2}$ and $\frac{\sigma_1}{\sigma_3}$ for data separated according to lithology and geological period.

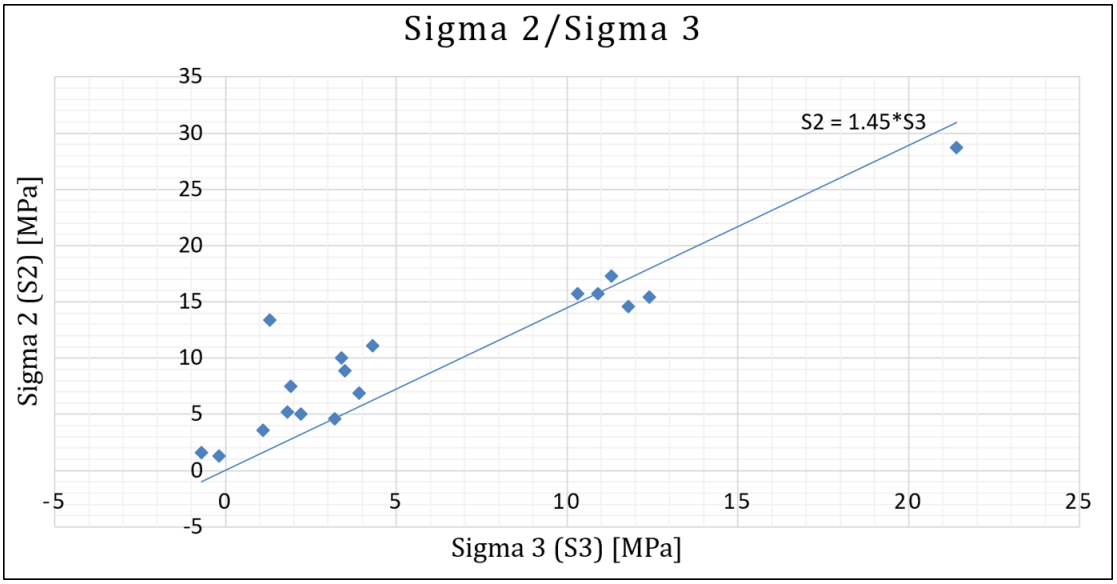

Figure A.7: σ_2 (S2)/ σ_3 (S3) stress ratio for all data points.

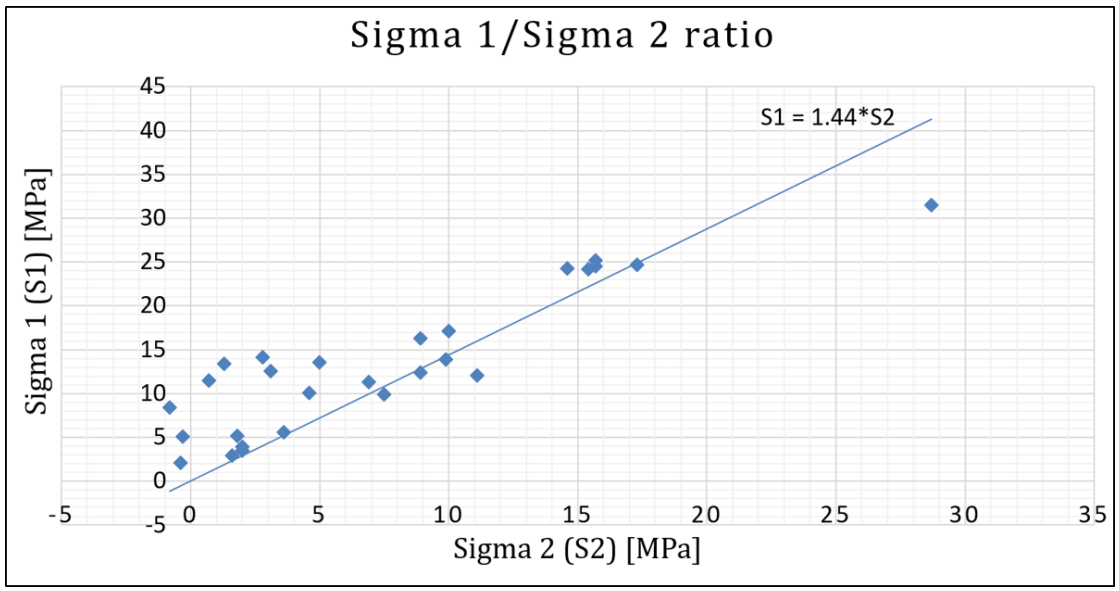

Figure A.8: σ_1 (S1)/ σ_2 (S2) stress ratio for all data points.

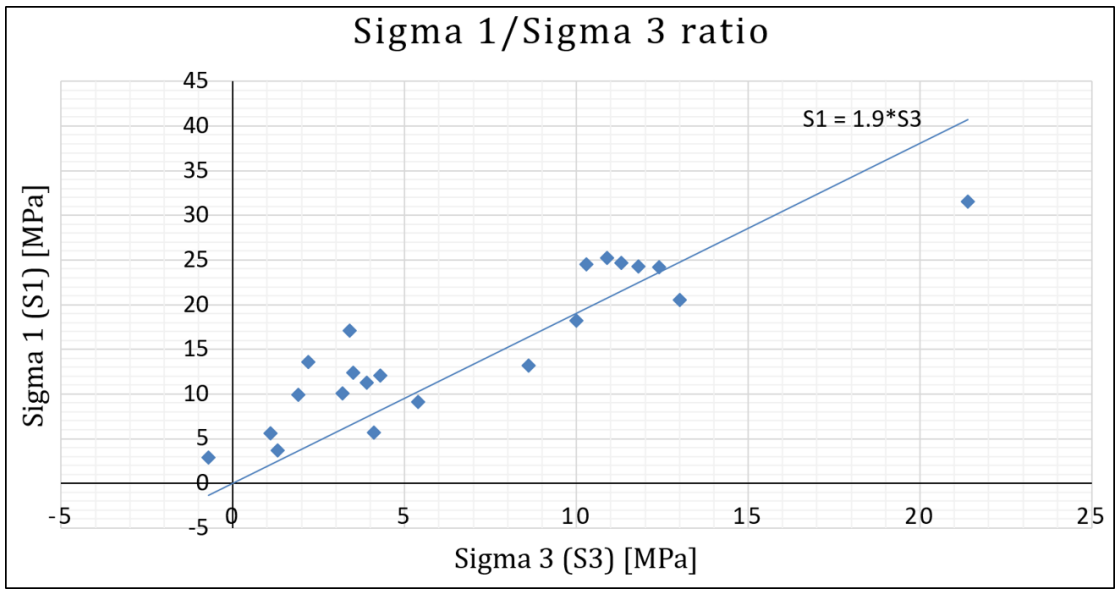

Figure A.9: σ_1 (S1)/ σ_3 (S3) stress ratio for all data points.

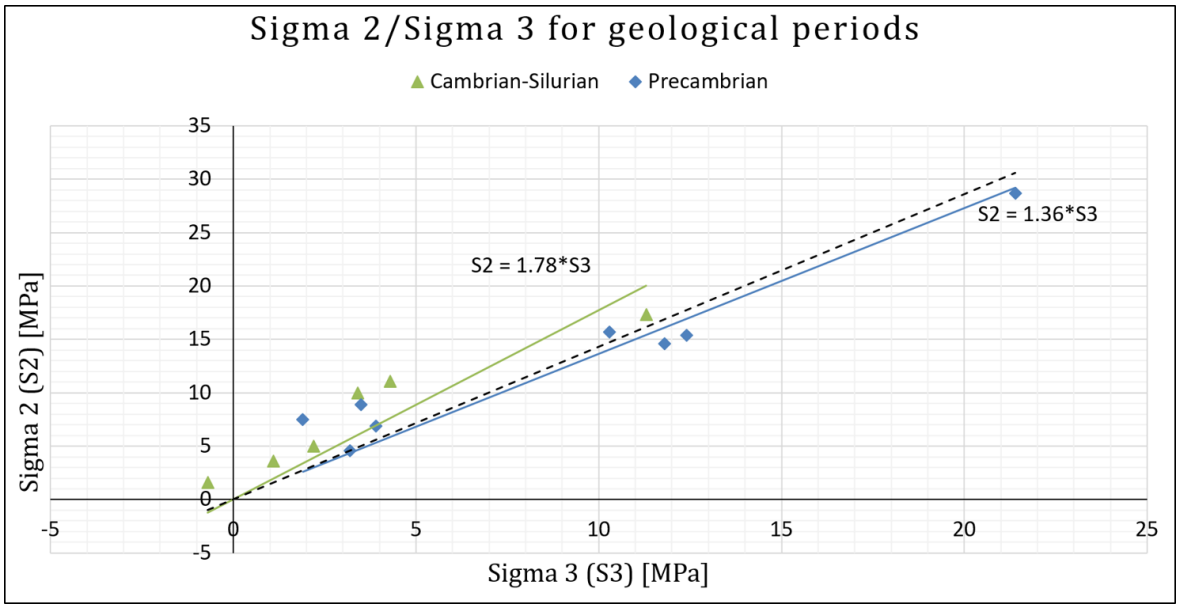

Figure A.10: σ_2 (S2)/σ_3 (S3) stress ratios separated according to geological periods. The dotted line represents σ_2/σ_3 ratio for all data entries.

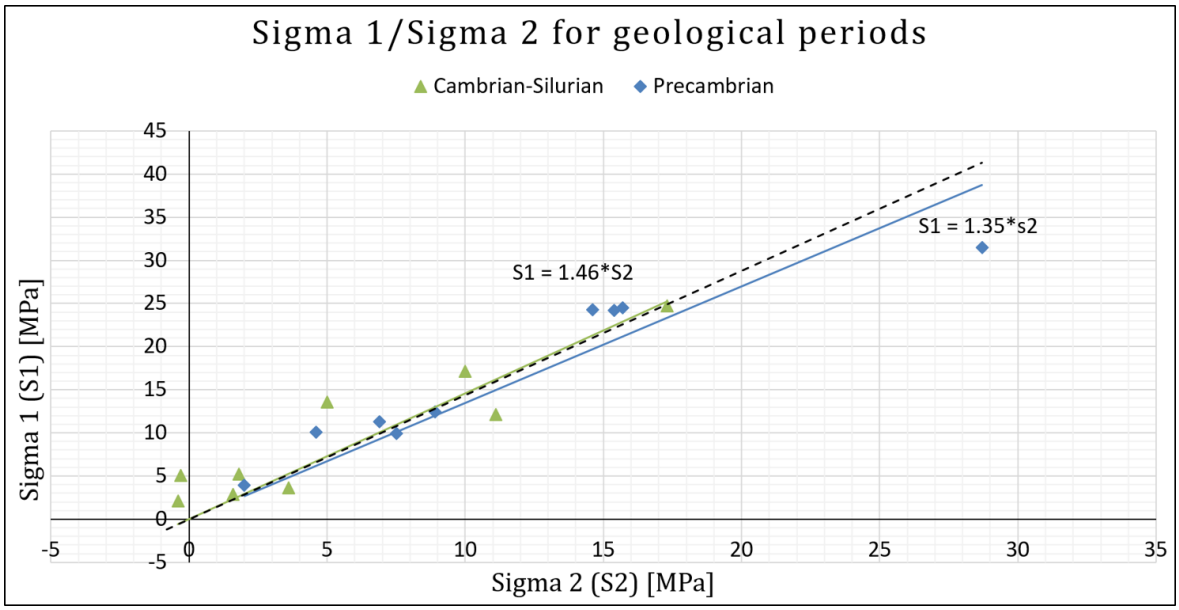

Figure A.11: σ_1 (S1)/σ_2 (S2) stress ratios separated according to geological periods. The dotted line represents σ_1/σ_2 ratio for all data entries.

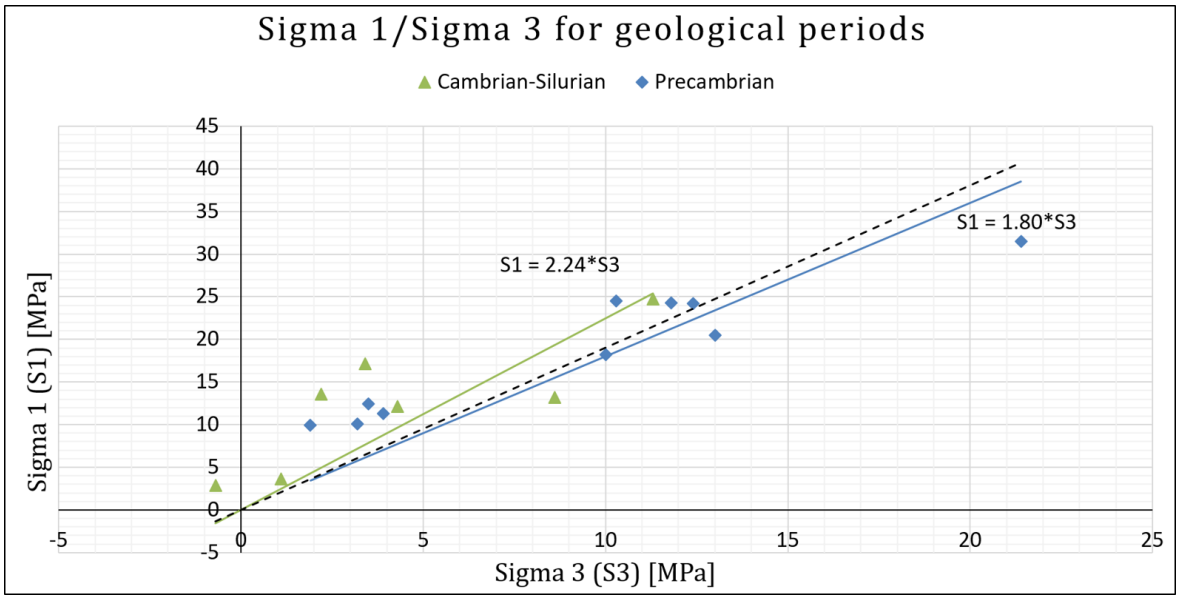

Figure A.12: σ_1 (S1)/σ_2 (S3) stress ratios separated according to geological periods. The dotted line represents σ_1/σ_3 ratio for all data entries.

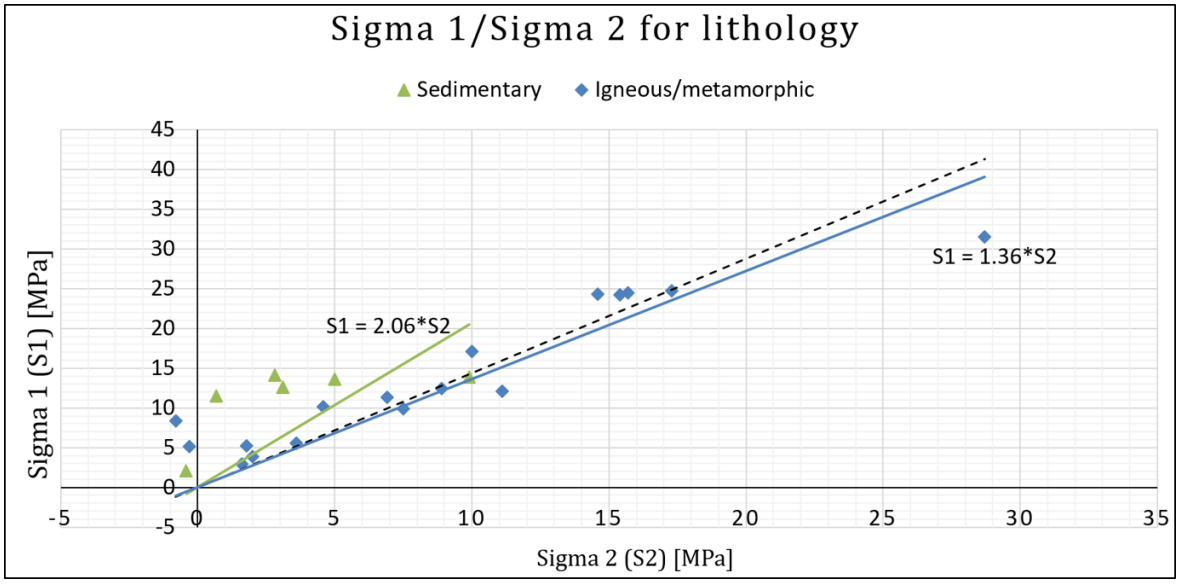

Figure A.13: σ_1 (S1)/σ_2 (S3) stress ratios separated according to lithology. The dotted line represents σ_1/σ_3 ratio for all data entries.

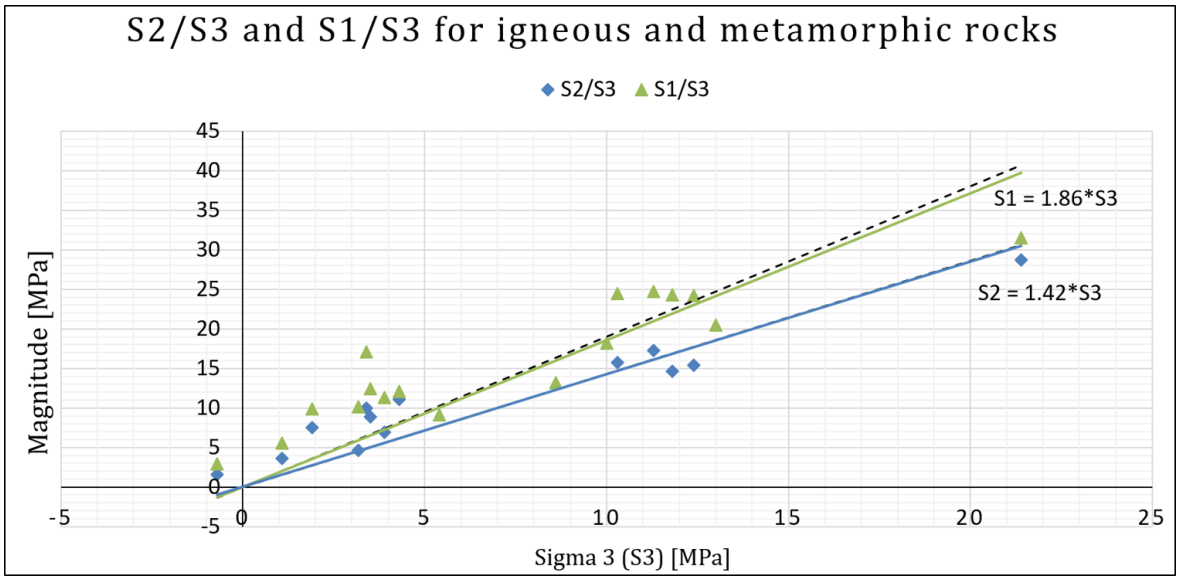

Figure A.14: σ_1 (S2)/σ_2 (S3) and σ_1 (S1)/σ_2 (S3) stress ratio for data points in igneous and metamorphic rocks. The dotted lines represent σ_2/σ_3 and σ_1/σ_3 ratios for all data entries.

Horizontal and vertical stress ratios

Figure A.15, A.16 and A.17 and show horizontal and vertical stress ratios $\frac{\sigma_H}{\sigma_V}$, $\frac{\sigma_h}{\sigma_V}$ and $\frac{\sigma_h}{\sigma_H}$ for all data entries.

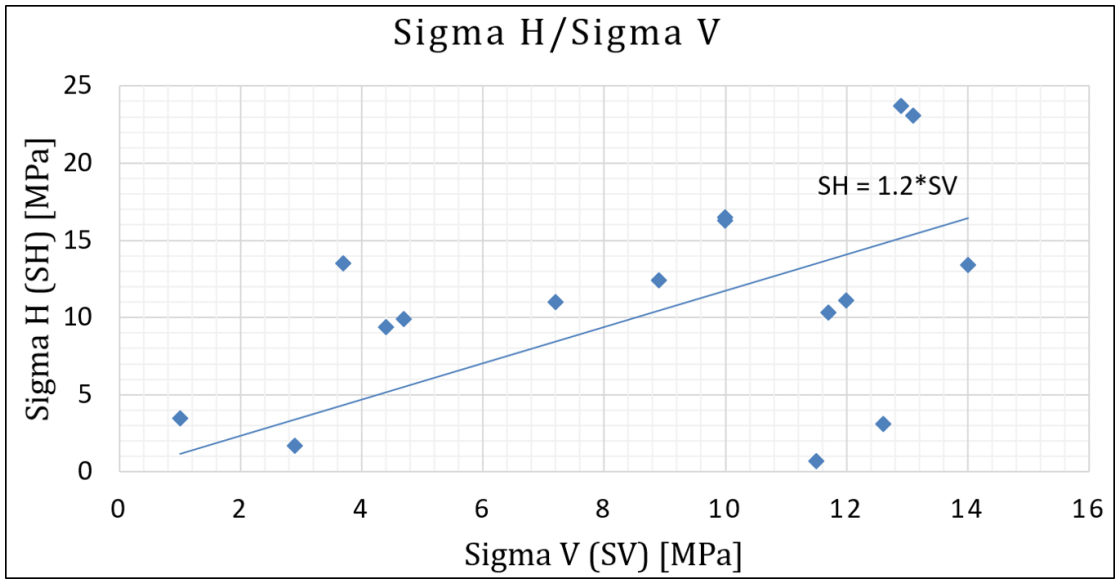

Figure A.15: σ_H (SH) / σ_V (SV) stress ratio for all data points.

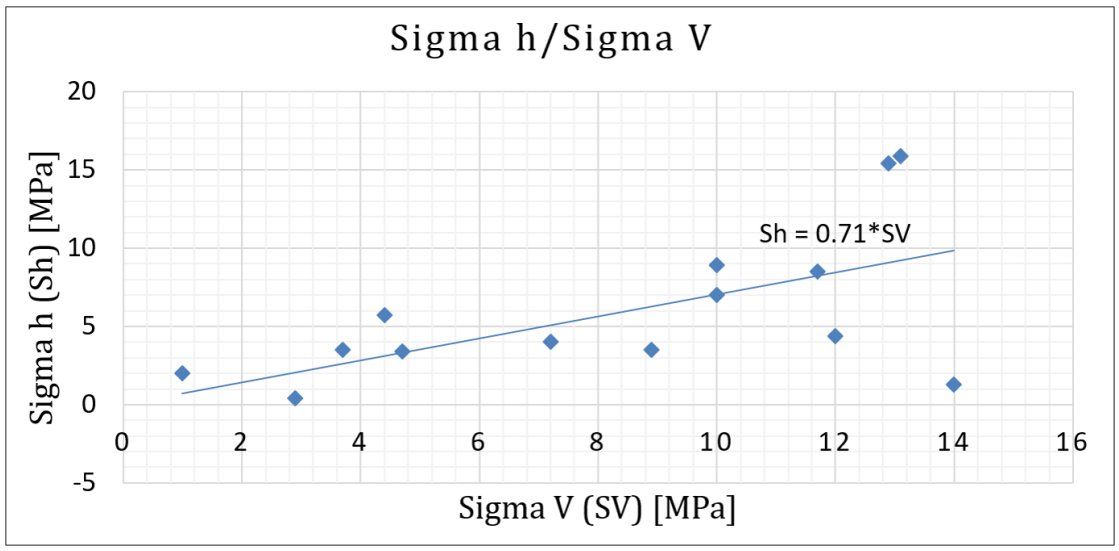

Figure A.16: σ_h (Sh) / σ_V (SV) stress ratio for all data points.

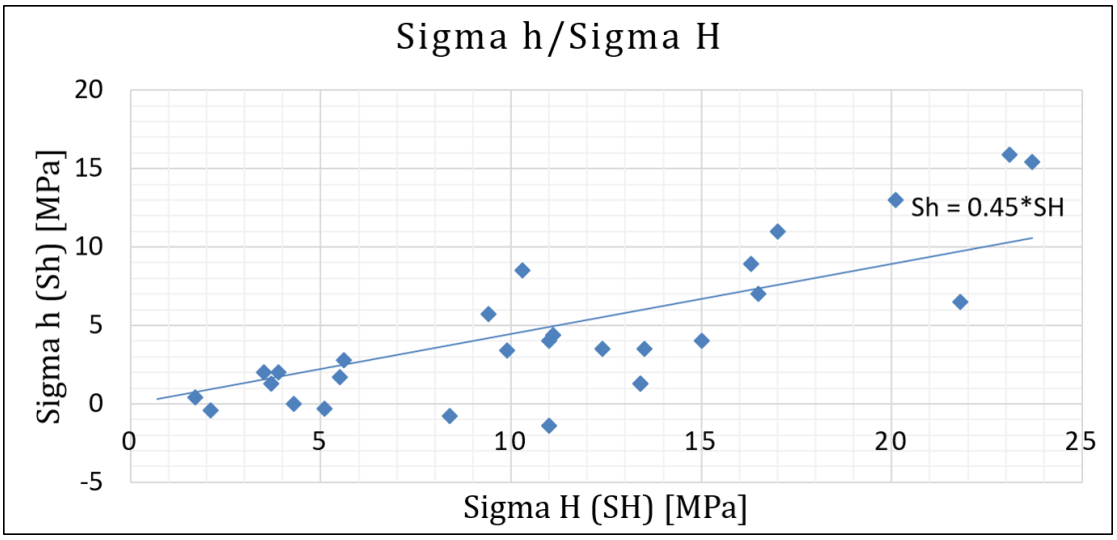

Figure A.17: σ_h (Sh)/ σ_H (SH) stress ratio for all data points.

A.6.2 Database tables

Table A.3, A.4, A.5, A.6 and A.7 presents the data collected in the database. See section 4.2 for description of the parameters and the acronyms.

Data from "Rock stress data" table

Table A.3: Collected in situ rock stress data, part 1.

ID	Company	Title	Year	Coordinates		Area	Method	Overburden	MASL
				Latitude	Longitude			[m]	[m]
1	Statoil		2007	61.11397	3.522206	Norwegian continental shelf	DIF		
2	Statoil		2007	61.08031	2.499736	Norwegian continental shelf	BO		
3	Statoil		2007	58.87262	2.390183	Norwegian continental shelf	DIF		
4	Statoil		2007	61.08032	2.499717	Norwegian continental shelf	DIF		
5	Statoil		2005	61.08035	2.499681	Norwegian continental shelf	DIF		
6	Statoil		2008	61,08028	2.499722	Norwegian continental shelf	DIF		
7	Statoil		2005	61.08033	2.499667	Norwegian continental shelf	DIF		
8	Statoil		2007	61.11397	3.522206	Norwegian continental shelf	DIF		
9	Statoil		2006	64.60846	9.719328	Norwegian continental shelf	DIF		
10	Statoil		2005	66.36443	5.577564	Norwegian continental shelf	DIF		
11	Statoil		2005	66.36443	5.577564	Norwegian continental shelf	BO		

Table A.3: Collected in situ rock stress data, part 1.

ID	Company	Title	Year	Coordinates		Area	Method	Overburden	MASL
				Latitude	Longitude			[m]	[m]
12	Statoil		1997	67.06885	7.010142	Norwegian continental shelf	BO		
13	Statoil		2006	71.58709	22.85601	Norwegian continental shelf	DIF		
14	Statoil		2006	71.58709	22.85601	Norwegian continental shelf	BO		
15	Statoil		2008	71.61375	23.06335	Norwegian continental shelf	DIF		
16	Statoil		2008	71.61375	23.06335	Norwegian continental shelf	DIF		
17	Statoil		2008	72.07242	22.47431	Norwegian continental shelf	BO		
18	Statoil		2008	72.07242	22.47431	Norwegian continental shelf	DIF		
19	Statoil		2008	72.07242	22.47431	Norwegian continental shelf	DIF		
20	Statoil		2008	72.62363	22.93094	Norwegian continental shelf	DIF		
21	Statens vegvesen	3D og 2D bergspenningsmålinger ved Lørentunnelen	2010	59.93363	10.79963	Oslo	OC 3D	20	70
22	Skanska Norge AS	3D og 2D bergspenningsmålinger Eiriksdal Kraftverk Høyanger	2010	61.2383	16.160397	Sogn og Fjordane	OC 3D	330	120
23	Skanska Norge AS	Hydraulisk splitting ved T55 Eiriksdal Kraftverk Høyanger	2010	61.2383	16.160397	Sogn og Fjordane	HF	430	120
24	Statkraft Energi AS	Hydraulisk splitting ved Ringedalen Kraftverk	2015	60.11663	6.62607	Hordaland	HF	300	465
25	Statkraft Energi AS	Hydraulisk splitting ved Nedre Røssåga kraftverk	2009	66.04289	13.78782	Nordland	HF	300	-50
26	Bane NOR SF	Follobanen: Bergmekanisk oppfølging (PPT)	2011	59.88939	10.76318	Oslo	OC 3D		10
27	NORSAR		2000	59.763	5.34	Hordaland	FM	18000	
28	NORSAR		1999	66.39	13.35	Nordland	FM	8000	
29	NORSAR		1999	62.19	4.74	Norwegian	FM	9000	

Table A.3: Collected in situ rock stress data, part 1.

ID	Company	Title	Year	Coordinates		Area	Method	Overburden	MASL
				Latitude	Longitude			[m]	[m]
30	NORSAR		1999	61.95	4.62	Norwegian continental shelf	FM	13000	
31	NORSAR		1999	61.555	4.29	Norwegian continental shelf	FM	24000	
32	NORSAR		1999	62.05	6.17	Møre og Romsdal	FM	10000	
33	NORSAR		1999	65.1	11.75	Trøndelag	FM	15000	
34	NORSAR		1999	61.89	4.68	Norwegian continental shelf	FM	21000	
35	NORSAR		1998	66.37	13.13	Nordland	FM	13000	
36	NORSAR		1998	66.39	13.09	Nordland	FM	11000	
37	NORSAR		1998	65.85	13.53	Nordland	FM	7000	
38	NORSAR		1998	60.35	5.867	Hordaland	FM	10000	
39	NORSAR		1997	60.97	3.72	Norwegian continental shelf	FM	19000	
40	NORSAR		1997	66.41	13.22	Nordland	FM	7000	
41	NORSAR		1997	66.5	12.4	Nordland	FM	11000	
42	NORSAR		1997	66.32	13.14	Nordland	FM	11000	
43	NORSAR		1997	66.32	13.15	Nordland	FM	11000	
44	NORSAR		1997	59.82	6.65	Hordaland	FM	12000	
45	NORSAR		1997	66.32	13.11	Nordland	FM	12000	
46	NORSAR		1996	69.42	24.04	Finnmark	FM	10000	
47	NORSAR		1996	61.05	2.9	Norwegian continental shelf	FM	240000	
48	NORSAR		1996	60.74	11.64	Hedmark	FM	32000	
49	NORSAR		1996	60.23	5.18	Hordaland	FM	7000	
50	NORSAR		1996	61.94	5.52	Sogn og Fjordane	FM	13000	
51	NORSAR		1996	59.84	5.13	Hordaland	FM	12000	
52	NORSAR		1996	61.64	3.39	Norwegian continental shelf	FM	17000	
53	NORSAR		1996	61.8	3.51	Norwegian continental shelf	FM	15000	
54	NORSAR		1996	61.82	3.51	Norwegian	FM	15000	

Table A.3: Collected in situ rock stress data, part 1.

ID	Company	Title	Year	Coordinates		Area	Method	Overburden	MASL
				Latitude	Longitude			[m]	[m]
55	NORSAR		1996	61.8	3.52	continental shelf Norwegian	FM	15000	
56	NORSAR		1996	61.02	3.79	continental shelf Norwegian	FM	20000	
57	NORSAR		1995	59.84	6.51	continental shelf Norwegian	FM	10000	
58	NORSAR		1995	61.71	3.98	continental shelf Norwegian	FM	10000	
59	NORSAR		1995	60.02	11.06	continental shelf Akershus	FM	18000	
60	NORSAR		1994	62.63	3.9	Norwegian continental shelf	FM	10000	
61	NORSAR		1994	60.38	9.89	Buskerud	FM	50000	
62	NORSAR		1994	60.17	11.06	Akershus	FM	13000	
63	NORSAR		1993	64.75	4.81	Norwegian continental shelf	FM	15000	
64	NORSAR		1993	62.61	4.14	Norwegian continental shelf	FM	17000	
65	NORSAR		1993	66.37	572	Norwegian continental shelf	FM	20000	
66	NORSAR		1993	64.99	5.19	Norwegian continental shelf	FM	10000	
67	NORSAR		1993	61.25	2.84	Norwegian continental shelf	FM	20000	
68	NORSAR		1992	59.27	10.88	Østfold	FM	10000	
69	NORSAR		1992	59.5	5.66	Rogaland	FM	12000	
70	NORSAR		1992	60.88	11.53	Hedmark	FM	12000	
71	NORSAR		1992	67.89	12.85	Nordland	FM	17000	
72	NORSAR		1991	69.33	24.02	Finnmark	FM	10000	
73	NORSAR		1991	79.02	3.59	Atlantic ocean	FM	10000	
74	NORSAR		1991	61.98	4.23	Norwegian continental shelf	FM	15000	
75	NORSAR		1991	67.91	9.97	Norwegian	FM	10000	

Table A.3: Collected in situ rock stress data, part 1.

ID	Company	Title	Year	Coordinates		Area	Method	Overburden	MASL
				Latitude	Longitude			[m]	[m]
76	NORSAR		1990	57.67	6.91	Norwegian continental shelf	FM	6000	
77	NORSAR		1990	66.04	6.26	Norwegian continental shelf	FM	30000	
78	NORSAR		1990	56.56	12.06	Norwegian continental shelf	FM	17000	
79	Skanska Norge AS	Hydraulisk splitting ved Storåselva Kraftverk	2016	64.27979	12.61814	Trøndelag	HF	29	200
80	Statens vegvesen	Bergspenningsmålinger Krågøy, Kvitsøy kommune	2011	59.06898	5.440003	Rogaland	OC 3D	75	-73
81	Statens vegvesen	Bergspenningsmålinger Krågøy, Kvitsøy kommune	2011	59.06898	5.440003	Rogaland	OC 3D	198	-196
82	SNSK AS	Bergmekaniske undersøkelser Gruve 7, R&P A24	1991	78.1565	16.02783	Svalbard	OC 2D	400	
83	SNSK AS	Bergmekaniske undersøkelser Gruve 7, R&P A24	1991	78.1565	16.02783	Svalbard	OC 2D	400	
84	SNSK AS	Bergmekaniske undersøkelser ved mellomstein i Svea	1995	77.89626	16.65914	Svalbard	OC 2D	275	
85	SNSK AS	Hydraulisk splitting Lunckefjell, Svalbard	2008	78.01749	16.76384	Svalbard	HF	82	
86	SNSK AS	Bergspenningsovervåkning med langtidsdoorstopper Svea Nord	2007	77.98505	16.71199	Svalbard	OC 2D	105	
87	SNSK AS	Bergspenningsovervåkning med langtidsdoorstopper Svea Nord	2007	77.96997	16.6615	Svalbard	OC 2D	335	
88	SNSK AS	Rock stress measurements by overcoring at "Svea Nord" coal mine in Svalbard	2000 and 3D	77.97861	16.69401	Svalbard	OC 2D	350	
89	SNSK AS	Rock stress measurements by overcoring at "Svea Nord" coal mine in Svalbard	2000 and 3D	77.97861	16.69401	Svalbard	OC 2D	50	
90	Eidsiva AS Vannkraft	Rendalen Kraftverk ingeniørgeologisk rapport	2008	61.81199	11.11962	Hedmark	OC 2D	130	300

Table A.3: Collected in situ rock stress data, part 1.

ID	Company	Title	Year	Coordinates		Area	Method	Overburden	MASL
				Latitude	Longitude			[m]	[m]
91	Lyse AS	Lysebotn 2 kraftverk	2010	59.05914	6.653742	Rogaland	OC 3D	700	-50
92	Bane NOR SF	Follobanen: Bergmekanisk oppfølging (PPT)	2012	59.89953	10.76186	Oslo	OC 2D		
93	NORSAR		1997	66.31	13.25	Nordland	FM	5000	
94	NORSAR		1992	67.77	14.88	Nordland	FM	10000	
95	Statens vegvesen	3D og 2D bergspenningsmålinger ved Lørentunnelen	2010	59.93345	10.7992	Oslo	OC 2D	31	
96	SNSK AS	Bergspenningsmålinger hydraulisk splitting i borhull 9110 Sentralfeltet, Svalbard	2007	77.98505	16.75608	Svalbard	HF	95	
97	SNSK AS	Numerisk analyse av samvirket mellom berg og bolt i kullgruven Svea Nord. Fjellspreningsdagen 2008	2007	77.96997	16.6615	Svalbard	OC	350	
98	SNSK AS	Numerisk analyse av samvirket mellom berg og bolt i kullgruven Svea Nord. Fjellspreningsdagen 2008	2007	77.96997	16.6615	Svalbard	OC 2D	95	
99	SNSK AS	Numerisk analyse av samvirket mellom berg og bolt i kullgruven Svea Nord. Fjellspreningsdagen 2008	2007	77.96997	16.6615	Svalbard	OC 2D	380	
100	SNSK AS	Numerisk analyse av samvirket mellom berg og bolt i kullgruven Svea Nord. Fjellspreningsdagen 2008	2007	77.98505	16.71199	Svalbard	OC 2D	340	
101	Statkraft Energi AS	Design and construction of high pressure tunnels at New Bjølvo hydropower plant	2001	60.4424	6.404528	Hordaland	OC 3D	890	0
102	Bane NOR SF	Holmestrand, resultater opp mot modellering, erfaringer, forbedringer (PPT)	2010	59.49335	10.3092	Vestfold	OC 3D	47	25
103	Bane NOR SF	Holmestrand, resultater opp mot modellering, erfaringer, forbedringer (PPT)	2010	59.49094	10.3099	Vestfold	HF	47	25
104	Rana Gruber AS	Stress measurements and rock excavation at Skaland mine, Norway. Fjellspreningsdagen 2010	2009	69.44666	17.32768	Troms	OC 3D		
105	Statens vegvesen	Finnfast, 2D bergspenningsmålinger i takhull	2008	59.11405	5.78635	Rogaland	OC 2D	150	
106	NGI	Fjellhallene på Sola	2005	58.9189	5.588118	Rogaland	HF	11	

Table A.3: Collected in situ rock stress data, part 1.

ID	Company	Title	Year	Coordinates		Area	Method	Overburden	MASL
				Latitude	Longitude			[m]	[m]
		planlegging av nytt industriområde							
107	Skanska Norge AS	Bergmekaniske beregninger, Tastavarden. Fjellspregningsdagen 1996	1996	58.98602	5.678471	Rogaland	OC 3D	27	43
108	Statens vegvesen	E16 Lærdalstunnelen. Høgt bergtrykk. Ønske om ferdig sikring ved stuff–går det? Fjellspreningsdagen 1997	1996	61.01426	7.452347	Sogn og Fjordane	OC 3D	1300	300
109	NGI	Predicted and measured performance, Norwegian Olympic Ice Hockey Cavern at Gjøvik	1990	60.79338	10.68394	Oppland	HF	40	
110	NGI	Bergmekaniske og ingeniørgeologiske undersøkelser før og under driving av Gjøvik olympiske fjellhall Fjellspreningsdagen 1993	1993	60.79338	10.68394	Oppland	OC 2D and 3D	25	
111	Bane NOR SF	Hydraulisk jekking ved høytrykksinjeksjon av berg. Maseroppgave NTNU	2015	59.81554	10.83254	Oslo	OC 3D	80	
112	Bane NOR SF	Hydraulisk jekking ved høytrykksinjeksjon av berg. Maseroppgave NTNU	2015	59.81207	10.83455	Oslo	OC 3D		
113	NGI	Fjellhaller i Rjukan– ingeniørgeologisk rapport.	1990	59.88259	8.688349	Telemark	OC 3D	25	
114	Eidsiva Vannkraft	Hydraulisk splitting i Rosten Kraftverk	2015	61.86052	9.41269	Oppland	HF	120	320
115	Eidsiva Vannkraft	3D bergspenningsmåling ved overboring Nedre Otta kraftverk	2017	61.79348	9.375416	Oppland	OC 3D	250	300

Table A.4: Collected in situ rock stress data, part 2.

ID	**Magnitudes** [MPa]						**Azimuth** [°]		**Stress regime**	**Bedrock** Lithology	Rock type	Geological period	**Topography**	**Mountain side** dist–ance	grad–ient	**Quality**
	σ_1	σ_2	σ_3	σ_H	σ_h	σ_V	σ_H	σ_h								
1							82		U							A
2							87		U							D
3							117		U							D
4							85		U							D
5							94		U							C
6							90		U							B
7							85		U							B
8							82		U							A
9							125		U							B
10							116		U							B
11							111		U							D
12							84		U							C
13							169		U							D
14							177		U							B
15							175		U							C
16							178		U							B
17							178		U							C
18							171		U							B
19							160		U							B
20							152		U							B
21	13.6	5	2.2	13.5	3.5	3.7	36	126	SS	Sedimentary	Limestone	Cambrian–Silurian	Under hill			B
22	24.2	15.4	12.4	23.7	15.4	12.9	165	74	RF	Metamorphic	Gneiss	Precambrian	Mountain side	200	0.57	A
23	20.5		13	20.1	13	7 T			RF	Metamorphic	Gneiss	Precambrian	Mountain side	165	0.57	A
24	18.2		10			8.1 T			U	Igneous	Granite	Precambrian	Mountain side	270	0.83	B
25	13.2		8.6			8.1 T			U	Metamorphic	Mica gneiss	Cambrian–Silurian	Under mountain	270	0.12	B
26	9.9	7.5	1.9	9.4	5.7	4.4	87	177	RF	Metamorphic	Tonalite to granite gneiss	Precambrian	Mountain side	270	0.33	C
27							85		RF							U
28							168		NF							U
29							82		U							U

Table A.4: Collected in situ rock stress data, part 2.

ID	Magnitudes [MPa]						Azimuth [°]		Stress regime	Bedrock			Topography	Mountain side		Quality
	σ_1	σ_2	σ_3	σ_H	σ_h	σ_V	σ_H	σ_h		Lithology	Rock type	Geological period		distance	gradient	
30							125		NF							U
31							103		RF							U
32							111		SS							U
33							167		NF							U
34							116		RF							U
35							14		SS							B
36							347		SS							B
37							115		RF							B
38							248		RF							C
39							76		SS							C
40							212		SS							B
41							73		SS							B
42							200		NF							C
43							200		NF							C
44							137		SS							C
45							176		RF							C
46							281		RF							B
47							37		U							C
48							299		RF							B
49							116		NS							C
50							200		NF							C
51							289		RF							D
52							288		SS							B
53							94		U							B
54							67		NS							B
55							96		U							B
56							90		NF							C
57							96		NS							U
58							300		U							C
59							329		NS							B
60							159		SS							C
61							117		RF							C
62							286		NF							B

Table A.4: Collected in situ rock stress data, part 2.

ID	Magnitudes [MPa]						Azimuth [°]		Stress regime	Bedrock			Topography	Mountain side		Quality
	σ_1	σ_2	σ_3	σ_H	σ_h	σ_V	σ_H	σ_h		Lithology	Rock type	Geological period		dist–ance	grad–ient	
63							285		RF							C
64							180		SS							B
65							99		NF							B
66							144		NF							D
67							121		RF							U
68							348		SS							C
69							292		SS							B
70							30		NF							B
71							60		NF							B
72							279		RF							C
73							174		SS							C
74							120		NF							C
75							100		NF							C
76							139		U							C
77							135		SS							C
78							188		U							B
79	9.1		5.4			2.1 T			U	Metamorphic	Garnet mica schist		Mountain side		0.32	C
80	2.9	1.6	-0.7	1.7	0.4	2.9	6		NF	Metamorphic	Greenstone	Cambrian–Silurian	Flat			D
81	12.1	11.1	4.3	11.1	4.4	12	75		NF	Metamorphic	Greenstone	Cambrian–Silurian	Flat			D
82	11.5	0.7		0.7		11.5	11		NF	Sedimentary	Sandstone	Paleogene–Neogene	Mountain side			C
83	12.6	3.1		3.1		12.6	7		NF	Sedimentary	Sandstone	Paleogene–Neogene	Mountain side			C
84	8.4	1.3	-0,2	8.4	-0.8	7.1 T	54		SS	Metamorphic	Shale					C
85	3.7		1.3	3.7	1.3	2.1 T	45	135	SS							C
86	13.9	9.9		17	11	2.3 T	70		RF	Sedimentary	Claystone, sandstone,	Paleogene–Neogene	Flat			C
87	14.1		2.8	15	4	8.2 T	67		SS	Sedimentary	Claystone, sandstone,	Paleogene–Neogene	Flat			A

Table A.4: Collected in situ rock stress data, part 2.

ID	Magnitudes [MPa]						Azimuth [°]		Stress regime	Bedrock			Topography	Mountain side		Quality
	σ_1	σ_2	σ_3	σ_H	σ_h	σ_V	σ_H	σ_h		Lithology	Rock type	Geological period		dist–ance	grad–ient	
88	16.3		8.9	16.5	7	10	63		SS				Valley between mountains			B
89		13.4	1.3	13.4	1.3	14	76	166	NF				Valley between mountains			C
90	18.2	5.2	1.8	4.3	0		135		U	Igneous	Granite	Cambrian–Silurian	Mountain side			A
91	25.2	15.7	10.9	23.1	15.9	13.1	165		RF				Mountain side			B
92				7			240		U	Metamorphic	Tonalite to granite gneiss	Precambrian	Mountain side			C
93							0		NF							C
94							63		NF							B
95	2.5		-0.2	2.1	-0.4		82		SS	Sedimentary	Limestone	Cambrian–Silurian	Under hill			D
96				5.6	2.8	3 T	45		SS							D
97				16.3	8.9	10	63		SS							U
98				13.4	1.3		78		U							U
99				11	1.3		72		U							U
100				21.8	6.5		47		U							U
101	24.7	17.3	11.3						U	Metamorphic	Gneiss or Amphibolite	Cambrian–Silurian	Mountain side	650	0.6	U
102	11.3	6.9	3.9	11	4	7.2	56	146	SS	Igneous	Basalt	Carboniferous–Permian	Hill top			B
103				5.5	1.7		50	140	U	Igneous	Basalt	Carboniferous–Permian	Hill top			C
104	12.4	8.9	3.5	12.4	3.5	8.9	43		SS	Igneous	Granite or migmatite	Cambrian–Silurian	Mountain side			B
105				5.1	-0.3		103		U	Metamorphic	Amphibolite augen gneiss	Cambrian–Silurian	Mountain side			C
106			3					50	U	Metamorphic	Gneiss	Precambrian	Mountain side			C

Table A.4: Collected in situ rock stress data, part 2.

ID	Magnitudes [MPa]						Azimuth [°]		Stress regime	Bedrock			Topography	Mountain side		Quality
	σ_1	σ_2	σ_3	σ_H	σ_h	σ_V	σ_H	σ_h		Lithology	Rock type	Geological period		dist–ance	grad–ient	
107	5.6	3.6	1.1						U	Metamorphic	Phyllite	Cambrian–Silurian	Hill side			U
108	31.5	28.7	21.4						RF	Metamorphic	Gneiss	Cambrian–Silurian	Mountain side			U
109				3.5	2	1	174	84	RF	Metamorphic	Granite gneiss	Precambrian Silurian	Hill side		0.3	B
110	4.3			3.9	2		153		U	Metamorphic	Granite gneiss	Precambrian	Hill side		0.3	B
111	24.3	14.6	11.8				169		RF	Metamorphic	Tonalite granite gneiss	Precambrian	Hill side		0.3	C
112	24.5	15.7	10.3				90		RF	Metamorphic	Tonalite granite gneiss	Precambrian				C
113	10.1	4.6	3.2	9.9	3.4	4.7			SS	Igneous	Rhyolite	Precambrian	Mountain side			C
114	5.7		4.1			3.2 T			RF				Mountain side		0.36	C
115	17.1	10	3.4	10.3	8.5	11.7	91	1	NF	Metamorphic	Mica schist	Cambrian–Silurian	Mountain side	170		C

Data from "Measurement uncertainty" table

Table A.5: Measurement uncertainty data.

ID	Number of measurements	Magnitude range			Azimuth			Dip from horizontal axis			Standard deviation			Azimuth range for σ_H
		σ_1	σ_2	σ_3	σ_1	σ_2	σ_3	σ_1	σ_2	σ_3	σ_1	σ_2	σ_3	
21	5	5.6	2.6	6.4	36	124	127	2	47	43	2.9	1.3	3.3	
22	5	6.8	6.6	5.6	345	75	183	12	4	77	3.4	3.3	2.8	
23	15	9.1		5.3							3.4		2	
24	19	7.8		3.7							3.1		1.1	
25	11	7.5		6.7							3.4		2	
26		3.8	3.8	5.6	249	145	14	24	27	61				
27								9		68				
28								58		6				
29								46		15				
30								65		14				
31								15		72				
32								36		16				
33								68		9				
34								5		74				
35								33		19				
36								22		11				
37								13		57				
38								13		57				
39								30		2				
40								29		7				
41								29		7				
42								58		23				
43								58		23				
44								7		29				
45								1		67				
46								5		70				
37								21		52				
48								19		58				
49								42		16				
50								63		24				
51								5		79				

Table A.5: Measurement uncertainty data.

ID	Number of measurements	Magnitude range			Azimuth			Dip from horizontal axis			Standard deviation			Azimuth range for σ_H
		σ_1	σ_2	σ_3	σ_1	σ_2	σ_3	σ_1	σ_2	σ_3	σ_1	σ_2	σ_3	
52								27		12				
53								40		3				
54								44		19				
55								40		3				
56								60		0				
57								44		19				
58								40		0				
59								47		12				
60								30		2				
61								13		57				
62								54		18				
63								0		90				
64								12		37				
65								72		9				
66								62		10				
67								18		58				
68								39		9				
69								0		30				
70								78		5				
71								58		23				
72								4		69				
73								0		0				
74								85		5				
75								60		5				
76								26		39				
77								10		1				
78								24		30				
79	23	6.3		4.3							2.2		1	
80	2	1.4	1.1	0.6	20	4	301	77	13	2				
81	1	2.5	1	0.8	275	73	164	74	15	6				
82	5	8.8	4.8					88						
83	5	10.9	5.7					81						
84	16				330	13								4
85	2			5										

Table A.5: Measurement uncertainty data.

ID	Number of measurements	Magnitude range			Azimuth			Dip from horizontal axis			Standard deviation			Azimuth range for σ_H
		σ_1	σ_2	σ_3	σ_1	σ_2	σ_3	σ_1	σ_2	σ_3	σ_1	σ_2	σ_3	
86	4	15.8	8.8											119
87	5	13.6	12.4											30
88	6	1.9	8.8											16
89	8	1.5	1.1											25
90	12	15.3	5.2		120									
91	4	2.1	2.8	2.4	166	256	1	23	6	67	1.2	1.7	1.5	
93								48		11				
94								55		6				
95	5	3.4	3.7											
97		1.9	4	8.8										16
98														25
99														12
100														35
101		3.2	1.2	2										
102		3.6	5	2.4	57	251	147	16	73	4				
105	6													36
106	2													58
108					154	49	266	20	36	47				
110		2.8	3.7											41
111	5	4.6	3.4	3.2	169	78	304	3	3	86				
112	6	4.8	6.2	2.2	90	184	339	7	18	70				
113					230	344	138	8	71	17				
114	20	15.7		5.1										
115	7	2	1.8	3.4	213	115	21	51	6	39	1	1	1.7	

Data from "Overcoring" table

Table A.6: Overcoring test data.

ID	Measurement data			Mechanical rock properties						Comments
	Number of measurements	Cell type	Diameter of rock core [mm]	E-modulus [GPa]	Poisson's ratio	Uniaxial compressive strength [MPa]	Friction angle [°]	P–wave velocity [$\frac{m}{s}$]	Density [$\frac{kg}{m^3}$]	
21	5	Triaxial NTNU/ SINTEF cell		56	0.19	146	28	2795	5435	
22	5	Triaxial NTNU/ SINTEF cell		33	0.14	231	23	2671	4049	
80	1	Borre probe		57	0.31					
81	2	Borre probe		57	0.31					
82	5	Doorstooper cell	62	19	0.05	110	12	2423	3611	
83	5	Doorstooper cell	62	54	0.16	123	12	2573	5083	
84	5	Doorstooper cell		11	0.35	58	17	2598	3872	Shale, Normal to stratification
84		Doorstooper cell		17	0.2					Shale, Parallel to stratification
84	11	Doorstooper cell		9	0.5	32	15	2480	3396	Normal to stratification
84		Doorstooper cell		14	0.36	41	9	2515	3923	Parallel to stratification
86	4	Doorstooper cell		30	0.18	125		2486	3138	Parallel to layering
87	5	Doorstooper cell		38	0.18	139	19	2581	4005	Parallel to layering
88	6	Doorstopper, triaxial NTNU/SINTEF	25	39	0.19	132		2617	4116	
89	8	Doorstopper, triaxial	29	27	0.29	56		2605	4277	

Table A.6: Overcoring test data.

ID	Measurement data			Mechanical rock properties						Comments
	Number of measurements	Cell type	Diameter of rock core [mm]	E-modulus [GPa]	Poisson's ratio	Uniaxial compressive strength [MPa]	Friction angle [°]	P–wave velocity $[\frac{m}{s}]$	Density $[\frac{kg}{m^3}]$	
		NTNU/SINTEF								
90	12	Doorstooper cell		34	0.2	87	18	2630		
95	5	Doorstooper cell		37	0.21	29		2693	5174	
101		Triaxial NTNU/ SINTEF cell		61	0.25	125		2990	6045	Amphibolite
101		Triaxial NTNU/ SINTEF cell		61	0.25	125		2990	6045	Quartz rich gneiss
104				60	0.19	140				Migmatite
105	6	Doorstopper cell	61	54	0.19	113	20	2966	4903	
107			62	84	0.25	49	35	2792		Phyllite Parallel with layering
107			20	38						Phyllite Normal to layering
108				64		120				Amphibolite gneiss
108				45		110				Diorite gneiss
110		Triaxial NTNU SINTEF cell		52	0.21	75				Granite gneiss
111	5	Triaxial NTNU/ SINTEF cell		64	0.18	192	16	2637	5629	
113		Triaxial NTNU/ SINTEF cell		21	0.14	186	18	2630	3900	
115	7	Triaxial NTNU/ SINTEF cell	61	43	0.22	50	19	2903	4860	

Data from "Hydraulic fracturing" table

Table A.7: Hydraulic fracturing test data.

ID	**Number of measurements**	**Number of cycles**	**Breakdown pressure** [MPa]	**Shut–in pressure** [MPa]	**Reopen pressure** [MPa]	**Pore pressure** [MPa]	**Comments**
23	15	1–3	29.3	9.4	15		
24	19	3	26.2	10	13		
25	16	3	21.8	8.6	13		
79	23	3	22.3	5.4	8		
85	2	3	8,5	1,1	5.5		Was carried out 7 measurements, but 5 were opening of existing fractures.
87	2	3	26.2	10	13		Was carried out 7 measurements, but only two were successful
102							Measurements done in four boreholes
106	2	4	22	5			
114	20	3	16.6	4.3	6.8		